STRUCTURAL BEHAVIOUR OF COMPOSITE GIRDERS USING HIGH STRENGTH FIBRE REINFORCED CONCRETE AND FIBRE REINFORCED POLYMERS

（高強度繊維補強コンクリートと FRP を用いた合成桁の力学的性状）

2016 年 3 月

埼玉大学大学院理工学研究科（博士後期課程）

理工学専攻（主指導教員 睦好 宏史）

ISURU SANJAYA KUMARA WIJAYAWARDANE

STRUCTURAL BEHAVIOUR OF COMPOSITE GIRDERS USING HIGH STRENGTH FIBRE REINFORCED CONCRETE AND FIBRE REINFORCED POLYMERS

（高強度繊維補強コンクリートと FRP を用いた合成桁の力学的性状）

A dissertation submitted in partial fulfilment of the requirement for the degree of
Doctor of Philosophy in Civil Engineering

by

Isuru Sanjaya Kumara Wijayawardane

Examination committee:
Prof. Hiroshi Mutsuyoshi (Chair)
Prof. Yoshiaki Okui
Prof. Masato Saitoh
Assoc. Prof. Takeshi Maki

Department of Civil and Environmental Engineering
Graduate School of Science and Engineering
Saitama University
Japan

March 2016

ABSTRACT

Fibre reinforced polymer (FRP) materials are being used for construction of the civil engineering structures because of their outstanding properties compared to the conventional construction materials. One of the main applications of the FRP is short span bridge construction. The superior features of the FRP include high tensile strength, high corrosion resistance, low weight, high fatigue resistance, etc. Furthermore, the use of the FRP reduces the life-cycle cost of a structure and the amount of carbon dioxide emission as compared to the prestressed concrete or steel bridges. The high durability of the FRP makes these materials suitable for short span bridges those are exposed to severe environmental conditions.

In most of the FRP bridges, steel bolts are used to connect the members together. Therefore, maintenance and repairing of the steel connections need to be carried out time to time. At the first stage of this study, glass fibre reinforced polymer (GFRP) and ultra-high strength fibre reinforced concrete (UFC) composite beams were developed to address that shortcoming. Non-corroding FRP bolts were used instead of the steel bolts and the flexural behaviour of the GFRP and UFC composite beams was studied. The GFRP and UFC composite beams were made by connecting precast UFC segments to the GFRP I-beam top flange using the FRP bolts and the epoxy adhesive. The four-point flexural tests were conducted on the large-scale GFRP and UFC composite beams by changing the FRP bolt diameter, bolt spacing and FRP bolt type in order to find out the suitable FRP bolt parameters. The experiment revealed that the FRP bolts can be used in the GFRP and UFC composite beams, instead of the steel bolts. Both the flexural capacity and the stiffness of the composite beams containing the steel bolts and the FRP bolts were similar. There was full composite behaviour until beam failure in the GFRP and UFC beams having FRP bolts and in the GFRP and UFC composite beams having steel bolts.

As well as the GFRP, the hybrid FRP (HFRP) also can be used for making the FRP and UFC composite beams. The GFRP consisted of glass fibres whereas the HFRP used in this study consisted of carbon and glass fibres. In both FRP types, the fibres were bonded together with the vinylester resin matrix. The polymer resin matrices contained in the GFRP, HFRP, FRP bolts, and the epoxy adhesive are susceptible to degrade their mechanical properties at glass transition temperature (T_g). Therefore, the flexural behaviour of the GFRP or HFRP (GFRP/HFRP) and UFC composite beams can be affected by elevated temperature. The temperature of the concrete bridge deck can reach 60°C or more when they are exposed to extremely hot climates or when they are located in hot industrial environments. Therefore, the second stage of this study was carried out to identify the influence of elevated temperature on

the mechanical properties of the materials used in the GFRP/HFRP and UFC composite beams and to investigate the flexural behaviour of the GFRP/HFRP and UFC composite beams at elevated temperature.

Experiments were conducted at temperatures between 20°C and 90°C to check the temperature dependence of the materials used in the GFRP/HFRP and UFC composite beams. The experiment results emphasized that the glass transition temperatures of the materials used in the GFRP/HFRP and UFC composite beams are in between 50°C and 60°C. The compressive strength of the GFRP, HFRP, and the FRP bolts is significantly affected by the glass transition. The tensile strength of the GFRP and the HFRP is greatly affected by the T_g of the vinylester resin whereas in the FRP bolts, the tensile strength is not significantly affected by the T_g. The compressive strength of the UFC also independent of temperature within 20°C and 90°C. The coefficients of thermal expansion of all the materials used in the GFRP/HFRP and UFC composite beams are constant at all temperatures between 20°C and 85°C. There is no influence on the longitudinal expansion rates of the materials by their glass transition temperatures. Shear strength of the FRP bolts rapidly reduced at the temperatures beyond 60°C whereas the shear capacity of the epoxy adhesive reduced with temperature regardless the T_g of the epoxy adhesive.

The flexural behaviour of the GFRP I-beams, GFRP-UFC composite beams, and the HFRP-UFC composite beams under room and elevated temperatures (between 20°C and 90°C) was studied. Prior to loading, all the beams except the beams at 20°C were heated up to the test temperature and kept constant at the same temperature for one hour. Similar to the material test results, the beam test results revealed that the flexural behaviour of the GFRP I-beams is influenced by the glass transition temperature of the vinylester resin. Both the flexural capacity and the stiffness of the GFRP I-beams are decreased at elevated temperature beyond the T_g of the vinylester resin. Use of the UFC segments significantly improves the ultimate flexural capacity and the stiffness of the GFRP I-beams at temperatures ranged from 20°C to 90°C. This is because the UFC segments can prevent premature delamination and kink failure of the GFRP I-beam compression flange. As a result, the tensile strength of the GFRP I-beam can be effectively utilized. It was confirmed that the bi-material bending effect in the GFRP/HFRP and UFC composite beams is negligible due to the close thermal expansion rates of the GFRP, HFRP, and the UFC materials. As well as the GFRP I-beams, the GFRP-UFC composite beams and the HFRP-UFC composite beams are affected by elevated temperature and their flexural capacities were decreased as the beam temperature increases. However, more than 85% of the

flexural capacity (compared to the flexural capacity at 20°C) of three beam types can be retained when the beam temperature is below 60°C. As the beam temperature increases beyond 60°C, the flexural capacity of these beams severely degraded. Furthermore, in these GFRP/HFRP and UFC composite beams, the failure mode depends on the shear capacity of the FRP bolts at the beam temperature.

Flexural behaviour of the GFRP I-beams and the GFRP and UFC composite beams was analysed using fibre model and the analysis results were verified by the experiment results. The fibre model can predict the flexural behaviour of the GFRP I-beams at temperatures between 20°C and 90°C. Regarding the GFRP and UFC composite beams, the fibre model results were be valid up to the slipping of the UFC segments. When there was no slip of the UFC segments, fibre model analysis results were agreed up to the failure of the composite beams. Under the actual circumstances, the GFRP and UFC composite beams may experience a large temperature gradient across beam top to bottom. According to the fibre model analysis, it was found that the stiffness of the GFRP and UFC composite beams, which is related to the main design criterion of the FRP bridges, is not significantly affected by the temperature gradient in the real situations. However, the flexural capacity of the GFRP and UFC composite beams at the slipping of the UFC segments is greatly influenced by the temperature of the beam top.

The high corrosion resistant GFRP and UFC composite beams were used as bridge girders to construct a short span pedestrian bridge in Japan. This bridge was constructed in a fishery harbour where corrosion is a major issue. The overall length and the width of the bridge are 6,000 mm and 960 mm, respectively. The static load tests conducted on the bridge confirmed the excellent performance of the GFRP and UFC composite beams.

DEDICATION

This dissertation is dedicated to my beloved wife

Anjalee Sumudu Shalika De Silva

&

My loving parents

Nandasiri Wijayawardena & Lakshmi Pragnawathi Gunapali Galhena

ACKNOWLEDGEMENT

This dissertation became a success with the support of many people. First of all, I would like to appreciate and express utmost gratitude to my advisor, Professor Hiroshi Mutsuyoshi for giving me valuable guidance and fruitful discussions throughout the FRP research project. I appreciate all the members of the examination committee, Professor Yoshiaki Okui, Associate Professor Takeshi Maki, and Professor Masato Saitoh for giving their comments and suggestions, which were very useful for this study.

I would like to greatly acknowledge the Japanese Ministry of Education, Culture, Sports, Science, and Technology (MONBUKAGAKUSHO) scholarship for being the financial support of my stay in Japan. I give sincere gratitude to the Saitama University, Japan for giving opportunity as well as the facilities to carry out this study successfully.

Very special thank should be given to the FRP project members, Mr. Yusuke Kanaya, Dr. Senanayaka Vidhanage Thilanka Janaka Perera, Mr. Daichi Masubuchi, Mr. Kuniaki Moriya, and Mr. Takaki Endo for their corporation and support in preparing and conducting the experiments. I would like to be thankful to Associate Professor Takashi Fujihara and Dr. Atsushi Sumida for their great support to this study. And also, I convey my sincere gratitude to the previous members of the FRP project in Saitama University, especially Dr. Nguyen Hai and Dr. Allan Manalo who gave support and important comments time to time.

I highly appreciate the numerous support given by the Associate Professor Shingo Asamoto, Assistant Professor Yao Luan, Mr. Kosuke Sato, Ms. Rie Nakamoto, Ms. Junko Yagi and Ms. Hitomi Tsukuda. I would like to extend my gratitude to all the friends in Saitama University, especially the students of the Structural Materials Laboratory for their supports and friendship.

Finally, I would like to thank my beloved wife, Anjalee Sumudu Shalika De Silva for understanding and giving her full support in all aspects. I would highly appreciate and be thankful to my parents, Nandasiri Wijayawardena and Lakshmi Pragnawathi Gunapali Galhena for the encouragements, care and support provided to make this achievement. I sincerely thank my loving brothers, Asitha Wijayawardane and Thilina Wijayawardane, and also other family members who gave enormous strength and encouragements.

Isuru Sanjaya Kumara Wijayawardane
Saitama University, Japan.
06 March 2016

Table of Contents

List of Tables

List of Figures

Abbreviations

FRP – Fibre reinforced polymer
GFRP – Glass fibre reinforced polymer
CFRP – Carbon fibre reinforced polymer
AFRP – Aramid fibre reinforced polymer
HFRP – Hybrid fibre reinforced polymer
CSM – Continuous strand mat
UFC – Ultra-high strength fibre reinforced concrete
GFRP/HFRP – Glass fibre reinforced polymer or hybrid fibre reinforced polymer
GFRP-UFC – GFRP and UFC
HFRP-UFC – HFRP and UFC
TF – Top flange
BF – Bottom flange
T_g – Glass transition temperature
α – Coefficient of thermal expansion
L_s – Steel pipe length
L_e – Effective length
L – Span length
W/C – Water/cement ratio
DSC – differential scanning calorimetry
ε_c – Compressive strain
ε_t –Tensile strain
ε_{cu} – Ultimate compressive strain
f'_{ck} – Compressive strength of concrete
E_c – Young's modulus of concrete
h – Beam height
n – Number of discrete horizontal elements
m – Number of longitudinal segments along the beam span
a – Number of longitudinal segments along the flexural span
b – Number of longitudinal segments along the shear span
ΣF_c – Resultant compressive force
ΣF_t – Resultant tensile force
M – Resultant moment
ϕ – Beam curvature/ bolt diameter
δ_{max} – Maximum beam deflection (at midspan)
D_1 is the number of horizontal divisions in the UFC slab cross-section
ΔA is the cross-sectional area of a UFC element
F_{shear} – Total shear force

Chapter 1

Introduction

A large number of bridges constructed using the conventional construction materials are low serviceable due to aging and deterioration. According to the U.S. department of transportation, 26.7% of the total bridges in the United States have been identified as structurally deficient [1]. Each country expends a huge amount of money on maintenance and renovation of the bridges annually and this problem can be minimized by implementing new materials and new technologies in bridge construction. Steel, prestressed, and reinforced concrete are the conventional construction materials used for bridges and the durability of these materials is severely affected by the corrosion. Aiming for non-corrosive materials and cost-effective construction methods can reduce the overall cost of a bridge during its life span.

Because of the excellent properties of the fibre reinforced polymer (FRP) composites, they have been used in many engineering applications (aerospace engineering, automobile engineering) as well as manufacturing of sports items, musical instruments etc. Since last few years, they are receiving attention as a suitable construction material in the civil engineering field. High corrosion resistance, high tensile strength-to-weight ratio, excellent fatigue resistance, and low weight are the outstanding features of the FRP. The FRP was first introduced in the civil engineering as FRP reinforcing bars and as retrofitting sheets for columns and beams. The superior properties of the FRP composites allow rapid construction of durable structures. Nowadays the FRP beams are being used as bridge girders in short span bridges. The high durability of the FRP material over the conventional construction materials reduces the maintenance cost of the FRP bridges and that results low life cycle cost of the FRP bridges [2]. The FRP composites can be pre-fabricated and transported to the construction site and this will accelerate and ease the overall construction process of an FRP bridges, and also that reduces the associated labour costs. Furthermore, the use of the FRP composite materials is environment friendly compared to the steel and the prestressed concrete, in terms of the low carbon dioxide emission during the manufacturing process of the materials [3]. Main shortcomings of the FRP materials are high initial cost, low stiffness, and lack of fire resistance compared to the conventional construction materials. The low stiffness of the FRP is the main reason for using them for construction of the short span bridges. However, the stiffness in the FRP composite beams can be enhanced with the use of the stiffeners and using a concrete slab, which will be discussed later.

1.1 Types of FRP composites used in civil engineering

CFRP composites

The carbon fibres have the highest stiffness and the tensile strength among the commonly used FRP materials. They are manufactured by controlled pyrolysis and crystallization of organic precursors at temperatures above 2000°C. The carbon FRP (CFRP) are durable in hot and moist environments and they can withstand fatigue loads. Studies carried out on the FRP composites showed that carbon fibre reinforced polymers have high durability compared to that of aramid or glass fibre reinforced polymers [4]. However, the CFRP is more expensive than the other FRP types.

GFRP composites

Glass fibre reinforced polymers (GFRP) are used in a wide range of civil engineering applications because it is less expensive compared to the other FRP materials. The glass fibres are processed form of glass, which are composed of a number of oxides. Unlike the carbon fibres, the glass fibres are particularly sensitive to moisture and need to be protected by the resin [5]. Glass fibres are susceptible to rupture and because of the creep, they tend to lose their strength under sustained stresses [6]. Other than the low cost of the GFRP, it has excellent thermal and electrical insulation properties compared to the CFRP.

AFRP composites

Aramid fibres were used to produce the first generation of FRP prestressing tendons in the 1980s in Europe and Japan [5]. They contain aromatic molecular chains and they are the lightest among the high-performance fibres. The high moisture absorption, difficulty in processing, low melting temperatures, and relatively low compressive strength compared to the other FRP materials made Aramid FRP (AFRP) less attractive in the structural applications.

HFRP composites

The physical and mechanical properties vary in different FRP types. Therefore, the combined features of the FRP types can be obtained by blending the different types of fibres together and manufacturing hybrid FRP (HFRP) profiles. Therefore, in the HFRP composites, there are two or more FRP types and the most commonly available HFRP consists of GFRP and CFRP. Use

of the HFRP profiles are economical because they are inexpensive than the CFRP as well as they have high tensile, flexural and compressive properties than those of the GFRP [7-11].

1.2 Literature review

1.2.1 Use of FRP and UFC for short span pedestrian bridges

High corrosion resistance of the FRP composites can be utilized to address the corrosion problem in bridges, so that, the durability of bridges can be increased and the maintenance and renovation costs can be reduced. There are large numbers of FRP bridges constructed worldwide and they confirmed the suitability and best performance [12-16]. Because the FRP composites are very expensive than the conventional construction materials, the initial cost of the FRP structures is very large. The prefabrication of the FRP structural elements such as beams and stiffeners can also increase the cost of the FRP systems compared to cheap in-situ construction methods. However, when the life cycle cost of the bridge is concerned, use of the FRP can be cheaper than the steel bridges or prestressed concrete bridges. Mostly, the GFRP is being used for the bridges because it is the cheapest among the FRP composites used in the civil engineering field. But the GFRP has low mechanical properties compared to the other FRP types such as the CFRP and the AFRP.

Based on the experiments carried out on the HFRP composite beams by Hai, et al. [17] in the Saitama University, a short span pedestrian bridge was constructed in Kure, Hiroshima prefecture, Japan in 2011. Fig. 1.1 shows the Kure pedestrian bridge and it is located in a fishery harbour where severe corrosion can take place. This is the first pultruded HFRP pedestrian bridge in Japan and the overall length and width of the bridge are 12 m and 0.896 m, respectively. This bridge was used to access a pontoon from the deck. Therefore, the bridge was simply supported at both ends. It was constructed using two I-shaped pultruded HFRP beams. Pultrusion is the manufacturing process of the FRP composite materials and during the pultrusion, the resin-coated fibres (glass, carbon, etc.) were pulled through a heated die. Schematic diagram of the pultrusion process is illustrated in Fig. 1.2. The HFRP I-beams consisted of CFRP and GFRP in the flanges and GFRP in the web. The main purpose of installing this HFRP short span bridge was to replace a corroded steel bridge using high corrosion resistant materials and thereby reduce the maintenance cost.

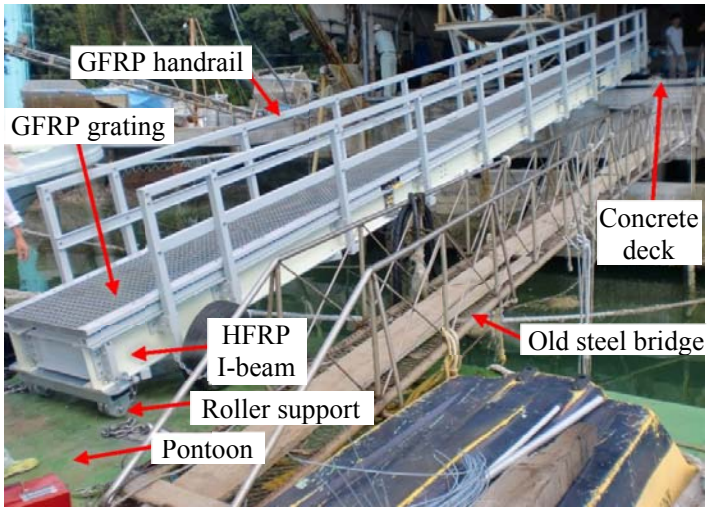

Fig. 1.1 HFRP short span pedestrian bridge in Kure city, Japan

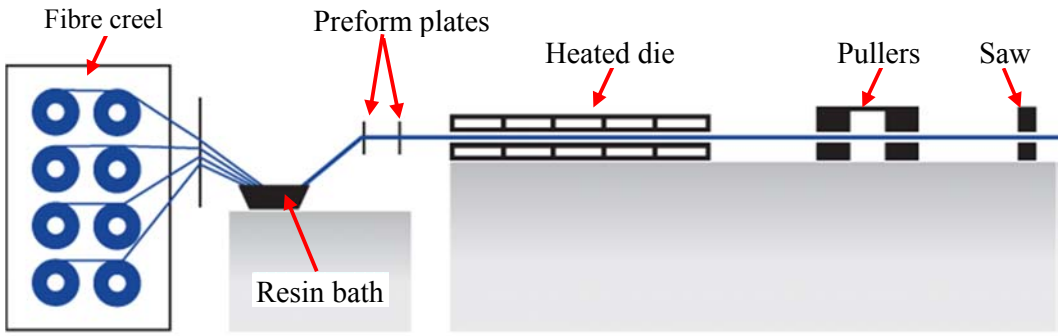

Fig. 1.2 Manufacturing of FRP by pultrusion

It has been identified that the premature delamination failure of the HFRP I-beam compression flange can occur when flexural load is applied on the beam [17, 18]. Fig. 1.3 shows the delamination failure of an HFRP I-beam. The layered structure in the HFRP is weak to undertake the tensile inter-laminar stresses developed in the compression flange. Consequently, the tensile capacity of the HFRP I-beam cannot be effectively utilized. To address this shortcoming of FRP I-beams, the compression flange need to be strengthened. This can be done using a reinforced concrete slab or fixing a steel section to the I-beam compression flange. Manalo, et al. [19], Nordin and Täljsten [20] investigated the flexural behaviour of the HFRP and concrete composite beams and the results showed that both the flexural capacity and stiffness of the composite beams were improved with the use of the top concrete slab. Typical reinforced concrete slabs required to be larger in cross-sectional area, in order to utilize high tensile capacity of the HFRP I-beams. The larger composite beams cause excess deformation

due to their heaviness and also, there will be difficulties in manufacturing and installation of these beams. Corrosion is the main problem in steel plates which prevents them using in the HFRP beams. These issues related with reinforced concrete and steel can be eliminated by using innovative materials such as ultra-high strength fibre reinforced concrete (UFC). The effectiveness of the FRP and UFC composite beams in pedestrian bridges has been reported in the literature [8, 21]. The UFC slab was precast and it was connected to the GFRP I-beams using steel bolts and epoxy adhesive. Fig. 1.4 illustrates the structure of the GFRP and UFC composite beam consisting steel bolts. Since the steel bolts are deteriorated by corrosion, the durability of the composite beam will be affected. Therefore, it is important to avoid this shortcoming and enhance the durability of the GFRP and UFC composite beams.

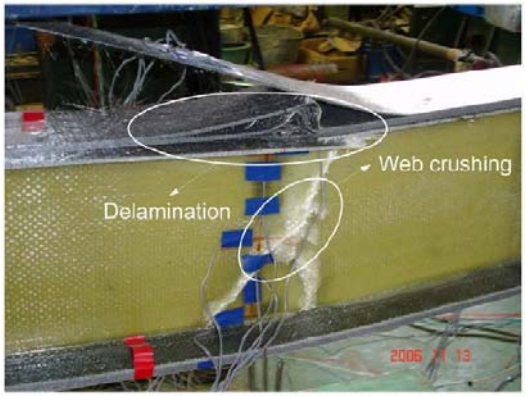

Fig. 1.3 Delamination failure of HFRP I-beam

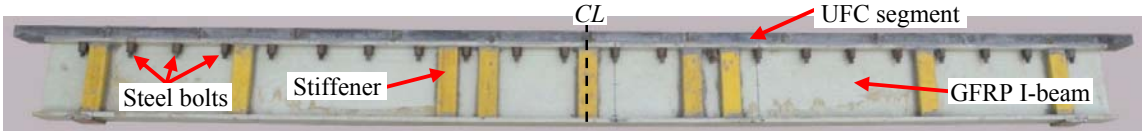

Fig. 1.4 GFRP and UFC composite beam

1.2.2 Influence of elevated temperature on FRP materials

The fibres and polymer resin matrix are the primary components in the FRP materials. In the FRP composites, most of the mechanical properties depend on the characteristics of the fibres. However, the polymer resin matrix which contributes to the fibre cohesion in the FRP materials also has some influence on the material properties of the FRP. This is because of some of the physical and mechanical properties of the FRP composite are inherited by their resin matrices.

Based on the thermal response of the polymer matrices used for manufacturing the FRP, they are divided into two categories, 1) thermoset resins, 2) thermoplastic resins.

Thermoset resins

The composite materials contain thermoset resins cannot be re-melted or reformed after curing. Reason for this is, during the curing, they form three dimensional molecular chains which are called 'cross-linking'. The higher the number of cross-linking, the more rigid and thermally stable the material will be. Thermosets are brittle in nature but sometimes they may soften to some extent at elevated temperature. This characteristic is sometimes used to create a bend or curve in tubular structures. Thermosets offer greater thermal and dimensional stability, better rigidity, and higher electrical, chemical, and solvent resistance. The most common resin materials used in thermoset composites are epoxy, polyester, bismaleimides, vinylester, phenolics, cyanate esters, and polyimides.

Thermoplastic resins

Thermoplastics can be melted by heating and solidified by cooling. Therefore, these materials are capable of repeated reshaping and reforming. This is happened because the thermoplastic molecules do not cross-link each other [22]. Their lower stiffness and strength values require the use of fillers and reinforcements for structural applications. Thermoplastics generally exhibit poor creep resistance at elevated temperature, as compared to thermosets. They are more susceptible to solvents than thermosets. Polypropylene and polyethylene are the most common thermoplastic resins used in FRP composites. They have excellent resistance to acids and alkalies and have good resistance to organic solvents. Their relatively low melting points allow for rapid processing at lower cost. Nylon and Acetal are also widely used because they are highly resistant to organic solvents and can obtain better mechanical properties compared to the other thermoplastic resins.

Behaviour of polymer resins at elevated temperature

The pure crystalline solids such as metals undergo a phase change from solid to liquid at a transition temperature and that temperature is called the melting temperature. In contrast to pure crystalline materials, the polymer resins contain non-crystalline amorphous regions. Therefore, the polymer resins belong to semi-crystalline category and there will be thermal transitions at

lower temperatures than the melting temperature. This temperature of the polymer resin is called as glass transition temperature (T_g). Sometimes T_g is referred as heat distortion temperature or heat deflection temperature. When the temperature is close to or above T_g, physical and mechanical properties of the polymer resin are influenced and they degrade [23-25]. As a result, the polymer resins in FRPs undergo changes from rigid to rubbery state [5]. Therefore, when the temperature exceeds T_g, the polymer matrix in the FRP which contributes to fibre cohesion and transfer of forces between the fibres becomes soft. Generally, the T_g of the vinylester resins used as the polymer matrix in the GFRP reinforcing bars is between 100°C and 120°C [23, 26]. However, the T_g of some commercially available FRP composite materials typically varies from 60°C to 82°C [27]. The deterioration of strength and stiffness properties of conventional pultruded FRP profiles as a function of temperature for various resin systems is given in Table 1.1 [28].

Table 1.1 Percentage of property retention of conventional pultruded profiles as a function of temperature

Property	Temperature (°C)	Property retained (%)	
		Glass fibre and polyester pultruded material	Glass fibre and vinylester pultruded material
Strength	37.8	85	90
	51.7	70	80
	65.6	50	80
	79.4	do not use	75
	93.3	do not use	50
Elastic modulus	37.8	100	100
	51.7	90	95
	65.6	85	90
	79.4	do not use	88
	93.3	do not use	85

1.2.3 Performance FRP composite structures subjected to elevated temperature

Because of the temperature dependence of the polymer resins contained in the FRP, it is important to study the performance of the FRP composite beams exposed to extreme temperature conditions. There are some studies conducted to investigate the influence of elevated temperature on the FRP composite beams used in short span pedestrian bridges, but

the maximum temperature taken into account was less than 40°C. Farhey [29] and Keller et al. [30] investigated the long term performance of short span FRP bridges and reported on the acceptable serviceability and durability of the FRP systems.

It has been proven that the structural design of the FRP bridges depends mostly on the deflection limit because of the low stiffness of the FRP composites [31]. The American Association of State Highway and Transportation Officials (AASHTO) and the Japan Society of Civil Engineers (JSCE) suggest that the deflection limit for pedestrian bridges should be less than $L/500$, where L corresponds to the bridge span [32, 33]. Therefore, the stiffness of the FRP composite bridges becomes a significant parameter. The temperature variation in the FRP composite bridges has some influence on the flexural behaviour due to low stiffness of the fibre reinforced composites [34, 35]. According to Dai et.al., the structures consisting of the FRP and concrete can experience 50°C or higher temperatures when they are located in harsh environments such as hot climates and industrial environments [36]. A field investigation carried out on short span GFRP bridge showed that the maximum temperature at the bridge deck can reach up to 60°C during summer [37]. However, depending on the environmental conditions and the bridge location, the maximum temperature of the bridge deck can be higher than 60°C. An experiment was conducted evaluating the performance of the FRP composite bridge deck prototypes under two extreme temperature conditions by Kwon et.al [38]. In this study, the FRP composite bridge decks were subjected to simulated traffic loads that induce repetitive stress cycles under -30°C and 50°C. The fatigue performance of each FRP deck prototype was compared with the response of the conventional reinforced concrete deck. The results signified that the progressive degradation in stiffness of the FRP composite bridge decks under two extreme temperatures by the cyclic loading on all the decks. The stiffness of the FRP composite bridge decks was more susceptible to elevated temperature compared to low temperature conditions.

In the GFRP or HFRP (GFRP/HFRP) and UFC composite beams, there are polymer resin materials contained in the GFRP, HFRP, FRP bolts, and epoxy adhesive. Therefore, these composite beams may undergo some changes due to deterioration of physical and mechanical properties of the materials at elevated temperature. Because of that, it's noteworthy to study the flexural behaviour of the GFRP/HFRP and UFC composite beams under such temperature conditions.

1.3 Objectives and scope

The aim of this study is to develop high corrosion resistant GFRP/HFRP and UFC composite beams for construction of short span pedestrian bridges. So that, such composite beams can be used in severe corrosive environments with minor maintenance. The scope of the study is given in Fig. 1.5. There are three main objectives as described below.

- Utilize the FRP bolts in the GFRP and UFC composite beams instead of steel bolts and investigate the flexural behaviour of such beams. In order to find out the most suitable FRP bolt parameters, large-scale GFRP-UFC beam flexural tests were conducted with FRP bolts changing diameter, bolt types, and bolt spacing.
- Investigate the influence of elevated temperature on the flexural behaviour of the GFRP/HFRP and UFC composite beams. Large-scale beam flexural tests were carried out at room and elevated temperatures (less than 90°C). As a secondary objective in the study, a number of material tests were conducted at room and elevated temperatures (less than 90°C) to study the influence of elevated temperature on the mechanical properties of the materials used in the GFRP/HFRP and UFC composite beams.
- Study the performance of a short span pedestrian bridge under the static loading, which was constructed using the GFRP and UFC composite beams. The flexural behaviour of the bridge was checked under three loading patterns.

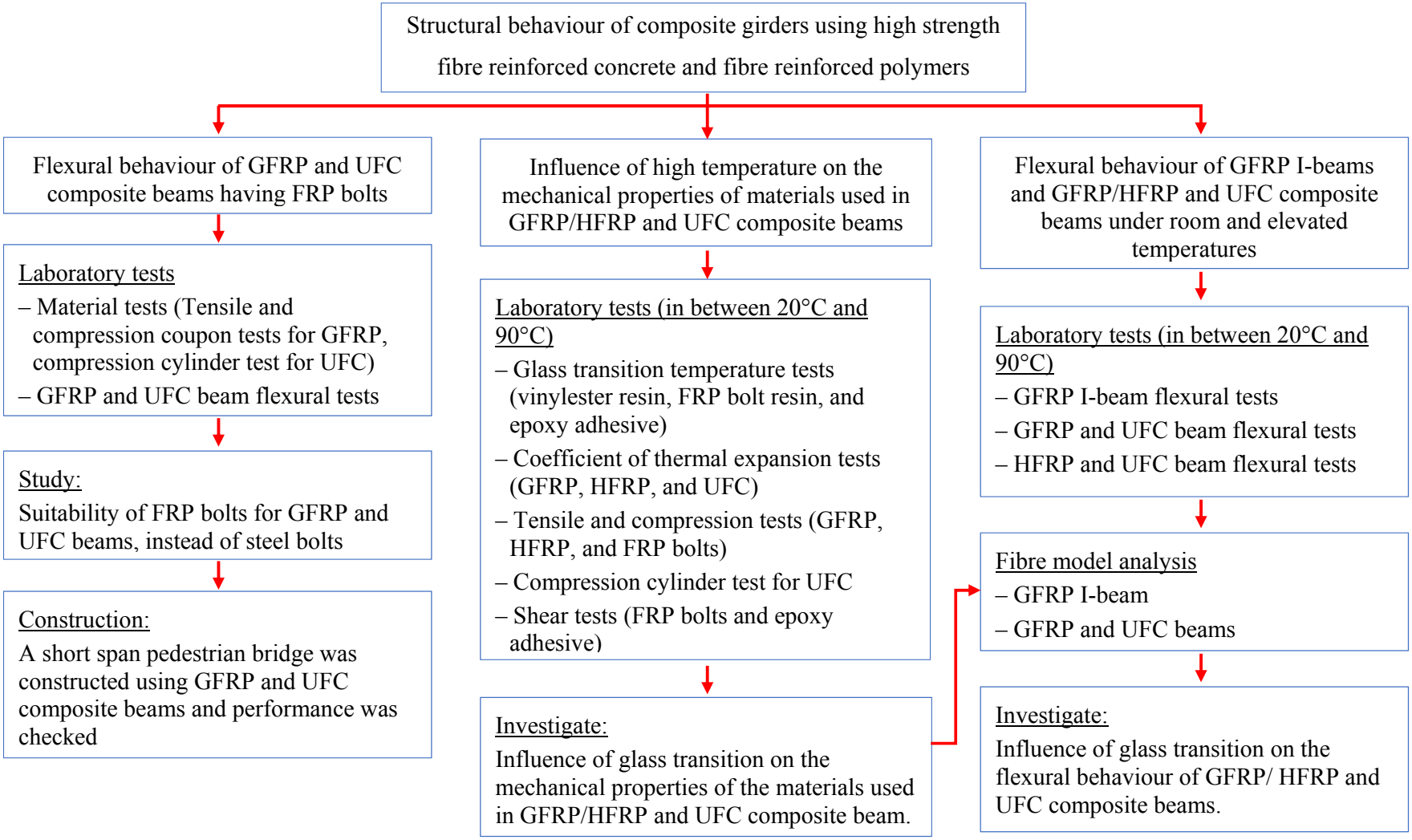

Fig. 1.5 Scope of study

1.4 Organization of the dissertation

There are four main parts in this dissertation; 1) suitability of FRP bolts for the GFRP and UFC composite beams, 2) investigate the influence of elevated temperature on the mechanical properties of the materials used in the GFRP/HFRP and UFC composite beams, 3) investigate the flexural behaviour of the GFRP/HFRP and UFC composite beams under room and elevated temperatures, and 4) performance of a short span pedestrian bridge subjected to static service loading, which was constructed using the GFRP and UFC composite beams. This dissertation consists of seven chapters and the details of each chapter is given below.

Chapter 1

Introduction including the literature review, motivation, objectives, and the scope of the study.

Chapter 2

Experimental works conducted to clarify the suitability of the FRP bolts in the GFRP and UFC composite beams is described in this chapter. The FRP bolts were used to connect the UFC slab to the top flange of the GFRP I-beams. Both the material tests and the composite beam flexural tests are explained in detail.

Chapter 3

Some researchers reported that the mechanical properties of the FRP composites are severely influenced by the glass transition temperature. This chapter describes the influence of elevated temperature on the mechanical properties of the materials used in the GFRP/HFRP and UFC composite beams. Degradation of the material properties of the FRP composites by glass transition is explained in this chapter.

Chapter 4

The influence of elevated temperature on the flexural behaviour of the GFRP I-beams, and the GFRP/HFRP and UFC composite beams is explained in this chapter. Details of the large-scale beam flexural tests conducted at room and elevated temperatures (in between 20°C and 90°C) including the specimen preparation, test setup, and heating method are demonstrated.

Chapter 5

In this chapter, the fibre model analytical method is described. The fibre model was used to analyse the flexural behaviour of the GFRP I-beams, and the GFRP-UFC (GFRP and UFC) composite beams. Verification of the analysis results by the experiment results is discussed. In the experiment, there was a small temperature gradient across the beam cross-section. Therefore, the fibre model analysis was used to predict the flexural behaviour of the GFRP-UFC composite beams under actual circumstances, where there is a large temperature gradient across beam cross-section.

Chapter 6

Details of a short span pedestrian bridge constructed using the GFRP and UFC composite beams is described in this chapter. Furthermore, the static loading test conducted to investigate the performance of the short span bridge also explained.

Chapter 7

Summarizes the main conclusions of this study and suggests the recommendations for future studies.

Chapter 2

Flexural Behaviour of GFRP and UFC Composite Beams Having FRP Bolts as Shear Connectors

2.1 Introduction

This chapter describes the development of high corrosive resistant GFRP and UFC composite beams for construction of short span pedestrian bridges. The previous experiments related to the GFRP and UFC composite beams, conducted in the Saitama University, used steel bolts and epoxy adhesive to connect the UFC slab to the GFRP I-beam [18]. However, the steel bolts in these composite beams are prone to corrosion and hence, the durability of the bridge is affected. In this study, corrosive resistance of the GFRP and UFC composite beams was improved using the FRP bolts and the flexural behaviour such beams was investigated. Large-scale beam tests were carried out by changing the FRP bolt diameter, FRP bolt spacing, FRP bolt type (bolts having heads and bolts without heads), and the gap between two consecutive UFC segments.

2.2 Materials

The GFRP and UFC composite beams consist of four main materials GFRP, UFC, FRP bolts, and epoxy adhesive. Details of the materials and the mechanical properties of them are explained in the following sections.

2.2.1 GFRP I-beams

The GFRP I-beams are manufactured by pultrusion process and they consist of glass fibres oriented in 0°, 90°, ±45° directions, continuous strand mat (CSM), and vinylester resin. The 0° and ±45° fibres in the GFRP mainly contribute to the tensile strength of the GFRP while the 90° fibres contribute to the lateral strength. The CSM consisted of randomly oriented glass fibres and those fibres help to reduce strong anisotropic properties in the GFRP. There is a significant contribution for the strength of the GFRP by the vinylester resin, which bonds the glass fibres together. Fibre layer composition of differently oriented glass fibre layers is given in Table 2.1 and the fibre lay-up in the GFRP I-beam's flange and the web is illustrated in Fig. 2.1. According to Table 2.1, fibre compositions in GFRP flange and web are different. This is

because, the flanges are designed to take the axial and flexural forces whereas the web is designed to undertake the shear force. Therefore in GFRP I-beams, the flanges are strong in the longitudinal direction of the beams, whereas the web is strong in the vertical direction.

The GFRP coupon tests were conducted to investigate the tensile strength, the compressive strength, and the Young's modulus of the GFRP flange and web. The test coupons were machined from a GFRP I-beam along the longitudinal direction. Details of the tensile and compression test specimens and the test methods are described in Section 3.1.3 and the effective mechanical properties of the GFRP flange and web are given in Table 2.2. According to the experiment results, the tensile strength, compressive strength, and the Young's modulus of the GFRP flange are significantly higher than that of the GFRP web. Main reason for this is the amount of differently oriented glass fibres in the flange and the web.

Table 2.1 Glass fibre layer composition in GFRP I-beam

Parameters		GFRP I-beam		
		GFRP 0°/90°	GFRP ±45°	GFRP CSM
Volume fraction (%)		53	53	25
Volume content (%)	Flange	50	41	9
	Web	43	43	14

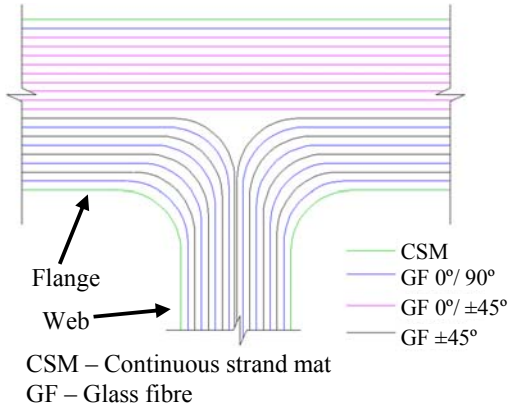

Fig. 2.1 Fibre lay-up in GFRP I-beam

Table 2.2 Mechanical properties of GFRP flange and web

Property	GFRP flange	GFRP web
Compressive strength (N/mm^2)	230	223
Tensile strength (N/mm^2)	448	306
Young's modulus (kN/mm^2)	21.0	17.8
Poisson's ratio	0.31	0.27

2.2.2 UFC

The UFC slab is the key component which is preventing the premature delamination failure of the compression flange of the GFRP I-beams. The primary advantages of using the UFC are its high compressive strength, low weight, and high durability compared to the conventional reinforced concrete. Watanabe et.al. and Mehta conducted experiments on UFC and reported the high durability of the UFC [39, 40]. In order to ease the manufacturing, transportation, and the installation processes of the UFC slab, it was designed as precast segments. Therefore, occurrence of some cracks and/or deflections in a long monolithic slabs due to their high slenderness ratio can be avoided. The UFC consists of steel fibres, premixed cementitious powder (ordinary Portland cement, Silica fume, and Ettringite), water, sand, and water reducing agent. Equal amounts of 0.2 mm diameter high strength steel fibres (tensile strength 2000 N/mm^2) having lengths 22 mm and 15 mm were used for making UFC. The volume ratio of the steel fibres is 1.75%. The mix proportions of the materials are given in Table 2.3. Curing of the UFC segments was done in two stages, in primary curing the segments were wet cured for 24 hours at 5°C to 40°C and in the secondary curing the segments were steam cured for 24 hours at 85°C.

Table 2.3 Mix proportions of materials for UFC

Unit quantity (kg/m^3)					Air content (%)
Water	Premixed cement	Sand	Water reducing admixture	Steel fibre	
205	1287	898	32.2	137.4	2.0

According to the test procedure explained in Section 3.1.4, the compressive strength and the Young's modulus of the UFC were obtained by the standard cylinder tests (50 × 100 mm), the test results are given in Table 2.4. Two sizes of UFC segments were used in this study and their

lengths were 300 mm and 250 mm. The 250 mm long segments were used only at the two ends of the GFRP and UFC beam. The cross-sectional dimensions of both segment types were identical (95 × 35 mm) and they were selected according to a previous study conducted in the Saitama University [18]. According to the experiment results of that study, the size of the UFC segments was decided to have a compression failure in the UFC slab and to avoid unsafe catastrophic tensile-brittle failure in the GFRP and UFC beams. The FRP bolts were embedded into the UFC segments during the casting of the segments and the embedment length is 30 mm. Manufacturing of the UFC segments was done in a factory to reduce the production time as well as the manpower.

Table 2.4 Mechanical properties of UFC

Compressive strength (N/mm^2)	Young's modulus (kN/mm^2)	Ultimate compressive strain (μ)
178	44.8	4930

2.2.3 FRP bolts and epoxy adhesive

Two shear connector types were used in the GFRP and UFC composite beams, 1) FRP bolts, and 2) 'Sikadur® – 30 Normal' epoxy adhesive. Fig. 2.2 and Fig. 2.3 show the FRP bolts and the epoxy adhesive used in the GFRP and UFC composite beams, respectively. The non-corrosive FRP bolts were used in the GFRP and UFC composite beams to improve the durability of the beams. The purpose of using the epoxy adhesive is to have a good bond between the top flange of the I-beams and the UFC segments and improve the composite behaviour of the beams. The mixing proportions of compound A and B (Fig. 2.3) of epoxy adhesive is 3:1.

The FRP bolts consist of the glass fibres in the core, oriented at 0° along the bolt axis and the core is covered with a high strength polymer material to form the threaded part. The FRP nut consists of high strength polymer only. The tensile, compressive, and shear strength tests were conducted for 16 mm diameter FRP bolts and the test methods are described in Section 3.1.5. The experiment results are given in Table 2.5. According to the method depicted in Section 3.1.6, epoxy adhesive shear tests were carried out and the effective shear strength was 9.6 N/mm^2.

Fig. 2.2 FRP bolts and nuts

Fig. 2.3 Epoxy adhesive

Table 2.5 Mechanical properties of FRP bolts and epoxy adhesive

Property	FRP bolts	Epoxy adhesive
Compressive strength (N/mm^2)	264	-
Tensile strength (N/mm^2)	255	-
Shear strength (N/mm^2)	140	9.6

2.3 Test variables and methodology of GFRP and UFC composite beam flexural test

Pultruded GFRP I-beams having overall length and height of 3,500 mm and 250 mm were used in this study. The flange is 14 mm in thickness and 95 mm in width. The web thickness is 9 mm. Cross-sectional details of the GFRP I-beam are given in Fig. 2.4. The GFRP and UFC composite beams were made by connecting the UFC segments to the top flange of the I-beam. The cross-sectional details of the GFRP and UFC composite beams are shown in Fig. 2.5. The test variables are FRP bolt diameter, FRP bolt spacing, FRP bolt type and the gap between two consecutive UFC segments. Five different GFRP and UFC composite beams were tested under four-point bending tests and the test variables are given in Table 2.6.

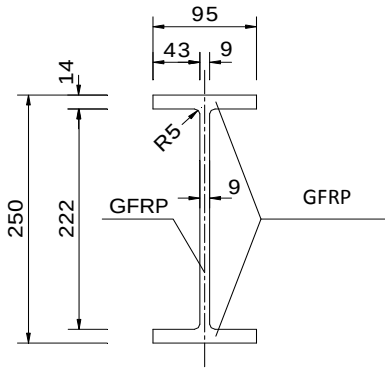

Fig. 2.4 Cross-sectional dimensions of GFRP I-beam (Units: mm)

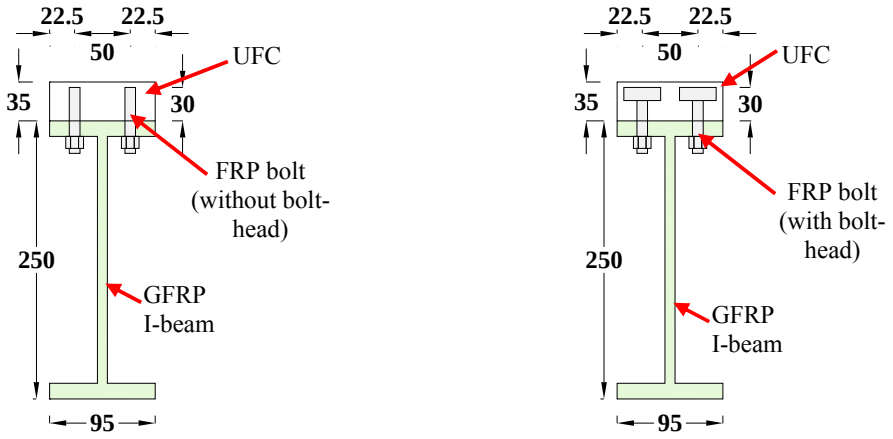

(a) G10-F16-B4 (b) Other composite beams

Fig. 2.5 Cross-sectional details of GFRP and UFC composite beams (Units: mm)

In beam G10-F16-B4, only the FRP threaded bars were used so that there were no bolt-heads inside the UFC segments. The gap between two consecutive UFC segments in beam G5-F16-BN4 was 5 mm whereas in all the other beams it was 10 mm. In the GFRP and UFC composite beam containing steel bolts, the bolt diameter and bolt spacing were chosen by push-out tests and the details of the experiment are available in literature [14]. The same bolt size and bolt spacing of the steel bolted GFRP-UFC (GFRP and UFC) composite beams were used for the GFRP-UFC beams having FRP bolts also. In addition to that, the GFRP and UFC composite beams having 10 mm and 16 mm diameter FRP bolts at 100 mm bolt spacing were tested to check the influence of different bolt diameters on the flexural behaviour of the composite beams. In order to study the influence of different bolt spacing (100 mm and 150 mm) on the flexural behaviour of the GFRP-UFC beams, two types of UFC segments were manufactured, 1) UFC

segments with four FRP bolts, and 2) UFC segments with six FRP bolts. The details of the UFC segments are given in Fig. 2.6. The I-beam top flange was drilled and the bolt-holes were created (at 100 mm or at 150 mm centre-to-centre spacing) to match the bolts which are embedded in the UFC segments. Before fixing the UFC segments to the I-beam, an epoxy adhesive layer was uniformly applied on the top flange. A constant torque of 20 Nm was applied on all the FRP bolts to have uniform tightness in all the UFC segments.

Table 2.6 Experimental variables

Specimen name	Material type	Bolt spacing (mm)	Segment joint spacing (mm)	FRP bolt diameter (mm)	Bolt-head in the UFC
G10-F16-B4	GFRP	150	10	16	No
G10-F10-BN6	GFRP	100	10	10	Yes
G10-F16-BN4	GFRP	150	10	16	Yes
G10-F16-BN6	GFRP	100	10	16	Yes
G5-F16-BN4	GFRP	150	5	16	Yes

Notations of the specimen names:
G: GFRP I-beam
10 or 5: Gap between consecutive UFC segments (filled with cement mortar)
F: FRP bolt
10 or 16: Bolt diameter (in mm)
B: Only threaded bar
BN: Bolts with head
4 or 6: Number of bolts per UFC segment

As shown in Fig. 2.7, GFRP stiffeners were attached at both sides of the I-beam web to avoid web buckling. The epoxy adhesive was used to attach the stiffeners and the nominal dimension of these stiffeners are 30 × 60 × 220 mm and their thickness is 4 mm. The gaps between the UFC segments (5 mm or 10 mm) were filled with cement mortar and the mix proportions of the materials are given in Table 2.7. The compressive strength and the Young's modulus of the filling cement mortar paste were 90.3 N/mm^2 and 31 kN/mm^2, respectively. The cement mortar filling of all the specimens were wet cured for 7 days before the bending test.

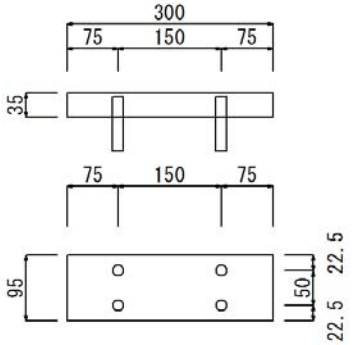

(a) UFC segment with four bolts

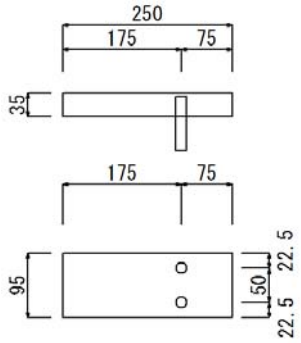

(b) Edge UFC segment of beams with 150 mm bolt spacing

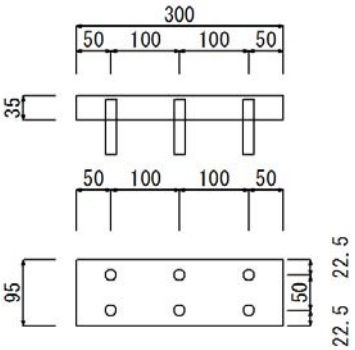

(c) UFC segment with six bolts

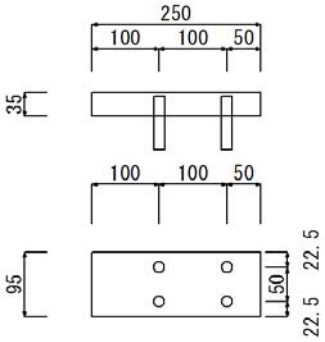

(d) Edge UFC segment of beams with 100 mm bolt spacing.

Fig. 2.6 Details of UFC segments (Units: mm)

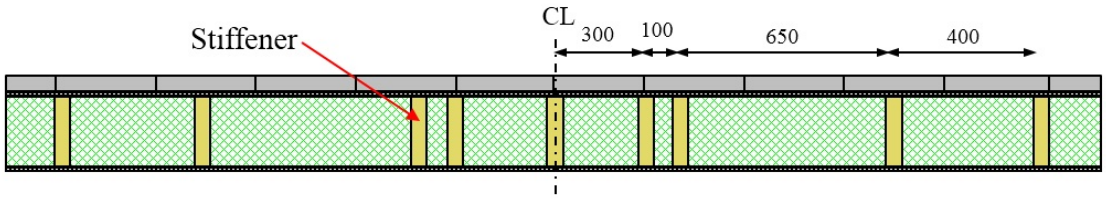

Fig. 2.7 Configuration of stiffeners in the GFRP and UFC composite beam (Units: mm)

Table 2.7 Mix proportions of cement mortar

W/C	Unit amount (kg/m^3)			
	Cement	Water	Fine aggregate	High performance water reducing agent
0.30	970.7	291.2	1026.9	0.01

The test setup of four-point flexural testing is illustrated in Fig. 2.8. The flexural span and the shear span of the beams were 700 mm and 1,250 mm, respectively. The load was applied at a constant rate by a manually operated hydraulic jack. A steel beam was used to equally spread the load between two loading points. Fig. 2.9 shows the four-point bending test of the GFRP and UFC composite beam.

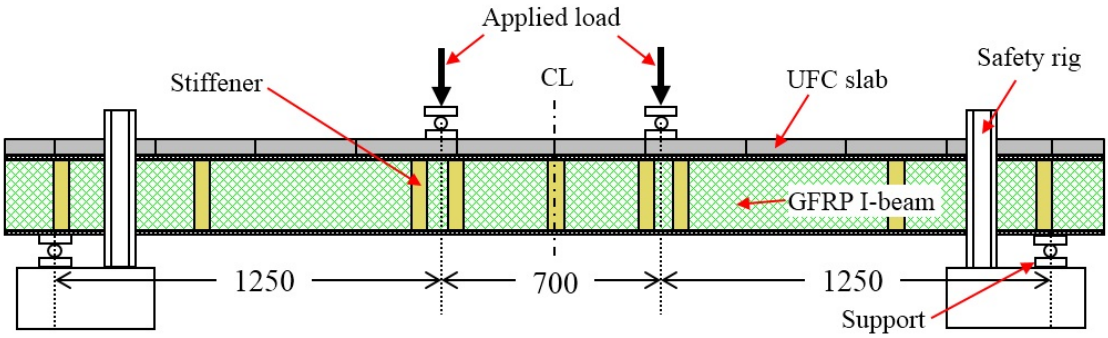

Fig. 2.8 Details of the experiment setup (Units: mm)

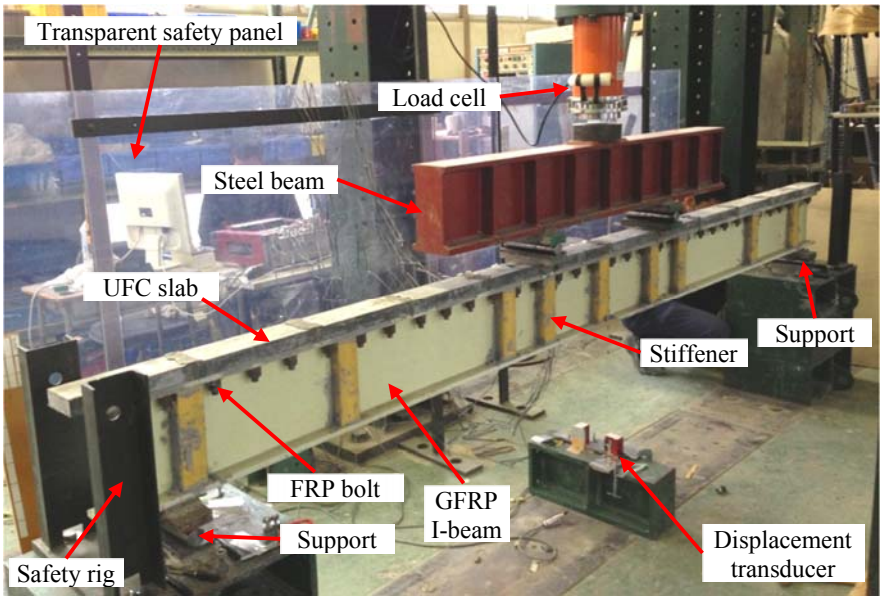

Fig. 2.9 Testing of the GFRP and UFC composite beam under four-point bending setup

As shown in Fig. 2.10a and b, fourteen strain gauges were attached along the midspan cross-section (C1 to C7) and along a cross-section (M1 to M7) in the shear span near to the loading point. The strain at the loading point was measured using two additional strain gauges attached

to the top surface of the UFC segments (Fig. 2.10c). In order to measure the midspan deformation, two deflection gauges were connected to the two sides of the bottom flange at midspan. During the beam test, the applied load, midspan deflection, and strain at midspan and near the loading point were measured until beam failure.

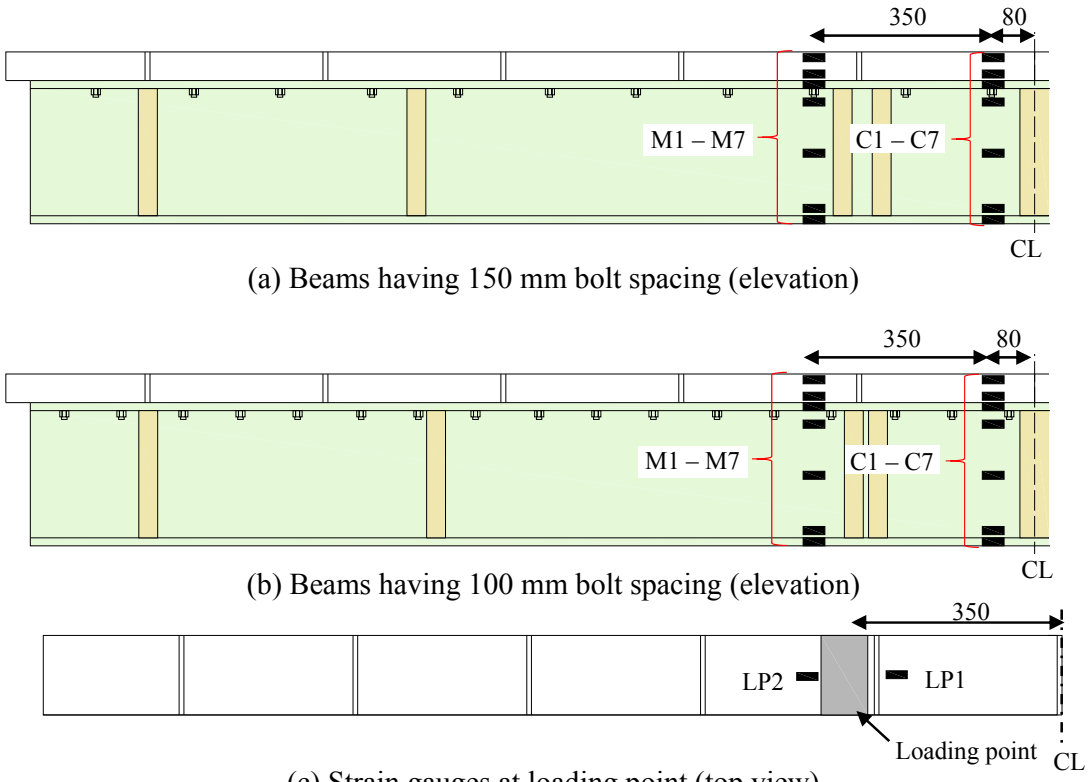

(a) Beams having 150 mm bolt spacing (elevation)

(b) Beams having 100 mm bolt spacing (elevation)

(c) Strain gauges at loading point (top view)

Fig. 2.10 Strain gauge locations in the GFRP and UFC composite beams (Units: mm)

2.4 Results and discussion

Fig. 2.11 shows the failure patterns of the GFRP and UFC composite beams. All the beams except G10-F16-B4 and G10-F10-BN6 were failed by crushing of the UFC segments followed by the crushing of the GFRP top flange and web. In G10-F16-B4 and G10-F10-BN6 beams, failure occurred by crushing of the UFC segments in the midspan. Results of the flexural beam test are summarized in Table 2.8. According to the test results, G10-F16-B4, G10-F10-BN6 and G10-F16-BN6 beams showed very high flexural capacity compared to that of G10-F16-BN4 and G5-F16-BN4 beams.

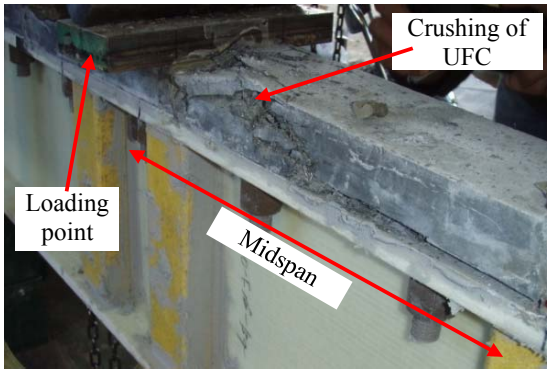

(a) G10-F16-B4 beam

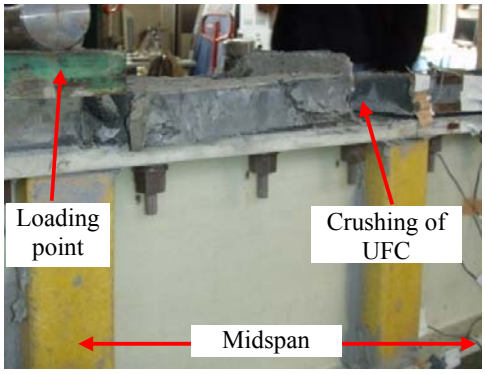

(b) G10-F10-BN6 beam

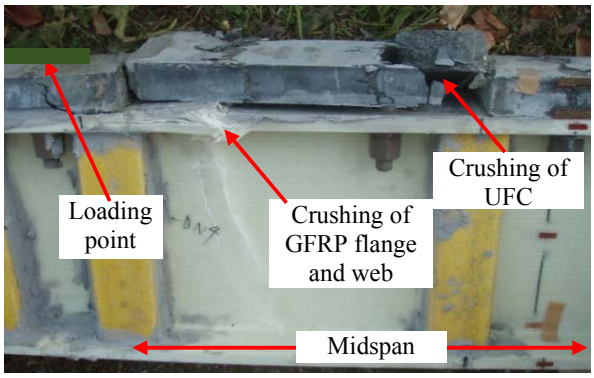

(c) G10-F16-BN4 beam

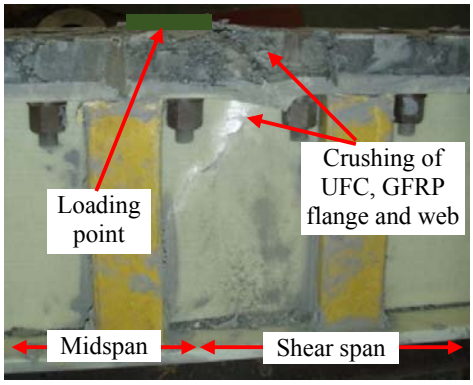

(d) G10-F16-BN6 beam

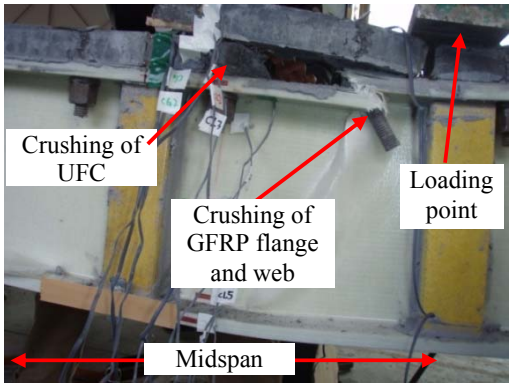

(e) G5-F16-BN4 beam

Fig. 2.11. Failure patterns of GFRP and UFC composite beams

Table 2.8 Flexural beam test results

Specimen name	Failure load (kN)	Midspan deflection at failure (mm)	Midspan tensile strain (μ)	Midspan compressive strain (μ)	Failure location
G10-F16-B4	199.8	64.1	11,400	3,007	FS
G10-F10-BN6	195.9	68.6	11,077	3,455	FS
G10-F16-BN4	154.9	54.6	9,227	Gauge damaged	FS
G10-F16-BN6	193.8	87.4	12,540	Gauge damaged	SS
G5-F16-BN4	163.8	60.4	10,079	Gauge damaged	FS

FS – Flexural span, SS – Shear span

2.4.1 Comparison of bolt type

Flexural behaviour of the GFRP and UFC composite beams consisting of either FRP bolts or the steel bolts was compared. The flexural behaviour of the GFRP and UFC composite beams having steel bolts can be found in literature [41]. Fig. 2.12 shows the load and deflection relationship of the composite beams having different bolt types. The mechanical properties of the steel bolts are given in Table 2.9 whereas those of the FRP bolts are given in Table 2.5. Beam G10-S16-BN4 had significantly high flexural capacity compared to beam G10-F16-BN4 (approximately 30% higher). The reason for this is the strength of the steel bolts are comparatively higher than that of the FRP bolts. Fig. 2.13 shows the broken FRP bolt-heads in beam G10-F16-BN4 at the beam failure, whereas in beam G10-S16-BN4, there were no damages in the steel bolts. In particular, beam G10-F16-B4 specimen containing FRP bolts without bolt-heads (only the threaded bar) showed similar flexural capacity to the composite beam having steel bolts (G10-S16-BN4). In beam G10-F16-BN4, because of the FRP bolt-head, the UFC cross-sectional area in the bending plane is smaller than that of beam G10-F16-B4. Therefore, the UFC segments with the FRP bolt-heads are weak compared to the UFC segments without bolt-heads. As a result, beam G10-F16-B4 signified high flexural capacity and stiffness compared to beam G10-F16-BN4. This concludes that the FRP bolts (without bolt-heads) can be utilized in the GFRP and UFC composite beams, instead of steel bolts.

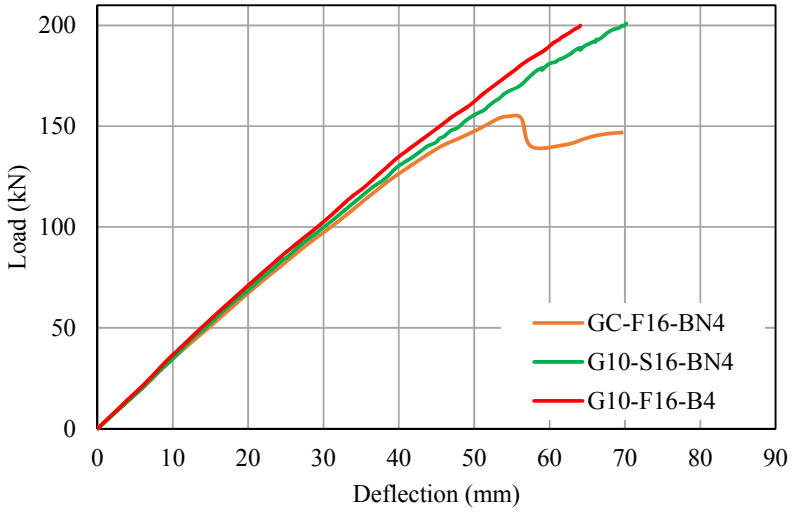

Fig. 2.12 Load and deflection relationship – different bolt types

Table 2.9 Mechanical properties of steel bolts

Property	Value
Shear strength (N/mm^2)	420
Tensile strength (N/mm^2)	700

Fig. 2.13 Broken FRP bolt-heads in G10-F16-BN4 beam

2.4.2 Comparison of UFC segment gap

Fig. 2.14 shows the load-deflection relationship of the GFRP and UFC composite beams having different segment gap (5 mm or 10 mm). The idea of keeping a gap between the UFC segments is to make easy the installation of the UFC segments. Both G5-F16-BN4 and G10-F16-BN4 beams have approximately same flexural capacities and stiffness. The difference between the flexural capacities of the two beams was approximately 4%. Therefore, the influence on the flexural behaviour of the GFRP and UFC composite beams caused by the gap (less than 10 mm) between the UFC segments is negligible.

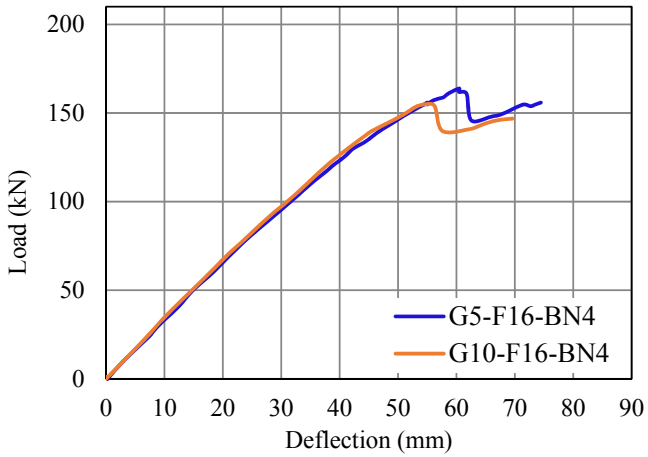

Fig. 2.14 Load and deflection relationship – different UFC segment gap

2.4.3 Comparison of bolt spacing

The influence of bolt spacing on the flexural behaviour of the GFRP and UFC composite beams was checked and the test results showed the beam with small bolt spacing has high flexural capacity (Fig. 2.15). The centre-to-centre bolt spacing of beam G10-F16-BN4 was 150 mm and that of beam G10-F16-BN6 was 100 mm. The difference between the flexural capacities of two beams was around 25%. High flexural capacity in beam G10-F16-BN6 was due to good bonding between the UFC slab and the I-beam flange. Beam G10-F16-BN4 showed slightly high stiffness than beam G10-F16-BN6 and this may be caused by the amount of FRP bolt content inside the UFC segments. In beam G10-F16-BN6, the high stiff UFC material was replaced by low stiff FRP bolt material compared to that of beam G10-F16-BN4.

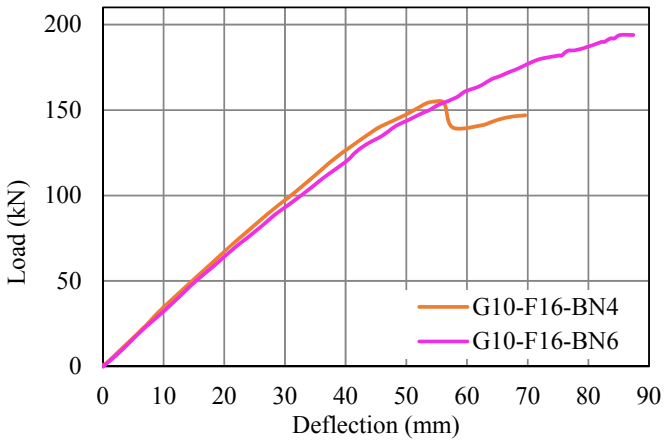

Fig. 2.15 Load and deflection relationship – different bolt spacing

2.4.4 Comparison of FRP bolt diameter

Beam G10-F10-BN6 and beam G10-F16-BN6 were tested to check the effect of bolt diameter on the flexural behaviour of composite beams. Fig. 2.16 shows the load and deflection behaviour of those beams. Both beams had almost same flexural capacities but in beam G10-F10-BN6, the stiffness is higher than beam G10-F16-BN6. The main reason for this was, in beam G10-F10-BN6, there was low amount of FRP material inside the UFC segments. The stiffness of the UFC segments increases when the volume of low strength (compared to UFC) FRP material is smaller in the UFC segments. This was observed in G10-F16-B4 and G10-F16-BN4 beams also (Fig. 2.12), where the beam G10-F16-B4 (no FRP bolt-heads) had high stiffness compared to beam G10-F16-BN4 (with FRP bolt-heads).

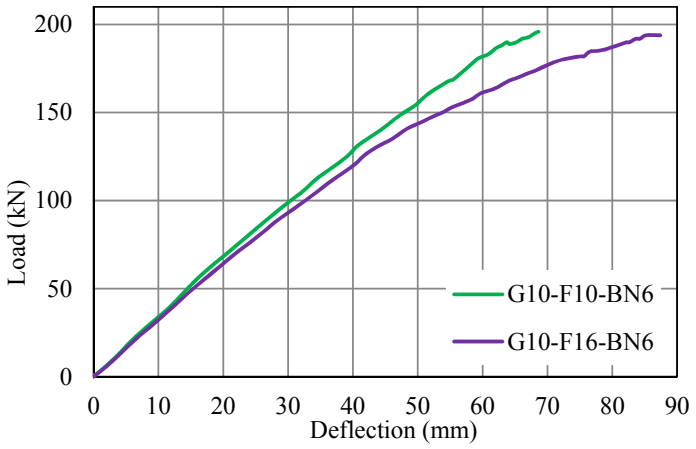

Fig. 2.16 Load and deflection relationship – different bolt diameters

2.4.5 Composite behaviour of test specimens

Strain distribution across the midspan cross-section is shown in Fig. 2.17. The values of seven strain gauges attached to the GFRP and UFC composite beams at the midspan (Fig. 2.10a and b) were used to obtain the graphs in Fig. 2.17. The 'section depth' was measured from the bottom of the GFRP and UFC composite beam. Due to crushing of the UFC, the strain gauges attached to the UFC segments were damaged in some of the composite beams at failure. Thus, the strain distribution of those beams at failure is not shown in Fig. 2.17c, d, and e. Except the beam G10-F10-BN6, all the other beams showed approximately linear strain distribution up to beam failure (Fig. 2.17). The sudden increase of the strain between G5 and G6 in beam G10-F10-BN6 was because of the slipping of the UFC segments (Fig. 2.17b).

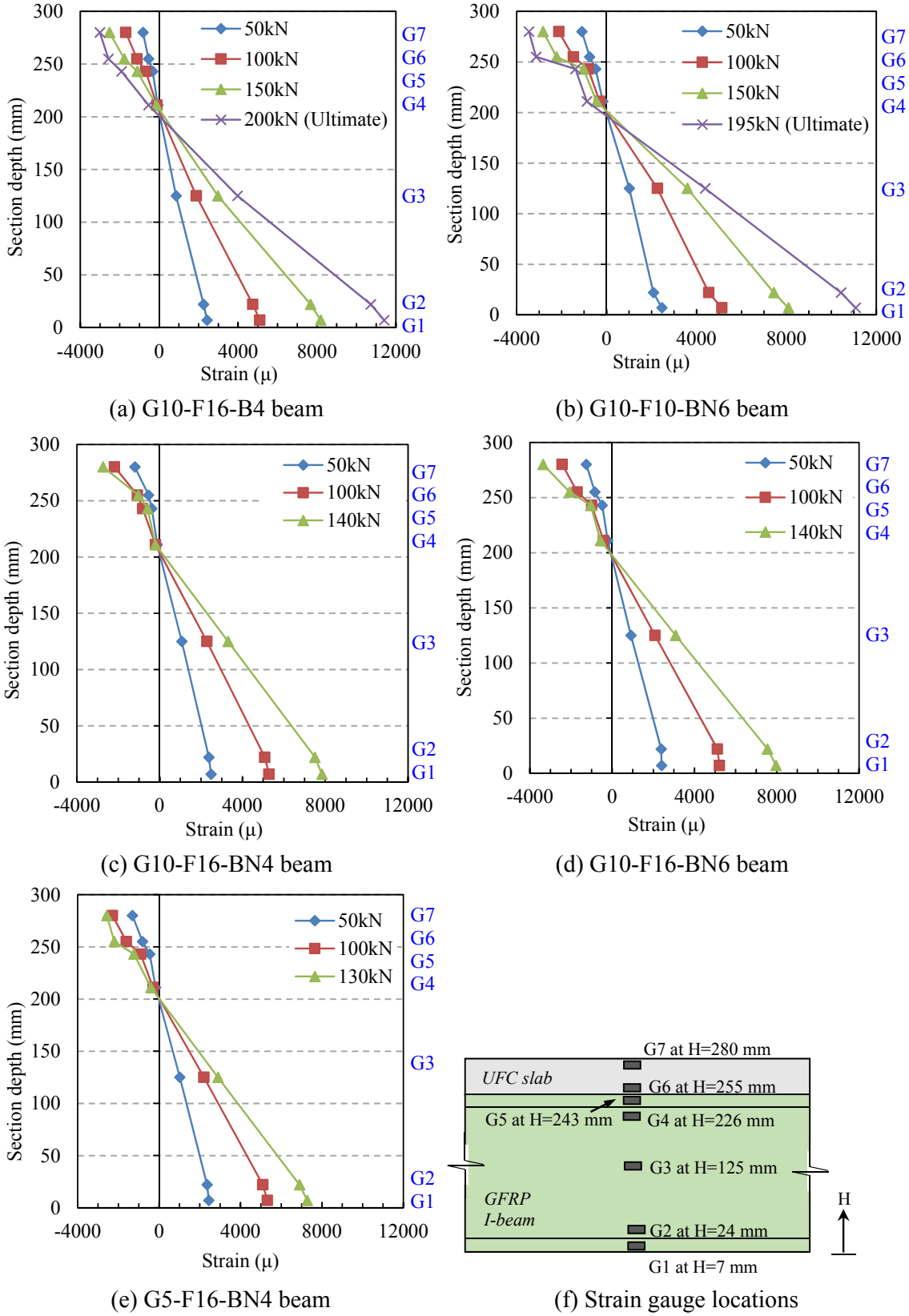

Fig. 2.17 Strain distribution across the midspan section of GFRP and UFC composite beam

As the UFC crushes at beam failure, the neutral axis of the composite beams slightly lowered.(Fig. 2.17a and b). The midspan strain distribution of the GFRP and UFC composite beams containing steel bolts is available in literature [18] and it was similar to that of FRP bolts. Therefore, the FRP bolts can be used in the GFRP and UFC composite beams and similar flexural performance compared to the steel bolts can be obtained.

2.5 Concluding remarks

This chapter describes the use of the FRP bolts in the GFRP and UFC composite beams as the shear connectors. Reason for using the FRP bolts was to enhance the durability of the GFRP and UFC composite beams, so that the maintenance and renovation costs of these beams can be reduced. The conclusions of the experiment are given below.

- The FRP bolts can be used instead of steel bolts in the GFRP and UFC composite beams and can have flexural capacity and stiffness similar to the GFRP and UFC composite beams with steel bolts. Because of the FRP bolts, the corrosion resistance of these composite beams will be increased and hence, they can be used for construction of short span pedestrian bridges in severe corrosive environments.
- The influence of the gap between the UFC segments on the flexural behaviour of the GFRP and UFC composite beams is very small where the gap is less than 10 mm. Provision of gaps between the UFC segments allows ease of fixing the UFC segments to the GFRP I-beams.
- The volume of the FRP material inside the UFC segment affects the stiffness of the composite beams. Therefore, the FRP bolts without bolt-heads are recommended to use as the shear connectors.

Chapter 3

Influence of Elevated Temperature on the Mechanical Properties of Materials Used in FRP and UFC Composite Beams

In Chapter 1, it was mentioned that the FRP materials containing a resin matrix (vinylester, epoxy, etc.) will lose their mechanical properties beyond the glass transition temperatures. Thus, the mechanical properties of the GFRP, HFRP, FRP bolts, and epoxy adhesive materials used for making the GFRP or HFRP (GFRP/HFRP) and UFC composite beam can also degrade at elevated temperature. This chapter describes the influence of elevated temperature on the physical and mechanical properties of the GFRP, HFRP, FRP bolts, and epoxy adhesive. Number of tests were conducted to check the influence of elevated temperature on the material properties and the test parameters are given in Table 3.1. The maximum temperature of the material tests was 90°C, which was determined based on the glass transition temperature of the materials.

3.1 Details of test specimens and methodology

The details of the GFRP I-beams are described in Section 2.2.1. The HFRP I-beams were manufactured by pultrusion process and their FRP layer composition is shown in Table 3.2. The fibre lay-up in the HFRP I-beam is illustrated in Fig. 3.1. In order to increase the flexural strength and the stiffness of the I-beam, the top and bottom flanges are made of CFRP and GFRP. Because the I-beam web undertakes comparatively lower stresses than the flanges, to reduce the manufacturing cost of the HFRP I-beam, its web is made of GFRP only (Fig. 3.1). All carbon fibres in the flanges are aligned in the longitudinal direction (oriented at 0°) while the glass fibres is oriented at 0°, 90°, and ±45° to provide integrity across the flange width and avoid strong anisotropic behaviour. The details of the FRP bolts and the epoxy adhesive are described in Section 2.2.3.

Table 3.1 Material tests and parameters

Test	Materials tested	Temperatures tested
Glass transition temperature	Vinylester resin (GFRP/HFRP)	-
	FRP bolt resin	-
	Epoxy adhesive	-
Coefficient of thermal expansion	GFRP I-beam (part)	Heated from 30°C to 85°C
	HFRP I-beam (part)	Heated from 30°C to 85°C
	UFC cuboid	Heated from 30°C to 85°C
Tensile strength	GFRP flange coupons	20°C, 50°C, 70°C, 90°C
	HFRP flange coupons	20°C, 50°C, 70°C, 90°C
	GFRP web coupons	20°C, 50°C, 70°C, 90°C
	FRP bolts	20°C, 50°C, 70°C, 90°C
Compressive strength	GFRP flange coupons	20°C, 60°C, 90°C
	HFRP flange coupons	20°C, 60°C, 90°C
	GFRP web coupons	20°C, 60°C, 90°C
	FRP bolts	20°C, 50°C, 70°C, 90°C
	UFC cylinders	30°C, 50°C, 70°C, 90°C
Shear strength	FRP bolts	20°C, 60°C, 90°C
	Epoxy adhesive	20°C, 60°C, 90°C

Table 3.2 Layer composition of HFRP I-beam

Parameters		HFRP I-beam			
		HFRP 0°	GFRP 0°/90°	GFRP ±45°	GFRP CSM
Volume fraction (%)		55	53	53	25
Volume content (%)	Flange	33	17	41	9
	Web	0	43	43	14

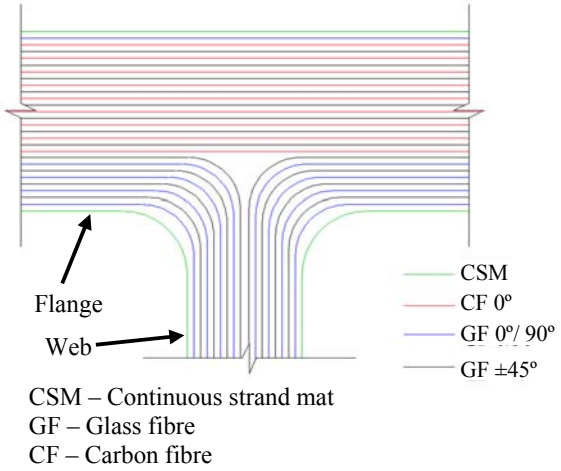

Fig. 3.1 Fibre layup in HFRP I-beam

3.1.1 Glass transition temperature test on GFRP, HFRP, FRP bolts and epoxy adhesive

The GFRP I-beams and the HFRP I-beams were consisted of vinylester resin. Therefore, the test for T_g of vinylester resin was conducted using the GFRP material. In addition to that, tests for the glass transition temperatures of the FRP bolts and the epoxy adhesive also carried out. Tests were conducted according to the differential scanning calorimetry (DSC) method described in the Japanese Industrial Standard K-7121 [42]. The specimens of the GFRP and the FRP bolts were prepared by chopping the materials whereas, the epoxy adhesive specimens were prepared by crushing of hardened (after curing for one week) adhesive. During the test, heat flow and temperature values of each material were measured separately using a differential scanning calorimeter. The T_g of the materials were determined from the graphs between the heat flow and temperature.

3.1.2 Coefficient of thermal expansion test on GFRP, HFRP and UFC

Thermal expansion rates of the HFRP I-beam flange, GFRP I-beam flange and web, and UFC material were measured in the longitudinal direction by slow heating tests. The temperature of the specimens was gradually increased from 30°C to 85°C over a period of 20.5 hours. Heating of the specimens was done inside an oven. The specimens used for measuring the coefficient of thermal expansion of the GFRP and the HFRP were obtained by cutting a 100 mm long section from a complete GFRP I-beam and an HFRP I-beam, respectively. As illustrated in Fig. 3.2a, five strain gauges were attached to both the GFRP and HFRP specimen at the mid-section

(one each at the top and bottom flanges and three in the web). A 20 × 20 × 100 mm cuboid specimen was used to obtain the coefficient of thermal expansion of the UFC in the longitudinal direction. As shown in Fig. 3.2b, expansion at the centre of the UFC specimen was measured using a strain gauge attached in the longitudinal direction.

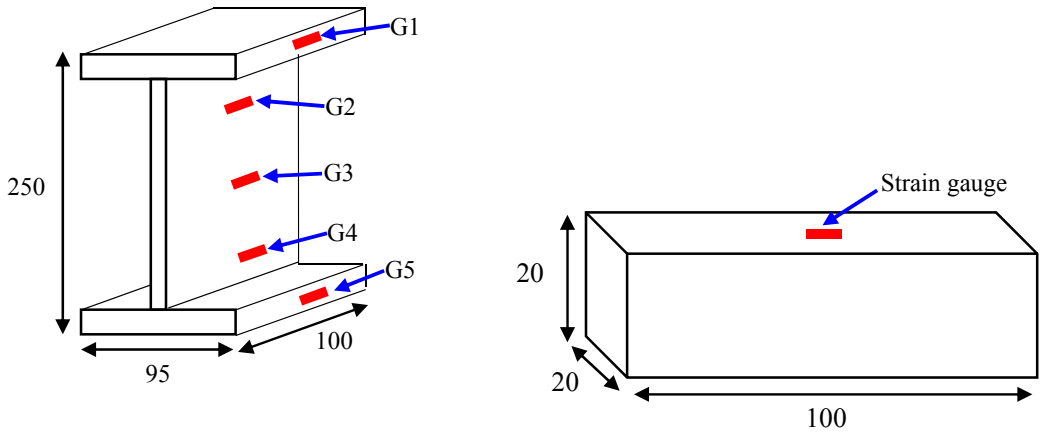

(a) GFRP/HFRP I-beam (b) UFC cuboid

Fig. 3.2 Strain gauge locations in coefficient of thermal expansion test specimens (Units: mm)

3.1.3 Tensile and compression tests on GFRP and HFRP coupons

In order to examine the influence of elevated temperature on the mechanical properties of the GFRP flange, GFRP web, and HFRP flange, tensile and compression coupon tests were carried out. The GFRP flange, HFRP flange, and GFRP web coupons were cut from the I-beam flange and web in the longitudinal direction. This is because, the longitudinal mechanical properties of GFRP and HFRP have major influence on the flexural behaviour of the GFRP/HFRP and UFC composite beams. Fig. 3.3 shows the cutting details of the flange and web coupons from a GFRP/HFRP I-beam.

The length of the GFRP flange, GFRP web, and the HFRP flange coupons was 800 mm. The two ends of each coupon were inserted into 34 mm diameter (outside) steel pipes and the space between coupon and pipe was filled with epoxy resin adhesive (Sho-bond™ Grout-W). The inside of the pipes was grooved to create a firm bond between the epoxy resin adhesive and the steel pipe, ensuring that slippage of the coupons through the pipe during tensile testing was avoided. All the specimens were cured for one week until the epoxy resin adhesive is fully hardened. Three specimens were tested at each temperature. In both tensile and compression

tests, the cross-sectional dimensions of the GFRP and HFRP flange coupons were 14 × 10 mm and the GFRP web coupons were 10 × 9 mm. Prior to application of loading in the tensile and compression coupon tests, the specimens were gradually heated up to the test temperature using an electric heater and held at that temperature for 90 minutes. All the specimens were wrapped with a heat insulating material in order to reduce heat loss and to ensure that the specimen remained at the test temperature. Specimen temperatures were monitored using a thermocouple fixed near the longitudinal strain gauge (Fig. 3.4 and Fig. 3.5) and an electric temperature controller was used to control temperature. Temperature deviations in the case of both tensile and compression specimens were within ± 3°C of the test temperature.

The tensile tests were carried out at 20°C, 50°C, 70°C, and 90°C and Fig. 3.4 shows the details of tensile test specimens. The effective length (l_e) of each GFRP or HFRP tensile test specimen was 200 mm and six strain gauges were attached to the specimen. The experimental setup of tensile testing is given in Fig. 3.6.

The compression tests were carried out at 20°C, 60°C, and 90°C and Fig. 3.5 shows the details of the compression test specimens. Their effective length (l_e) and the length of the steel pipe (l_s) were 45 mm and 50 mm, respectively.

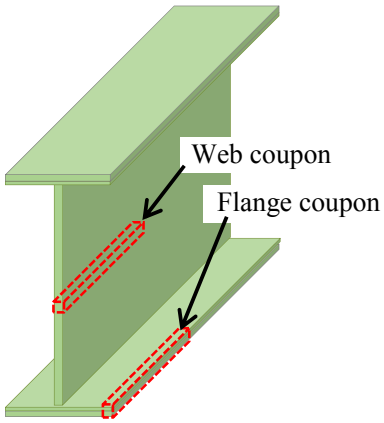

Fig. 3.3 Cutting details of flange and web coupons from a GFRP/HFRP I-beam

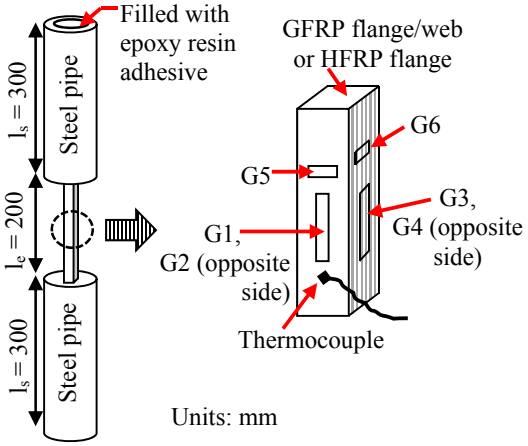

Fig. 3.4 Details of tensile test specimen

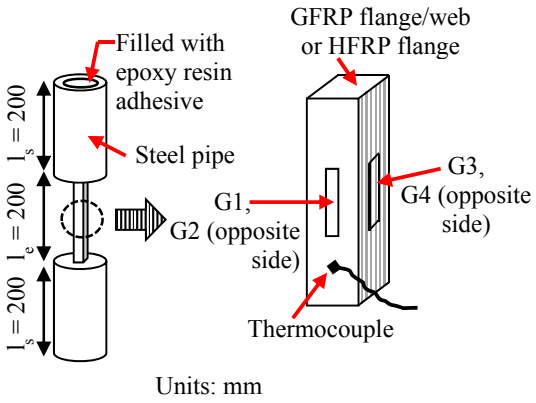

Fig. 3.5 Details of compression test specimen

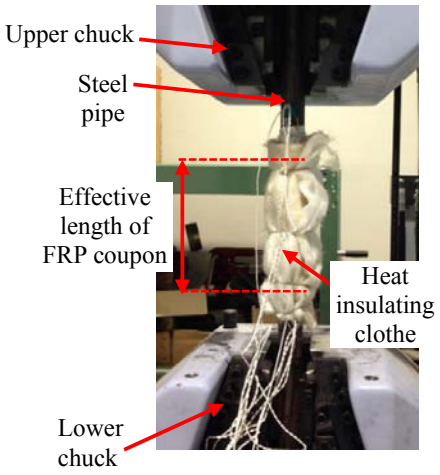

Fig. 3.6 Experimental setup for tensile testing

3.1.4 Compression test on UFC

The UFC segments used in this study were 300 mm in length, 95 mm in width, and 35 mm in height. The manufacturing process and other details of the ultra-high strength fibre reinforced concrete can be found in Section 2.2.2. Compression tests were conducted on standard cylinders (50 × 100 mm) cast during the manufacturing of the UFC segments. Test specimen details are shown in Fig. 3.7. The compression tests were carried out at 30°C, 50°C, 70°C, and 90°C. The heating method was similar to that used in the GFRP and HFRP coupon tests, in which the UFC specimens were gradually heated up to the required temperature and held there for 90 minutes prior to loading.

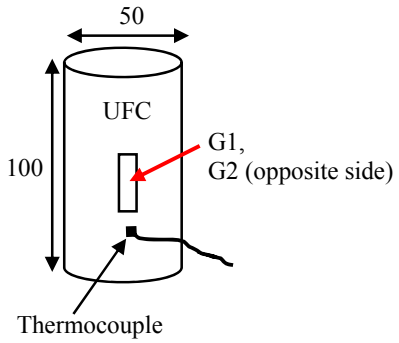

Fig. 3.7 Details of UFC compression test specimen (Units: mm)

3.1.5 Tensile, compression and shear tests on FRP bolts

In the GFRP/HFRP and UFC composite beams, 16 mm diameter FRP bolts (without bolt-head) were used to connect the UFC segments to the GFRP I-beam flange. The FRP bolts contain glass fibres and these bolts can improve the corrosion resistance of the GFRP/HFRP and UFC composite beams. Chapter 2 describes the reason for choosing 16 mm diameter FRP threaded bars for the GFRP and UFC composite beams. As illustrated in Fig. 3.8 and Fig. 3.9, the ends of FRP bolt tensile and compression test specimens were embedded into steel pipes using similar preparation method as used for the coupon tensile and compression test specimens. Fig. 3.8 and Fig. 3.9 show the details of the FRP bolt tensile and compression test specimens, respectively. The threaded part at the mid-area of the FRP bolts was removed and smoothened in order to form a flat surface to attach strain gauges. Special precautions were taken to avoid damaging the glass fibres in the core of the FRP bolt while removing the threaded part. In FRP bolt tensile test specimens, three strain gauges were attached (Fig. 3.8) whereas in FRP bolt compression specimens, only G1 strain gauge was attached (Fig. 3.9). The effective length (l_e) and steel pipe length (l_s) in the FRP bolt tensile test specimen were 200 mm, whereas in the compression test specimens, these lengths were 40 mm and 50 mm, respectively. The heating and heat controlling methods were similar to those used in the GFRP/HFRP coupon tensile and compression tests. The FRP bolt tensile and compression tests were carried out at temperatures of 20°C, 50°C, 70°C, and 90°C.

The FRP bolts provide the main shear connection between the GFRP/HFRP I-beam flange and the UFC segments. Shear strength of the FRP bolts was determined by lap-shear tests conducted at 20°C, 60°C, and 90°C. Fig. 3.10 shows the details of the FRP bolt lap-shear test specimen. The lap-shear test specimens were made using three steel plates of 5 mm in thickness, which were fabricated with 18 mm diameter holes. The steel plates were fastened together using a pair

of 80 mm long FRP bolts. Two thermocouples were attached to the specimen, one inside the steel plate (near the shear failure plane) and the other one outside (on the FRP nut). Before applying the load, the specimen was gradually heated inside a heat insulated steel box until the test temperature was achieved and held constant under that temperature for 90 minutes. The test setup is illustrated in Fig. 3.11.

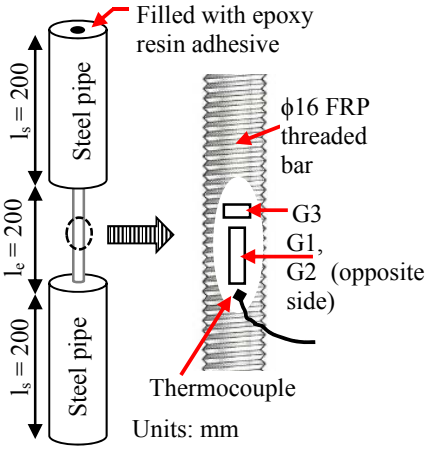

Fig. 3.8 Details of FRP bolt tensile test specimen

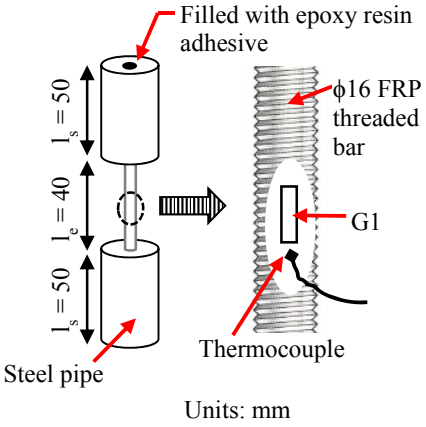

Fig. 3.9 Details of FRP bolt compression test specimen

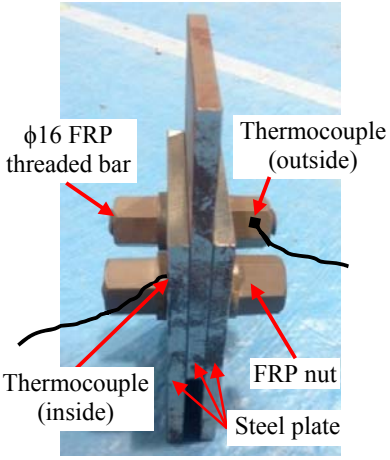

Fig. 3.10 Details of FRP bolt lap-shear test specimen

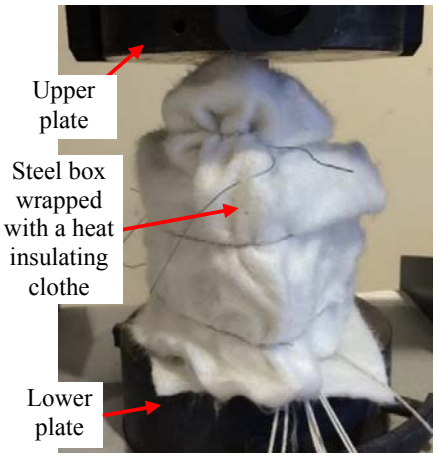

Fig. 3.11 Test setup of FRP bolt/epoxy adhesive lap-shear test

3.1.6 Shear test on epoxy adhesive

The epoxy adhesive provides a good bonding between the UFC segments and the GFRP/HFRP I-beam flange. The lap-shear tests were conducted on the epoxy adhesive at 20°C, 60°C, and

90°C and the cross-sectional details of the epoxy adhesive shear test specimen are given in Fig. 3.12. In order to replicate the actual epoxy bonding conditions, specimens were made by cutting the GFRP plates and the UFC parts from an actual GFRP I-beam flange and from UFC segments, respectively. The UFC parts were attached to each side of the GFRP plate using the epoxy adhesive. The bottom of the specimen was given a level base using the cement mortar (Fig. 3.12). All the specimens were cured for 7 days until the epoxy adhesive become fully hardened. The effective shear area of the test specimen was 10,000 mm^2 (100 × 50 mm × 2 sides). Prior to the shear test, the specimens were heated up to the required temperature inside a heat insulated steel box using the same method as in the FRP bolt shear test (Fig. 3.11). The temperature of the UFC parts and the GFRP plate was measured using three thermocouples (Fig. 3.12).

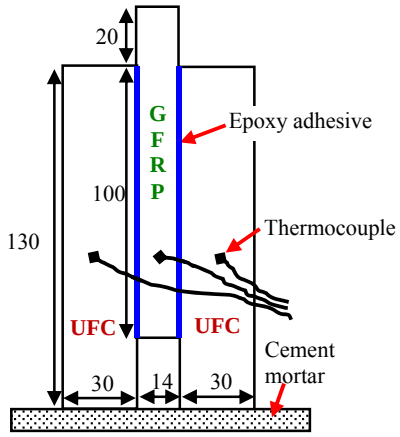

Fig. 3.12 Cross-sectional details of epoxy adhesive lap-shear test specimen (Units: mm)

3.2 Material test results and discussion

3.2.1 Results of glass transition temperature tests

The measured glass transition temperatures of vinylester resin used in the GFRP and HFRP, the resin inside the FRP bolts, and the epoxy adhesive are given in Table 3.3. The glass transition temperature in the vinylester resin, FRP bolt resin, and epoxy adhesive was in between 50°C and 60°C. Therefore, deterioration of mechanical properties of these materials can be anticipated beyond 60°C. Based on the glass transition temperature values of materials and the maximum surface temperature on actual FRP bridges, 20°C to 90°C was selected as the temperature range for the other material tests.

Table 3.3 Glass transition temperatures of materials

	GFRP/HFRP (vinylester resin)	Resin of FRP bolt	Epoxy adhesive
Glass transition temperature (T_g) (°C)	58	53	56

3.2.2 Results of coefficient of thermal expansion tests

The longitudinal coefficients of thermal expansion (α) of the GFRP flange, HFRP flange, GFRP web, and UFC were obtained from a slow heating tests and are given in Table 3.4. The coefficient of thermal expansion of the GFRP flange, HFRP flange, GFRP web, and UFC were constant with temperature. The α of the GFRP flange, HFRP flange, and UFC are not significantly different to each other. So that, the bi-material bending effect (the bending occurred in composite beams at elevated temperature due to the mismatch of the α values in the constituent materials) resulted by the temperature variations would be very small in the GFRP/HFRP and UFC composite beams. Details of α values of concrete, GFRP, and CFRP are available in literature. The coefficients of thermal expansion of an FRP composite depends upon both the fibre type used and fibre layup in the matrix [43]. The α of GFRP is similar to that of concrete. The axial coefficients of thermal expansion of ordinary concrete, GFRP, and CFRP bars are 10×10^{-6}/°C, 9 to 10×10^{-6}/°C, and 0.6 to 1.0×10^{-6}/°C, respectively [44]. The HFRP used in this study contains both GFRP and CFRP and hence, the coefficient of thermal expansion should be in between those of GFRP and CFRP. This was confirmed by the experiment results and the α of HFRP was lower than that of the GFRP (Table 3.4).

Table 3.4 Coefficients of thermal expansion of materials

	GFRP flange	GFRP web	HFRP flange	UFC
Coefficient of thermal expansion (α) ($x10^{-6}$ °C^{-1})	9.6	13.7	4.1	11.6

3.2.3 Results of tensile tests

Fig. 3.13 shows the relationship between temperature and tensile strength of the GFRP flange, HFRP flange, GFRP web, and FRP bolts. The tensile strength of the GFRP flange and the GFRP web coupons fell significantly (more than 20%) at temperatures beyond 70°C and 50°C,

respectively. The degradation in tensile strength of the GFRP may be resulted by the glass transition of the vinylester resin. However, both flange and web coupons lost their tensile strength significantly when the temperature increases from 20°C to 50°C due to softening of the vinylester resin.

In contrast to the GFRP flange and GFRP web coupons, the tensile strength of the HFRP flange coupons retained beyond the glass transition temperature of the vinylester resin. Between 50°C and 90°C, the tensile strength of the HFRP coupons reduced only by 6.7%. In general, the tensile strength of the HFRP is not significantly influenced by temperatures less than 90°C and this can be explained by the orientation of the glass fibres. The HFRP consists of high amount of carbon fibres oriented at 0° to the longitudinal direction, whereas the GFRP flange and GFRP web contain less number of glass fibre layers oriented at 0° direction. Therefore, the tensile strength is not significantly affected in the FRP materials having a large number of fibres oriented in the longitudinal direction. In addition to 0° oriented fibres, to enhance the isotropic properties in the GFRP and HFRP, there are glass fibre layers oriented at 90°, ±45° and randomly oriented continuous strand mat (CSM) in these FRP types. Fibre lay-up in the GFRP I-beam and the HFRP I-beam is illustrated in Fig. 2.1 and Fig. 3.1, respectively.

Similar to HFRP coupons, the FRP bolts also did not exhibit a significant reduction in tensile strength with temperature (Fig. 3.13). The reason for this is, in the FRP bolts all glass fibres are oriented at 0° to the longitudinal direction.

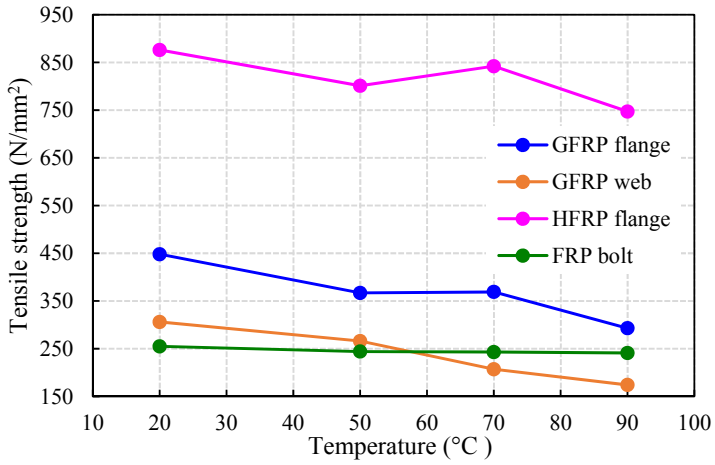

Fig. 3.13 Tensile strength of GFRP flange, HFRP flange, GFRP web, and FRP bolt

Regardless of temperature, brittle tensile failure was observed in the GFRP flange, GFRP web, and HFRP flange tensile test specimens (Fig. 3.14a and b). On the other hand, there were two failure patterns observed in the FRP bolt specimens (Fig. 3.14c), 1) slippage of FRP part within the bolt and 2) brittle failure. Figures of failure patterns of all tensile test specimens are given in Appendix 1.

The relationships between temperature and Young's modulus of the GFRP flange, HFRP flange, and the GFRP web are shown in Fig. 3.15. In all FRP types, Young's modulus declines as temperature increases. However, at temperatures beyond 50°C, this declination became steeper due to the deterioration of the vinylester resin in the GFRP and HFRP coupons by glass transition. The relationship of the Young's modulus of the UFC with temperature will be discussed in the next section.

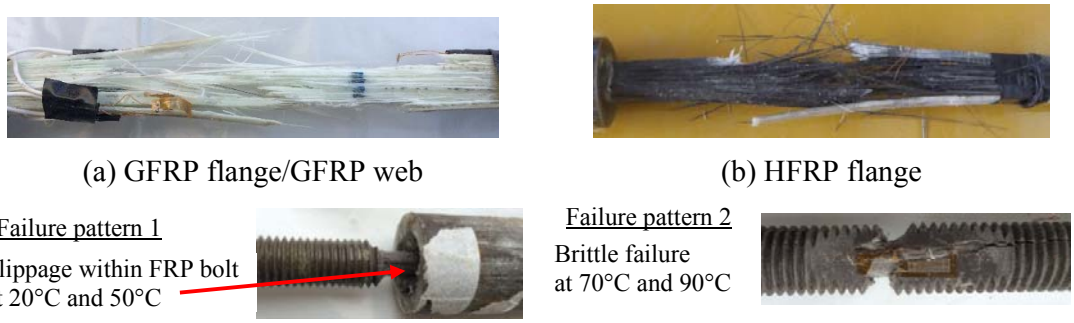

Fig. 3.14 Failure patterns of tensile test specimens

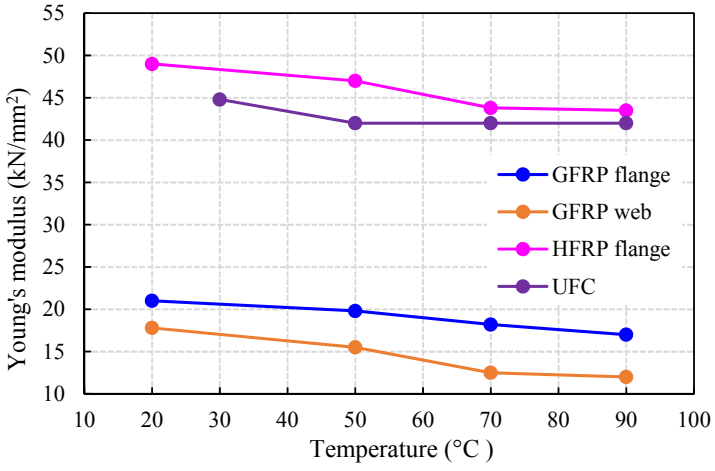

Fig. 3.15 Young's modulus of GFRP flange, HFRP flange, GFRP web, and UFC

3.2.4 Results of compression tests

Relationships of the compressive strengths of the GFRP flange, HFRP flange, GFRP web, FRP bolts, and UFC with temperature are shown in Fig. 3.16. The GFRP flange, HFRP flange, GFRP web, and FRP bolts lose their compressive strength as the temperature increases. The compressive strength of the GFRP flange was fallen rapidly beyond 60°C, while in FRP bolts, the compressive strength was suddenly reduced at temperatures above 50°C. However, the compressive strength of the HFRP flange and GFRP web coupons reduced continuously from 20°C to 90°C (Fig. 3.16). It was found that the T_g of the GFRP, HFRP, and FRP bolt materials is between 50°C and 60°C. Therefore, the main reason for the deterioration of the compressive strength of those materials beyond 50°C can be the glass transition of their resin matrix.

According to the compressive test results, the UFC material was characterized by high compressive strength at all temperatures. The UFC contains no material that are affected by the glass transition and hence its compressive strength remains constant with temperature (Fig. 3.16). Furthermore, the Young's modulus of UFC also does not depend on temperature (Fig. 3.15).

The failure patterns of the GFRP flange, HFRP flange, and GFRP web compression test specimens were almost the same, shown in Fig. 3.17a and b. At failure, crushing and delamination were observed in the GFRP and HFRP specimens at 20°C and 60°C, but the specimens at 90°C failed by kinking and crushing. The kinking of the GFRP and HFRP laminates in the coupons at 90°C is a sign of softening of the vinylester resin due to the glass transition. The FRP bolts failed by crushing at all temperatures and the typical failure pattern is shown in Fig. 3.17c. Images of failure patterns of compressive test specimens at all temperatures are given in Appendix 1.

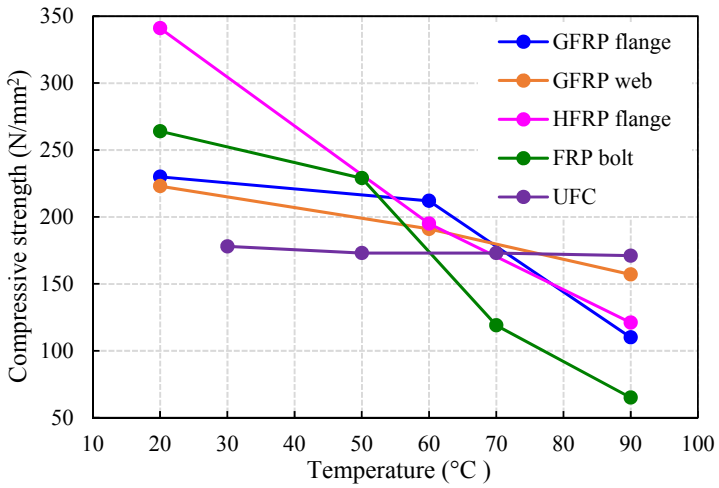

Fig. 3.16 Compressive strength of GFRP flange, HFRP flange, GFRP web, FRP bolt, and UFC

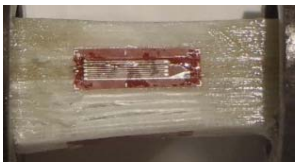

Delamination and crushing at 20°C and 60°C

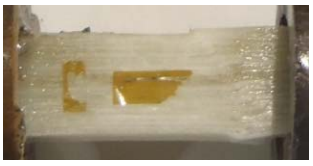

Kinking and crushing at 90°C

(a) GFRP Flange/GFRP web

Delamination and crushing at 20°C and 60°C

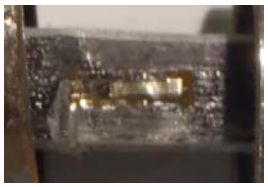

Kinking and crushing at 90°C

(b) HFRP Flange

Bolt crushing at all temperatures

(c) FRP bolt

Fig. 3.17 Failure patterns of GFRP coupons, HFRP coupons, and FRP bolt compression test specimens

3.2.5 Results of shear tests

As shown in Fig. 3.18, the shear capacity of both FRP bolts and epoxy adhesive deteriorates significantly at elevated temperature. The sudden fall in the shear capacity of the FRP bolts after 60°C may be caused by the glass transition of the bolt resin at 53°C. The effect of temperature on the shear strength of the epoxy adhesive is very severe. The shear capacity of epoxy adhesive dropped by approximately 82% between 20°C and 90°C. Fig. 3.19 shows the typical failure patterns of the FRP bolt and epoxy adhesive lap-shear test specimens. Failure patterns of all the FRP bolt and epoxy adhesive shear test specimens are given in Appendix 1.

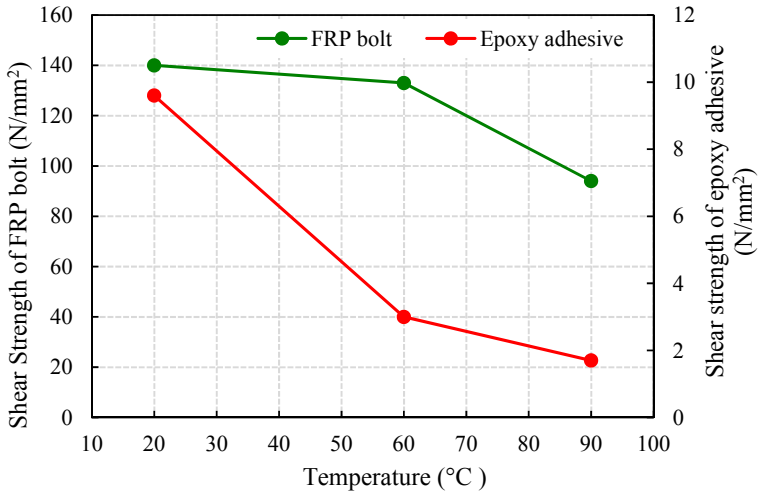

Fig. 3.18 Shear strength of FRP bolt and epoxy adhesive

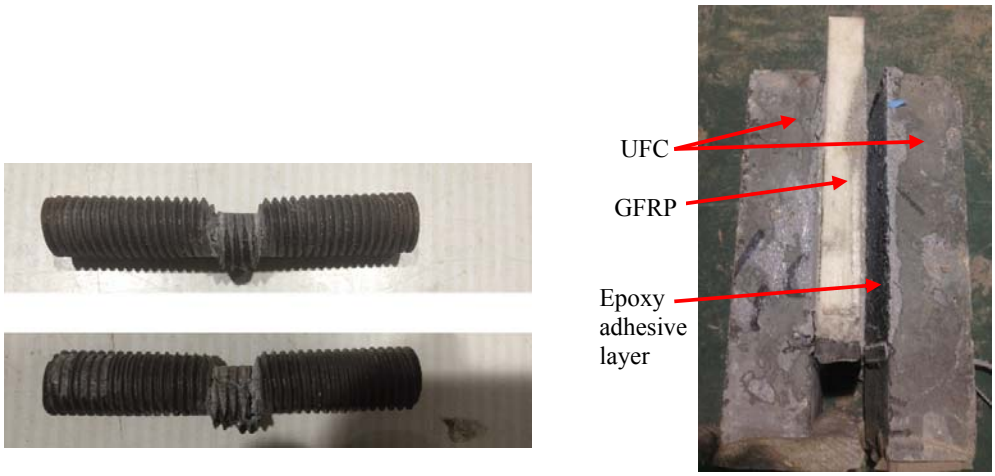

(a) FRP bolts (b) Epoxy adhesive

Fig. 3.19 Typical failure patterns of lap-shear test specimens

3.3 Concluding remarks

This chapter demonstrates the temperature dependence of material properties of the GFRP flange, GFRP web, HFRP flange, FRP bolts, UFC, and epoxy adhesive. Number of tests were carried out within the temperatures 20°C and 90°C. The main conclusions of the study are as follows.

- The glass transition temperatures of the materials used in the GFRP/HFRP and UFC composite beams are in between 50°C and 60°C. Therefore, the flexural capacity and the stiffness of the GFRP/HFRP and UFC composite beams can be significantly reduced at temperatures beyond 60°C.
- The coefficients of thermal expansion (in the longitudinal direction of the composite beam) of GFRP flange, HFRP flange, GFRP web, and UFC are constant at all temperatures between 20°C and 85°C. There is no significant influence on the longitudinal thermal expansion rates of these materials by their glass transition temperatures.
- Tensile strength of the GFRP flange and GFRP web is greatly affected by the glass transition of the vinylester resin whereas in the HFRP flange and in the FRP bolts, the tensile strength is not significantly affected by glass transition of polymer resin matrix.
- In contrast to the tensile strength, the compressive strength of the GFRP flange, GFRP web, HFRP flange, and the FRP bolts is significantly affected by the glass transition of their polymer resin matrices. The UFC doesn't contain temperature dependent materials and hence, its compressive strength remained almost constant with the temperature.
- Shear strength of the FRP bolts is rapidly reduced at the temperatures beyond 60°C, caused by the glass transition of the resin inside the FRP bolts. On the other hand, the shear capacity of the epoxy adhesive significantly reduced with temperature regardless its glass transition temperature.

Chapter 4

Flexural Behaviour of FRP I-beams and FRP-UFC Composite Beams Subjected to Elevated Temperature

4.1 Introduction

In Chapter 3 the influence of the elevated temperature on some of the material properties of the GFRP, HFRP, UFC, FRP bolt, and epoxy adhesive were investigated. According to that, the glass transition temperature of materials is in between 50°C and 60°C. And also the American concrete institute (ACI) states that the T_g of some commercially available FRP systems typically varies from 60°C to 82°C [27]. It has been found that some mechanical properties of the composite materials containing resin components (epoxy, vinylester, etc.) deteriorate beyond T_g [28]. Dai et.al and Sirimanna et.al conducted exposure tests of outdoor FRP structures [36, 37]. They found that the maximum surface temperature of those FRP structures can reach 60°C during extreme climate conditions or when they are located in hot industrial environments. Therefore, the flexural behaviour of the GFRP/HFRP and UFC composite beams can be influenced by elevated temperature if they are constructed in such heated environments. In this study, large-scale flexural beam tests were carried out on FRP composite beams at elevated temperature and the flexural behaviour of those beams is demonstrated.

4.2 Test variables and methodology

Three FRP beam types were used in this study, 1) GFRP I-beams, 2) GFRP and UFC composite beams, and 3) HFRP and UFC composite beams. The GFRP I-shaped beam specimens were manufactured by the pultrusion process using glass fibres and vinylester resin. In the HFRP I-beams, flange consisted of both GFRP and CFRP and the web consisted of GFRP only. The overall length, width, and height of the GFRP/HFRP I-beams are 3,500 mm, 95 mm, and 250 mm, respectively. In both beam types, the flange thickness is 14 mm and that of the web is 9 mm. Cross-sectional dimensions of the GFRP I-beams are shown in Fig. 4.1a and those were identical for the HFRP I-beams also.

The cross-sectional details of the GFRP-UFC (GFRP and UFC) composite beams and the HFRP-UFC (HFRP and UFC) composite beams are shown in Fig. 4.1b and c, respectively. The GFRP/HFRP and UFC composite beams were fabricated by fixing UFC segments to the GFRP/HFRP I-beam top flange using 16 mm diameter FRP bolts and epoxy adhesive. The

centre-to-centre spacing of the FRP bolts along the GFRP/HFRP and UFC beams is 150 mm and the bolts were tightened to a torque of 20 Nm. Elevation details of the GFRP/HFRP and UFC composite beams are given in Fig. 4.2. All the beams were fitted with nine GFRP stiffeners on each side of the web using epoxy adhesive to prevent web buckling (Fig. 4.2). The nominal dimension of these stiffeners are 30 × 60 × 220 mm and their thickness is 4 mm. The spacing between the stiffeners is illustrated in Fig. 2.7. In GFRP/HFRP and UFC composite beams a 10 mm spacing was kept between two consecutive UFC segments. Providing these gaps make easy the installation of the UFC segments and those gaps were filled with cement mortar. The material mix proportions of the filling mortar is given in Table 2.7. The compressive strength and the Young's modulus of the filling cement mortar paste were 90.3 N/mm^2 and 31 kN/mm^2, respectively. The cement mortar filling of all the specimens were wet cured for 7 days before the bending test.

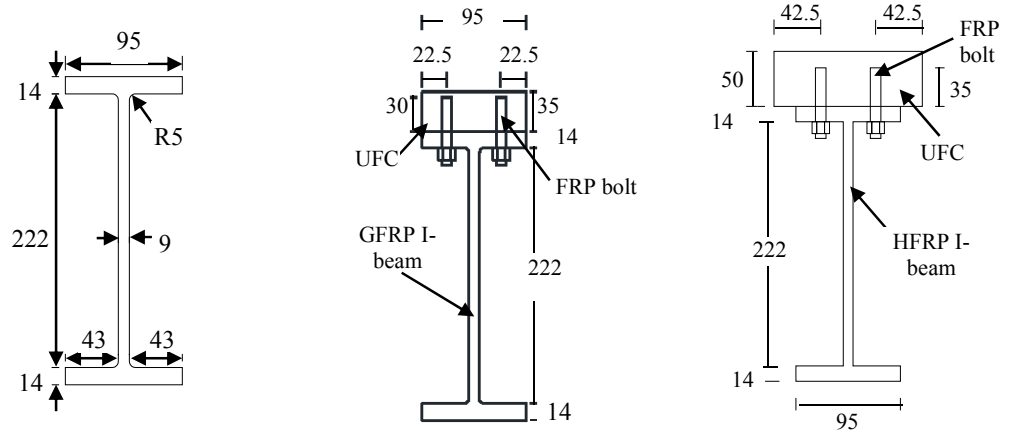

(a) GFRP I-beam (b) GFRP and UFC composite beam (c) HFRP and UFC composite beam

Fig. 4.1 Cross-sectional details of beams (Units: mm)

In total, eight beams (two GFRP I-beams, three GFRP-UFC composite beams, and three HFRP-UFC composite beams) were tested. The experimental variables of the bending test are given in Table 4.1. All the beams were tested under four-point bending test and a schematic diagram of the four-point bending test setup is shown in Fig. 4.2. The flexural and shear spans of the beams were 700 mm and 1,250 mm, respectively. The reason for testing the GFRP I-beams was to compare the flexural behaviour of the GFRP I-beams and the GFRP and UFC composite beams at elevated temperature. Therefore, the impact of the UFC segments on the flexural

behaviour of the GFRP and UFC composite beams subjected to elevated temperature can be determined.

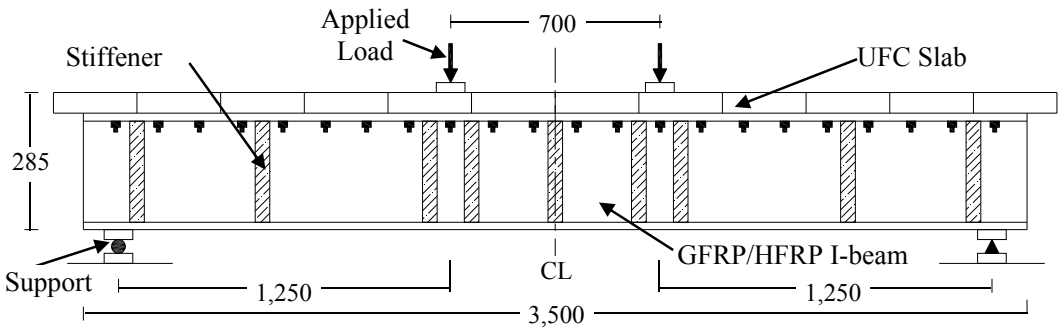

Fig. 4.2 Elevation of the GFRP/HFRP and UFC composite beams (Units: mm)

Table 4.1 Experiment variables

Specimen name	Beam type	Test temperature (°C)	Presence of UFC segments
G-60	GFRP I-beam	60	No
G-90	GFRP I-beam	90	No
GC-20	GFRP-UFC beam	20	Yes
GC-60	GFRP-UFC beam	60	Yes
GC-90	GFRP-UFC beam	90	Yes
HC-20	HFRP-UFC beam	20	Yes
HC-60	HFRP-UFC beam	60	Yes
HC-90	HFRP-UFC beam	90	Yes

Before applying the load, the beams except GC-20 and HC-20 were gradually heated up to the required temperature and held there for 60 minutes. GC-20 and HC-20 were tested under room temperature conditions. The beams were heated inside a heat insulated steel box fitted with ten electric heaters. The electric heaters were fixed at the outside of the steel box. The locations of the heater are shown in Fig. 4.3.

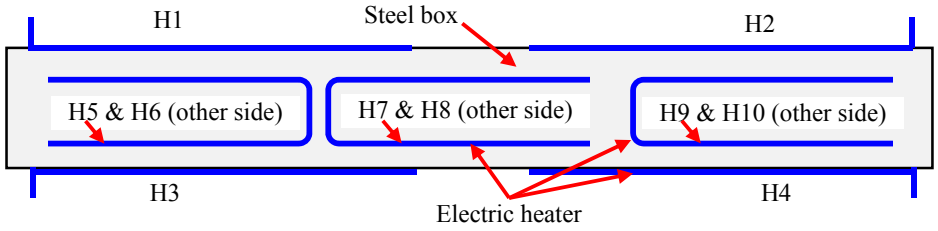

Fig. 4.3 Electric heater locations in the steel box

The temperature at the flexural and shear spans of the beams was measured using the thermocouples attached to the UFC (in GC-60, GC-90, HC-60, and HC-90 only), the GFRP/HFRP top flange, the GFRP web, and GFRP/HFRP bottom flange. In order to monitor the temperature throughout the beam, thermocouples were attached to the beams at both shear spans and the flexural span (Fig. 4.4). Heating of a beam prior to a bending test is illustrated in Fig. 4.5. The load was applied using a manually operated hydraulic jack and the load was transferred to the loading points equally by a levelled steel beam (Fig. 4.5). Changes in strain at the midspan of the GFRP/HFRP and UFC composite beams were measured using seven high temperature strain gauges (G1 to G7 in Fig. 4.4), while in the case of GFRP I-beams there were only five strain gauges (G3 to G7). Maximum midspan deflection was recorded throughout the experiment using two displacement transducers, one fixed to each side of the bottom flange (Fig. 4.5).

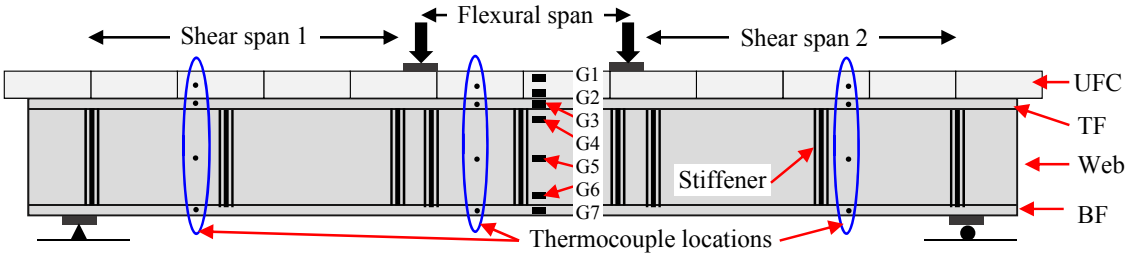

Fig. 4.4 Thermocouple and strain gauge locations in the GFRP/HFRP and UFC composite beams

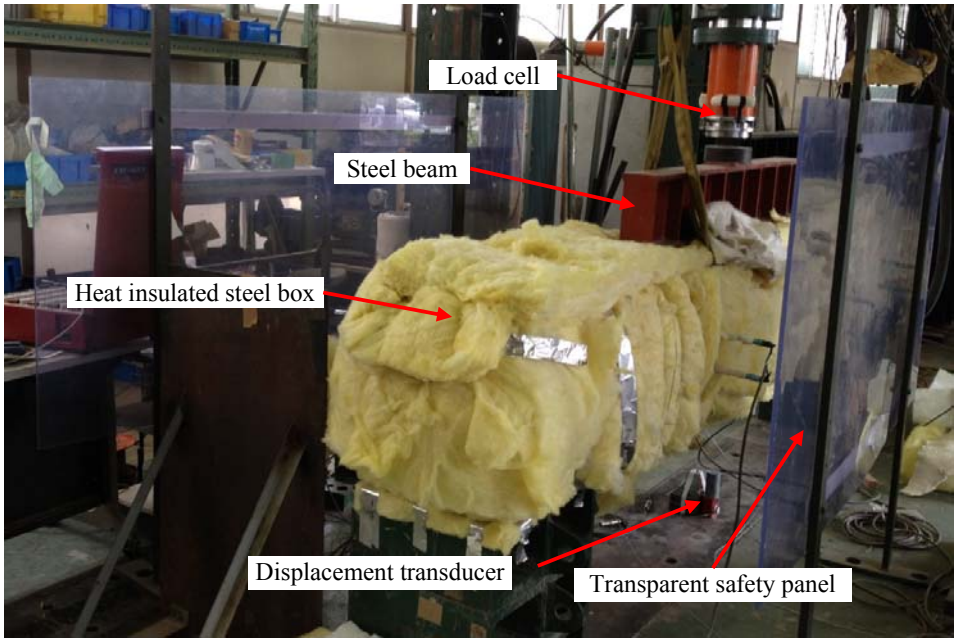

Fig. 4.5 Heating of a beam prior to four-point bending test

4.3 Results and discussion

Fig. 4.6 shows the temperature distribution in the GFRP I-beams and the GFRP/HFRP and UFC composite beams in the shear spans and the flexural span. It can be observed that the temperature distribution in the beam cross-sections (in flexural and shear spans) is approximately similar to each other. Generally, the bottom flange (BF) temperature was low compared to the other parts of the beams and this was caused by the upward movement of heat through convection.

Fig. 4.7, Fig. 4.8, and Fig. 4.9 show the failure patterns of the GFRP I-beams, GFRP-UFC composite beams, and HFRP-UFC composite beams, respectively. For comparison, the failure pattern of the GFRP I-beam at 20°C (G-20) from previous experiment was included in Fig. 4.7 [18]. Delamination and crushing failure similar to that exhibited by the GFRP compression test coupons were seen in the GFRP I-beams when the temperature was below 60°C (G-20 and G-60 beams). In both cases, the failure location was at the loading point in the shear span (Fig. 4.7a, b). In contrast to G-20 and G-60 beams, in G-90 beam, failure was due to kinking of the compression flange and web at midspan. This was caused by the glass transition of the vinylester resin in the GFRP I-beam at 90°C. A kink failure similar to this was observed in compressive tests on both the GFRP flange and GFRP web coupons at 90°C (Fig. 3.17a). The details of the compression test of the GFRP coupons are demonstrated in Section 3.2.4.

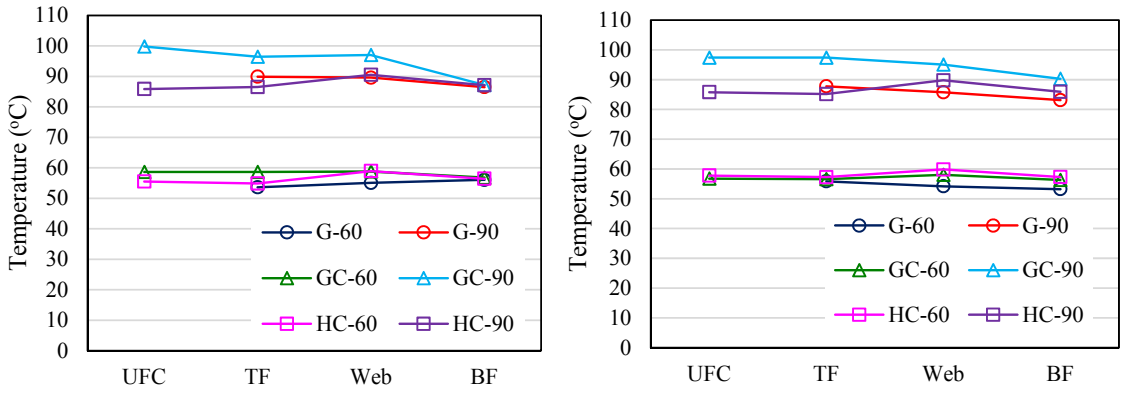

(a) Shear span 1

(b) Shear span 2

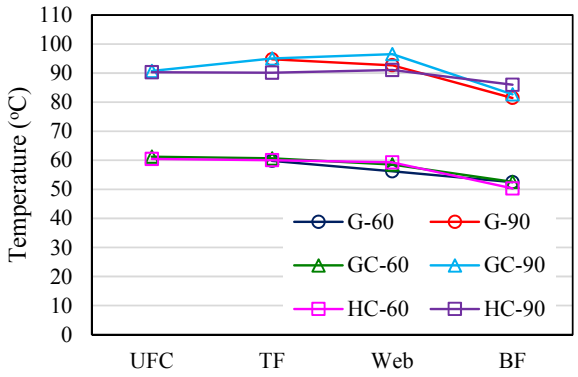

(c) Flexural span

TF: Top flange BF: Bottom flange

Fig. 4.6 Temperature distribution in the beams

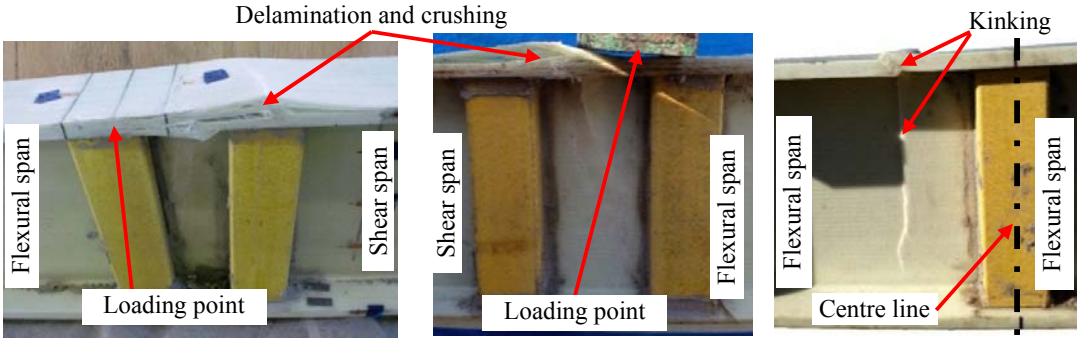

(a) G-20 beam (b) G-60 beam (c) G-90 beam

Fig. 4.7 Failure patterns of GFRP I-beams

Fig. 4.8 shows the failure patterns of the GFRP and UFC composite beams, which were all different. Beams GC-20 and GC-60 failed due to crushing of the UFC segments in the flexural span. In GC-60 beam, a very small movement of all the UFC segments in the shear span was observed (Fig. 4.8b). The slip of the UFC segments occurred because of the failure of the epoxy adhesive. The failure pattern of the GC-90 beam was completely different to GC-20 and GC-60 beams. It was failed through shearing of both the epoxy adhesive and the FRP bolts followed by kinking and crushing of the GFRP top flange and web in the shear span (Fig. 4.8c). There was no damage to the UFC segments and four UFC segments became completely detached from the GFRP top flange.

As shown in Fig. 4.9, the HFRP and UFC composite beams failed in the shear span at all temperatures considered in this study. In all the HFRP and UFC composite beams, the UFC segments fixed to the shear span have been completely detached from the HFRP I-beam and there were no damages observed in the UFC segments (Fig. 4.9). This type of failure pattern was observed in GC-90 also (Fig. 4.8). The cause for this failure is the shear failure of the FRP bolts and the epoxy adhesive. As the UFC segments detach from the HFRP I-beam at failure, crushing of the HFRP flange and the GFRP web was observed in HC-20 and HC-60 beams while in beam HC-90, kinking of the HFRP I-beam flange and web was observed.

Practically, the bi-material bending effect (the bending occurred in a composite beam at elevated temperature due to the mismatch of the α values in the constituent materials) must be largest in the GFRP/HFRP and UFC composite beams subjected to the highest temperature. Therefore, the bi-material bending effect should be maximum in beams GC-90 and HC-90. According to the experiment results, the maximum midspan deflection of the GC-90 beam before loading was approximately 1 mm (downward direction), or around 1.5% of the deflection at failure. In case of HC-90 beam, the maximum midspan deflection prior to loading was also approximately 1 mm (upward direction), or around 2% of the deflection at failure. This concludes that the bi-material bending effect in the GFRP/HFRP and UFC composite beams at elevated temperature (less than 90°C) due to different thermal expansion rates of the materials is negligible. This result was expected because of close coefficients of thermal expansion rates of the GFRP flange, HFRP flange, and UFC (Table 3.4). The upward deflections in beam HC-90 is because the UFC is having larger coefficient of thermal expansion compared to that of the HFRP.

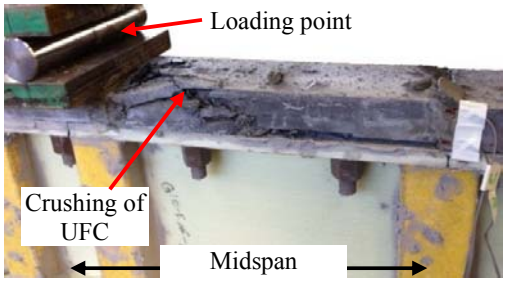

(a) GC-20 beam

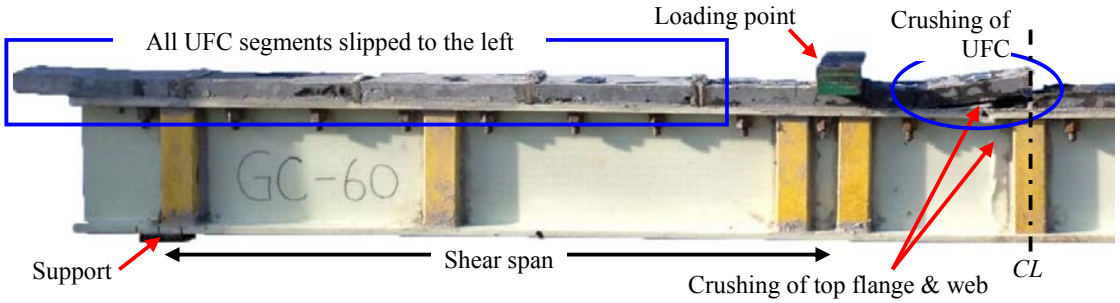

(b) GC-60 beam

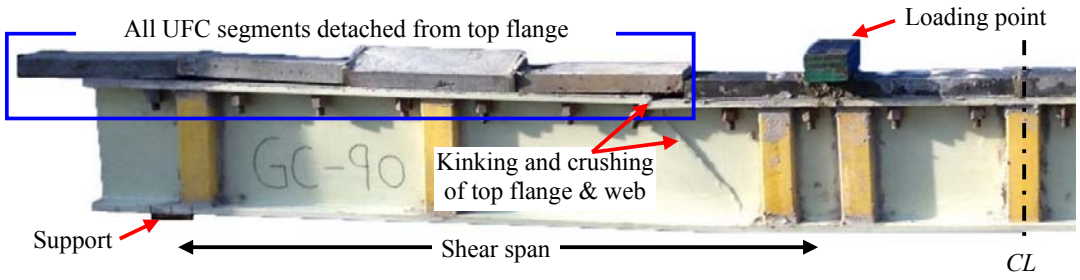

(c) GC-90 beam

Fig. 4.8 Failure patterns of GFRP and UFC composite beams

Failure details of all beams are summarized in Table 4.2. Experimental results show that the ultimate load carrying capacity of the GFRP I-beams, GFRP-UFC composite beams, and HFRP-UFC composite beams falls when the temperature increases. In the case of the GFRP I-beams, the reduction in flexural capacity is 11% as the temperature increases from 20°C to 60°C and it is 57% when the temperature increases from 60°C to 90°C. In the case of GFRP and UFC composite beams, the reduction in ultimate flexural capacity is 14% as the temperature increases from 20°C to 60°C and that is 40% when the temperature increases from 60°C to 90°C. On the other hand, the GFRP and UFC composite beams exhibited 83%, 75%, and 147% flexural capacity higher than those of the GFRP I-beams at 20°C, 60°C, and 90°C, respectively.

Therefore, the UFC segments have utilized the tensile properties of the GFRP effectively and hence the flexural capacity of the GFRP I-beams have been improved significantly. In the HFRP and UFC composite beams, the ultimate flexural capacity reduced by 14% when the temperature increases from 20°C to 60°C and it was reduced by 32% when the temperature increases from 60°C to 90°C.

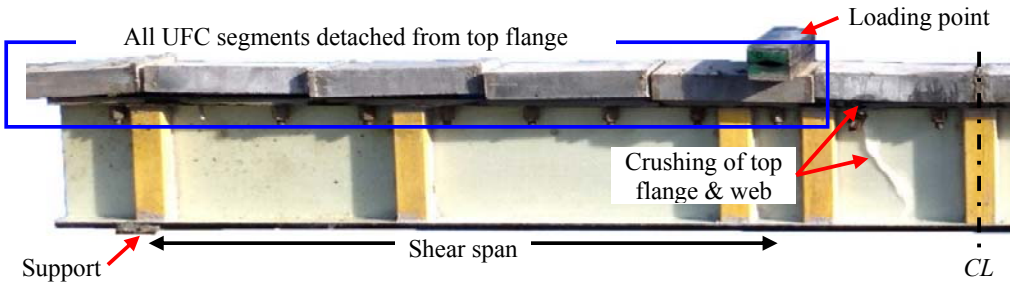

(a) HC-20 beam

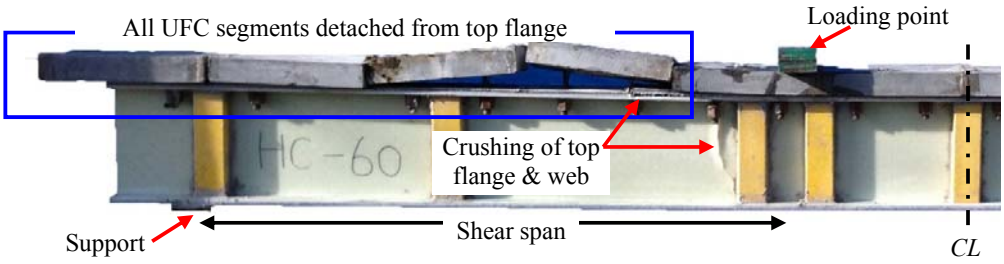

(b) HC-60 beam

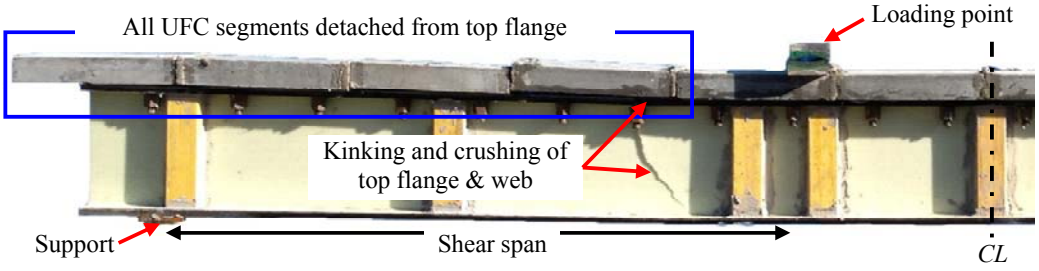

(c) HC-90 beam

Fig. 4.9 Failure patterns of HFRP and UFC composite beams

Fig. 4.10 shows the relationship between the normalized flexural capacity and temperature of the GFRP I-beams, GFRP-UFC beams, and HFRP-UFC beams. In all beam types, more than 85% of their flexural capacity was retained up to 60°C. However at 90°C, the retained flexural

capacity of the GFRP I-beam, GFRP-UFC beam, and HFRP-UFC beam dropped to 38%, 50%, and 58%, respectively. This is attributed to the degradation of material properties of the GFRP/HFRP I-beams and the shear connectors (FRP bolts and epoxy adhesive) beyond their glass transition temperatures.

Table 4.2 Failure details of test specimens

Beam	Ultimate load (kN)	Deflection (mm)	Midspan compressive strain (μ)	Midspan tensile strain (μ)
G-20	108.9	67.4	6980	7492
G-60	96.9	64.4	6858	6386
G-90	41.1	29.7	2667	3020
GC-20	199.8	64.1	3007	11400
GC-60	169.9	72.8	2403	Gauge damaged
GC-90	101.9	66.2	1794	6785
HC-20	245.8	45.4	2555	6374
HC-60	210.8	49.4	1980	6330
HC-90	142.9	46.2	1517	4954

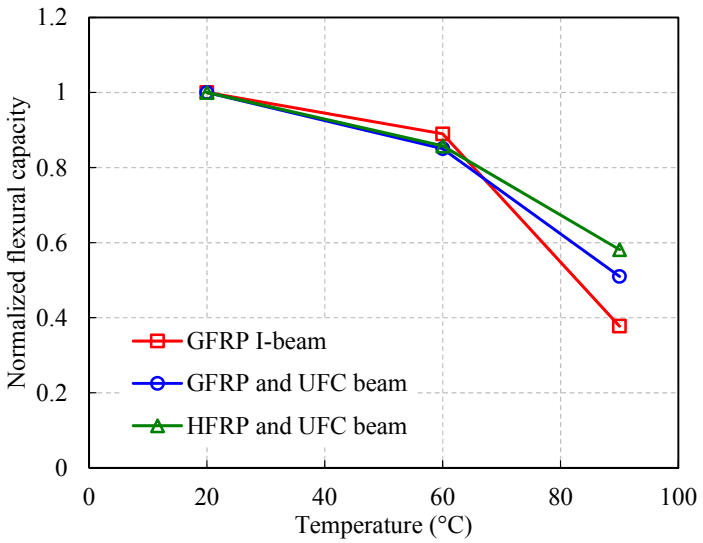

Fig. 4.10 Normalized flexural capacity of GFRP I-beams, GFRP-UFC beams, and HFRP-UFC beams

Fig. 4.11, Fig. 4.12, and Fig. 4.13 show the load and deflection relationships of the GFRP I-beams, GFRP-UFC composite beams, and HFRP-UFC composite beams, respectively. According to Fig. 4.11, all the GFRP I-beams exhibited linear load-deflection relationship until failure. The greatly reduced ultimate flexural capacity of beam G-90 compared to that of beam G-60 may be due to the deterioration of the GFRP material properties resulting from the glass transition. Similar to the flexural capacity, the stiffness of the GFRP I-beams and the GFRP and UFC beams decreased as the temperature increases (Fig. 4.11 and Fig. 4.12). The reason for the reduction of the stiffness of these beams is due to softening of vinylester resin by glass transition. However, with the installation of the UFC segments at the compression flange, the stiffness of the GFRP I-beams was significantly improved.

In the HFRP and UFC composite beams, large size (cross-sectional area) UFC segments were used because the tensile capacity of HFRP is greater than that of the HFRP. Because of the high tensile strength of the HFRP and larger UFC segments, the flexural capacity of the HFRP and UFC composite beams were larger than that of the GFRP and UFC composite beams under the same temperature. According to the Fig. 4.13, the stiffness of the HFRP and UFC composite beams was not significantly changed until the occurrence of slipping of UFC segments.

The decrease in the flexural capacity of the GFRP/HFRP and UFC composite beams at elevated temperature is mainly caused by the degradation of the material properties due to the glass transition of the vinylester resin, FRP bolt resin, and epoxy adhesive. The sudden deflection changes in beams GC-60 and GC-90 at 144 kN and 89 kN were due to slipping of the UFC segments in the shear span (Fig. 4.12). In GC-20 beam, there was no noticeable slipping was observed. As shown in Fig. 4.13, there was a slipping of the UFC segments in HC-60 and HC-90 beams at 180 kN and 71 kN, respectively. Furthermore, it was noted that in beam HC-20 there was a sudden increase in deflection at 220 kN. However, as observed in HC-60 and HC-90 beams, there was no reduction in the load when the deflection increases. Therefore, the cause of increase of deflection in beam HC-20 is different from that of HC-60 and HC-90 beams and it may be due to crushing of the cement mortar filling or due to a small slip of the FRP bolts inside the bolt-holes.

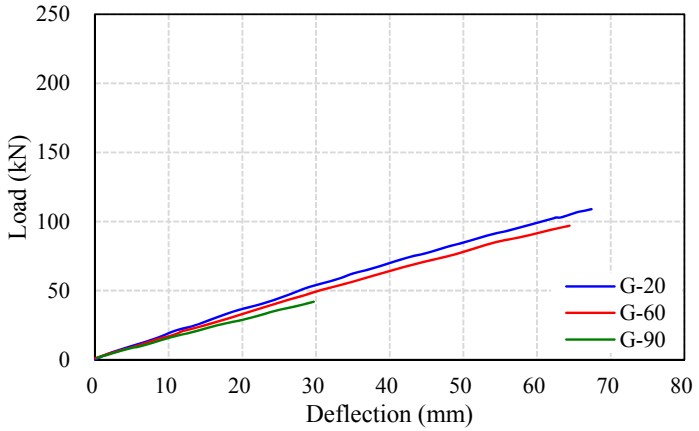

Fig. 4.11 Load-deflection relationship of GFRP I-beams

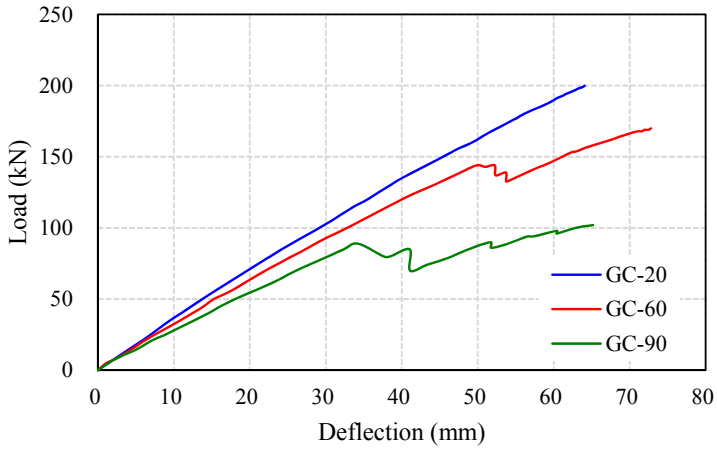

Fig. 4.12 Load-deflection relationship of GFRP and UFC composite beams

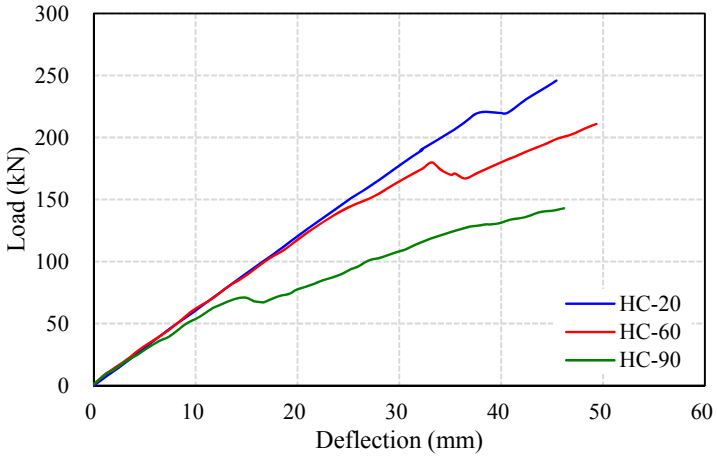

Fig. 4.13 Load-deflection relationship of HFRP and UFC composite beams

The strain distribution at midspan cross-section of the GFRP and UFC composite beams is shown in Fig. 4.14. The locations of the strain gauges on the beam are illustrated in Fig. 4.14a and the height to each strain gauge (cross-section depth) was measured from the beam bottom. According to Fig. 4.14b, there was a very small slip between the UFC segments and the I-beam top flange in beam GC-20 and therefore, the strain distribution remained almost linear up to beam failure. In the case of GC-60 beam, there was a linear strain variation at the midspan even after slipping of the UFC segments and this may be due to the residual shear capacity of the epoxy adhesive at 60°C (Fig. 4.14c). It should be noted that there is a slight downward movement of the neutral axis in GC-60 after slipping of the UFC segments. In contrast to the other GFRP and UFC beams, the strain distribution at midspan of beam GC-90 was non-linear after slipping of the UFC segments and the distribution is characterized by the partial shear interaction (Fig. 4.14d).

Fig. 4.15 shows the strain distribution across midspan cross-section of the HFRP and UFC composite beams. The strain gauge locations in the midspan section of the beams are as illustrated in Fig. 4.15a. Similar to beam GC-20, in beam HC-20, there was a very small slip between the UFC and the HFRP I-beam. Therefore in beam HC-20, the midspan strain variation until beam failure was linear (Fig. 4.15b). This confirms that the sudden increase in beam HC-20 at 220 kN was not due to the failure of epoxy adhesive. In contrast to beam HC-20, the midspan strain distribution of HC-60 and HC-90 beams was non-linear until the beam failure. This is very similar to the midspan strain distribution in beam GC-90 and the partial shear interaction can be seen in HC-60 and HC-90 beams (Fig. 4.15c and d) after the occurrence of UFC slip. Furthermore, after the occurrence of the UFC slippage in HC-60 and HC-90 beams, downward movement of the neutral axis was observed from Fig. 4.15c and d.

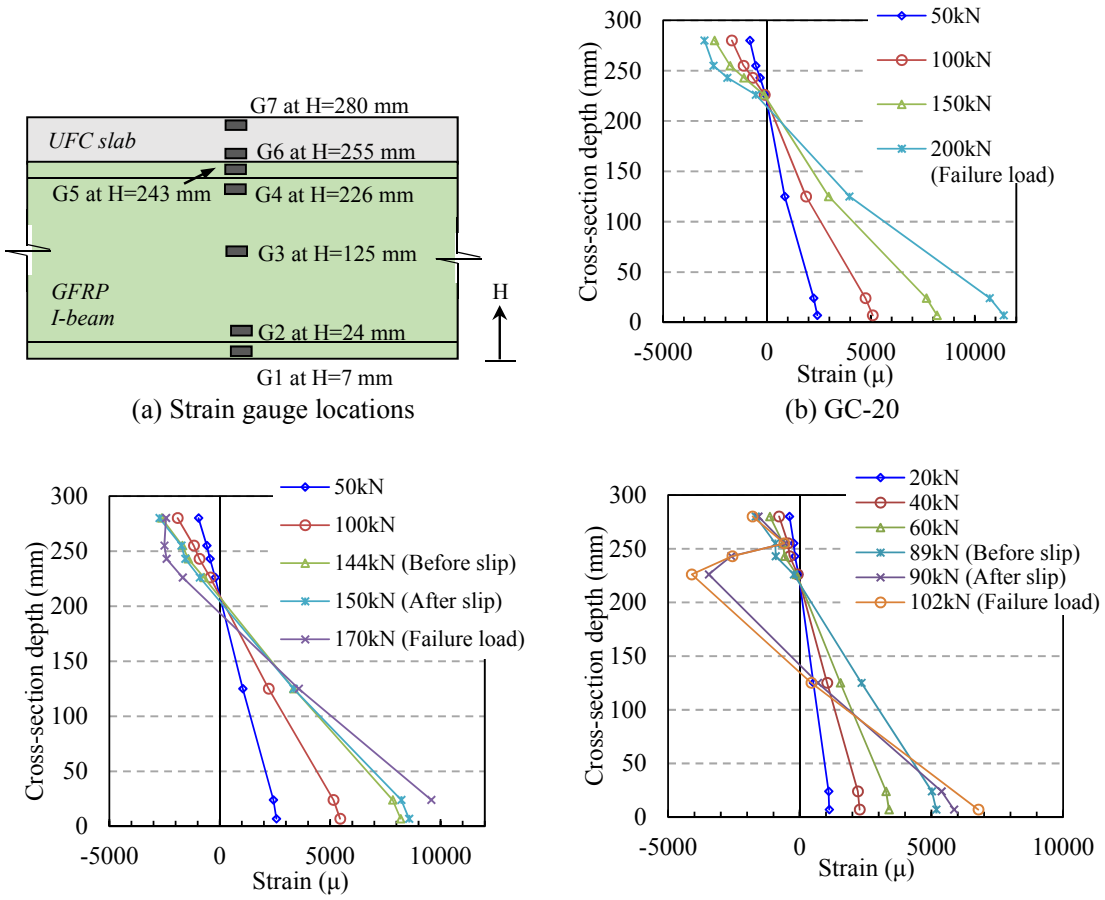

Fig. 4.14 Longitudinal strain distribution across midspan cross-section of GFRP and UFC composite beams

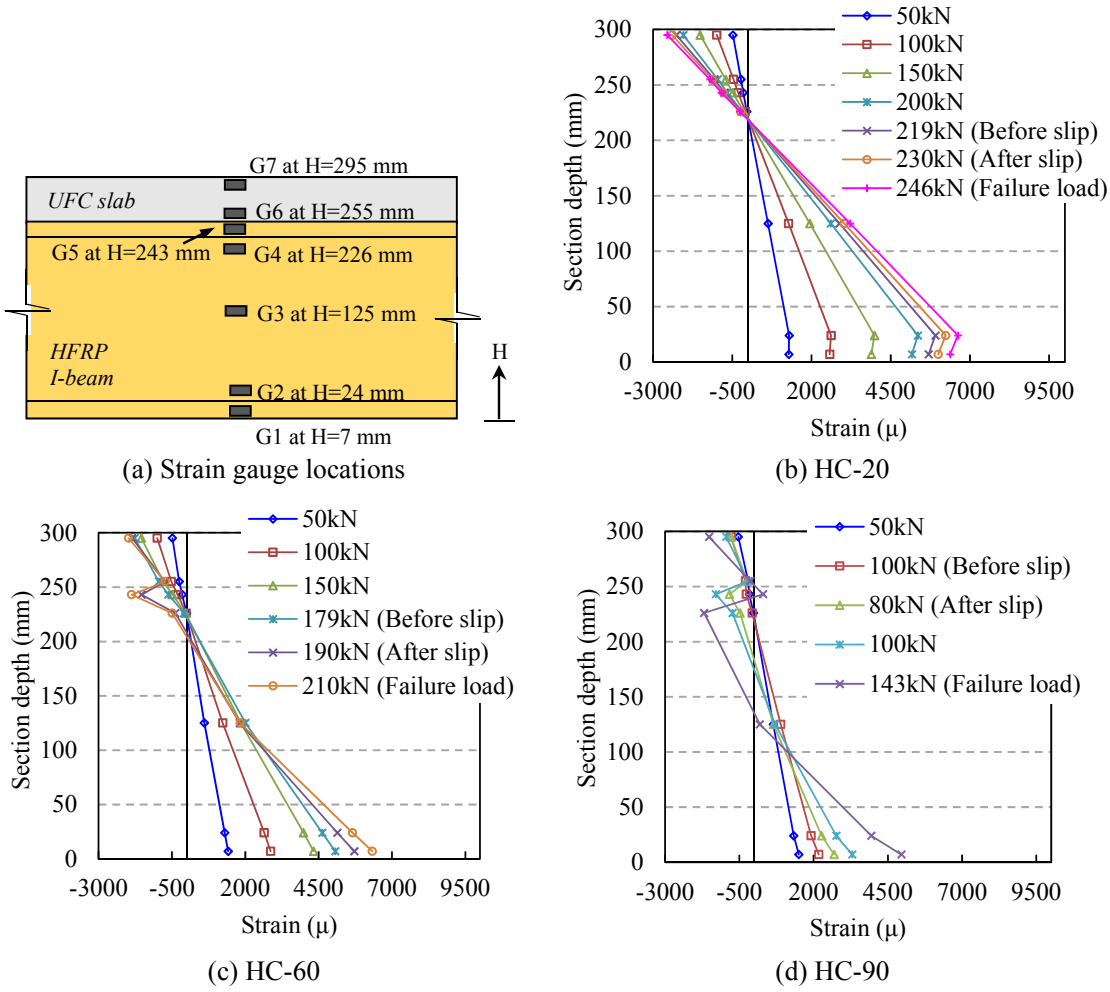

(a) Strain gauge locations

(b) HC-20

(c) HC-60

(d) HC-90

Fig. 4.15 Longitudinal strain distribution across midspan cross-section of HFRP and UFC composite beams

4.4 Concluding remarks

This section demonstrates the influence of temperature on the flexural behaviour of the GFRP I-beams, GFRP-UFC composite beams, and HFRP-UFC composite beams. According to the large-scale beam bending tests, the following conclusions were made.

- The flexural capacity and the stiffness of the GFRP I-beams, GFRP-UFC composite beams, and HFRP-UFC composite beams are degraded by elevated temperature due to glass transition of the vinylester resin. However, more than 85% of the flexural capacity (compared to the flexural capacity at 20°C) of three beam types can be retained when the

beam temperature is below 60°C. As the beam temperature increases beyond 60°C, the flexural capacity of these beams was severely degraded.

- The use of the UFC segments significantly improves the ultimate flexural capacity and the stiffness of the GFRP I-beams at temperatures in between 20°C to 90°C. This is because the UFC segments can prevent the premature delamination and kink failure of the GFRP I-beam compression flange. As a result, the tensile strength of the GFRP I-beam can be effectively utilized. Similarly, the UFC segments will improve the flexural capacity and the stiffness of the HFRP I-beams.
- The bi-material bending effect in the GFRP/HFRP and UFC composite beams is negligible due to approximately close thermal expansion rates of the GFRP, HFRP, and UFC materials.
- The slippage of the UFC segments observed in the GFRP/HFRP and UFC composite beams above 60°C was due to the failure of the epoxy adhesive caused by elevated temperature. It was found that the full composite behaviour of the GFRP/HFRP and UFC beams lose after the slippage of the UFC segments and there will be partial interaction between the UFC segments and the GFRP/HFRP I-beams.
- Both the GFRP-UFC composite beams and the HFRP-UFC composite beams are affected by elevated temperature and their flexural capacities are reduced when the beam temperature increases. The failure mechanism (flexural failure or shear failure) of these composite beams was governed by the shear capacity of the FRP bolts at the beam temperature.

Chapter 5

Fibre Model Analysis

In this chapter, the flexural behaviour of the GFRP I-beams and the GFRP-UFC composite beams was predicted using a simple fibre model analysis (FMA) and the analysis results were verified by the experimental results described in Chapter 4. Fibre model is a one dimensional model and it has been used successfully by researchers to analyse the flexural behaviour of the reinforced concrete beams, FRP beams, and FRP-concrete composite beams [41, 45-49]. In this method, the theoretical moment-curvature relationship of the GFRP and UFC composite beam sections can be determined based on the strain compatibility and internal force equilibrium principles. An important feature of the FMA is that it can account for the different behaviour of constituent materials of the GFRP and UFC composite beams. In addition, the FMA is comparatively less time-consuming and cost-effective compared to the commercial finite element software packages.

5.1 Calculation procedure in the fibre model analysis

The fibre model is a finite element analytical program which was written using Microsoft Visual Basic™ computer language. Therefore, it has the advantage of working compatibility with Microsoft Excel™ software. The sequence diagram of the fibre model analysis is shown in Fig. 5.1. As illustrated in Fig. 5.2, in the fibre model, the composite beam is divided into 'm' longitudinal segments along the span (with '*a*' divisions in the flexural span and '*b*' divisions in each shear span, so $m = a + 2b$). And also the midspan cross-section is divided into 'n' discrete horizontal elements as shown in Fig. 5.3a. The basic assumptions in the analysis are as follows. 1) the GFRP and UFC composite beam behaves under Euler-Bernoulli beam theory, 2) there is full interaction between the UFC segments and the GFRP I-beam top flange until beam failure and hence, there is no slip at the UFC-GFRP interface, 3) temperature within each part of the GFRP and UFC composite beam (UFC slab, GFRP top flange, GFRP web, and GFRP bottom flange) remains constant, and 4) the bending effect due to the mismatch of the coefficient of thermal expansion values of the materials is negligible. Fig. 5.4 shows the material models (UFC model and GFRP model) used for the FMA at T°C temperature. To model the UFC slab, a bi-linear stress-strain relationship (for high strength concrete) proposed by Japan Society of Civil Engineering (JSCE) [50] was used (Fig. 5.4a). The GFRP I-beam was modelled using the GFRP model shown in Fig. 5.4b. The GFRP model was developed using

the material properties of GFRP, described in Chapter 3. In the analysis of the GFRP I-beams, the cross-sectional dimensions of the UFC slab was considered as zero.

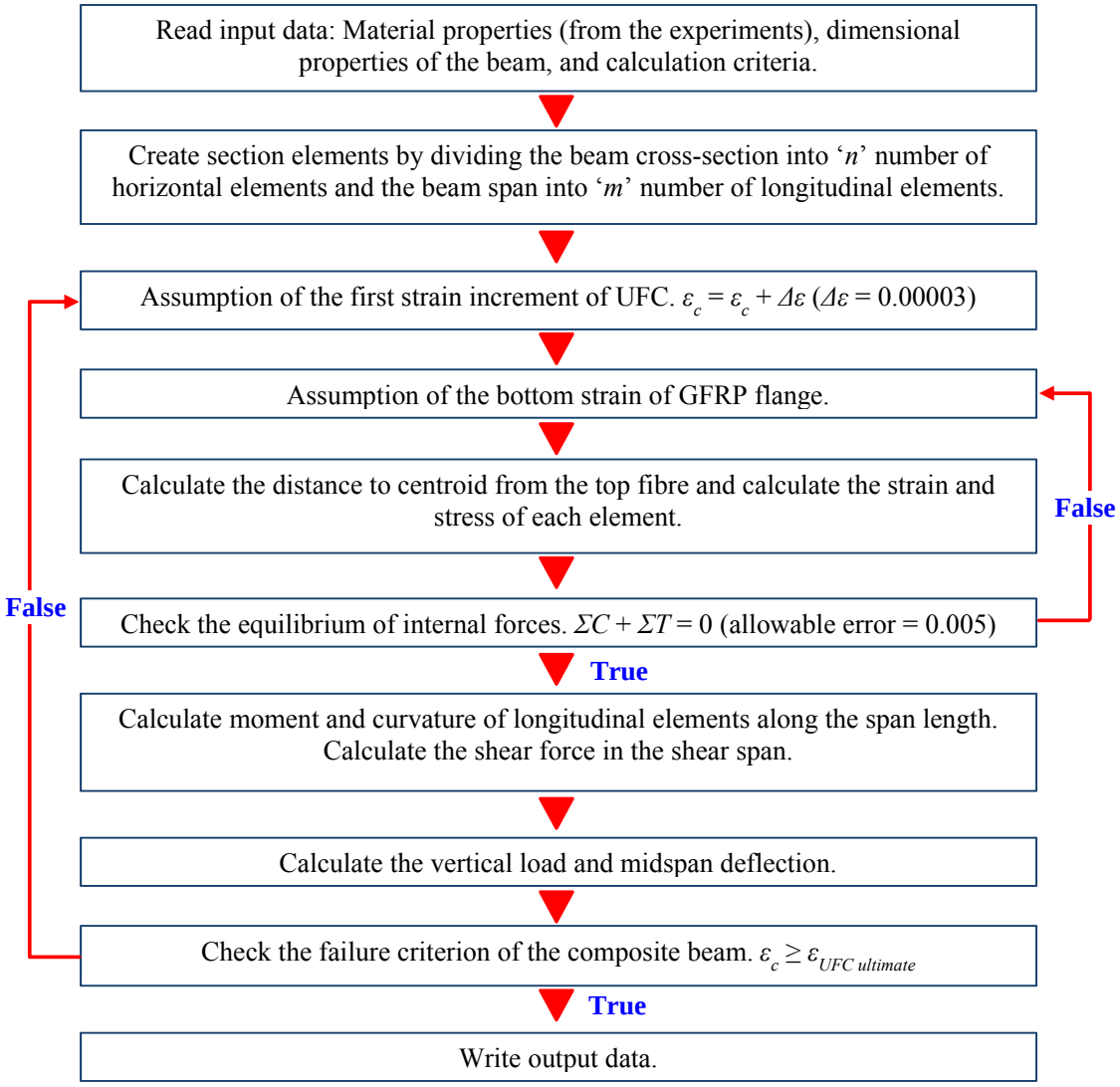

Fig. 5.1 Sequence diagram of fibre model analysis

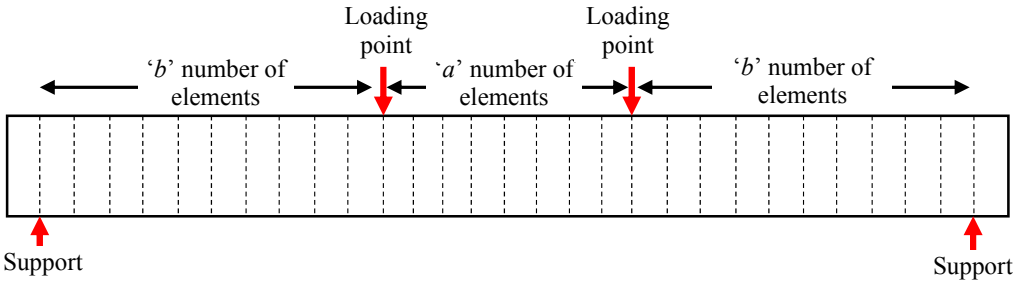

Fig. 5.2 Horizontal discrete elements in the fibre model analysis

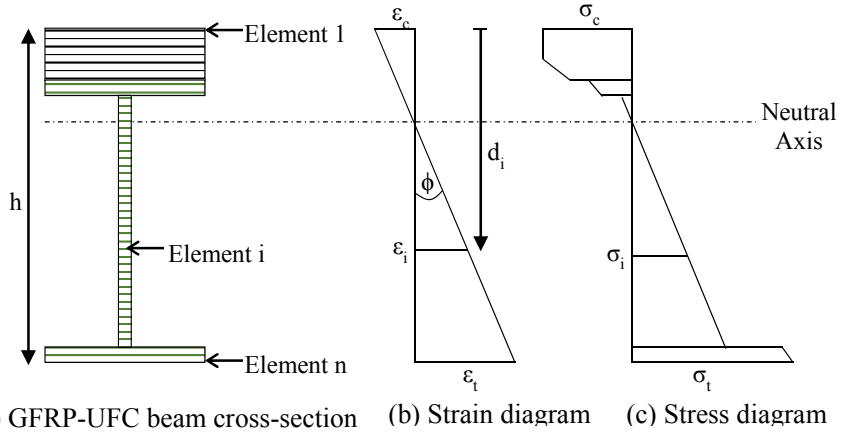

Fig. 5.3 Fibre model analysis: discrete elements in GFRP and UFC composite section, strain and stress diagrams

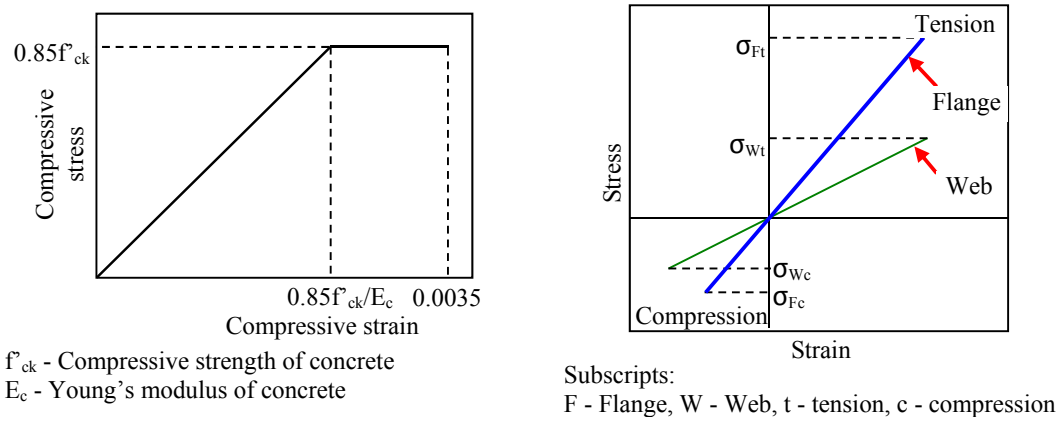

(a) UFC bi-linear model at T°C temperature

(b) GFRP model at T°C temperature

Fig. 5.4 Material models used in the fibre model analysis

As shown in Fig. 5.3a, the distance to the i^{th} horizontal element from the beam top is $i \times h/n$, where h is the overall beam height. In the fibre model, the initial compressive and tensile strains (ε_c and ε_t) at the midspan section are assumed to be 30μ. Based on the linear strain distribution in the cross-section (Fig. 5.3b), the strain at the centre of i^{th} element (ε_i) is determined by equation (1), where d_i is the distance to the centroid of the i^{th} element from the beam top (Equation 2).

$$\varepsilon_i = \varepsilon_c - \frac{d_i(\varepsilon_c+\varepsilon_t)}{h} \tag{1}$$

$$d_i = \frac{h(i-0.5)}{n} \tag{2}$$

The stress in each element of the GFRP and UFC beam cross-section is calculated (Fig. 5.3c) from the element strain and the stress-strain models (Fig. 5.4a & b) corresponding to the beam temperature being considered. Internal forces in each element are calculated considering the element stress and the cross-sectional area of the element, and the force equilibrium is checked using equation (3) where ΣF_c and ΣF_t are the resultant compressive and tensile forces acting on the GFRP and UFC beam cross-section, respectively.

$$\sum F_c - \sum F_t = 0 \tag{3}$$

If equation (3) is not satisfied by the assumed ε_c and ε_t strains, an iterative method is used in the fibre model to achieve force equilibrium. However, it is very difficult and time consuming to obtain the exact force equilibrium so that a 0.005 allowable error is considered in the FMA. Once the force equilibrium is obtained, the resultant moment (M) and the curvature (ϕ) are calculated using equations (4) and (5).

$$M = \sum F_i d_i \tag{4}$$

Where, F_i is the element force of the i^{th} element.

$$\phi = (\varepsilon_c + \varepsilon_t)/h \tag{5}$$

Thereafter, the curvature of each section of the longitudinal segments (ϕ_j) is calculated by the fibre model and then the maximum deflection at the midspan (δ_{max}) is calculated according to equation (6), where l_j is the length of the longitudinal segment.

$$\delta_{max} = \sum_{j=1}^{0.5a+b} \phi_j l_j \tag{6}$$

The total shear force developed at the UFC-GFRP interface is calculated using the element strain values in the shear span (Equation 7), where D_1 is the number of horizontal divisions in

the UFC slab cross-section, ΔA is the cross-sectional area of a UFC element and E_c is the Young's modulus of concrete.

$$F_{shear} = \sum_{i=0.5a}^{0.5a+b} \sum_{j=1}^{D_1} E_c(\varepsilon_{i,j} - \varepsilon_{i+1,j})\Delta A \quad (7)$$

In this method, loop calculations are carried out by increasing the ε_c and ε_t (at 30μ steps) until the ultimate compressive strain (ε_{cu}) of the UFC (in the GFRP I-beams ε_{cu} is the compressive strain of the compression flange) is reached or until the total shear force at the UFC-GFRP interface exceeds the shear capacity of the FRP bolts (only in GFRP-UFC beams). The total shear capacity of the FRP bolts and the epoxy adhesive at the beam temperature was determined from the lap-shear test data described in Chapter 3.

5.2 Fibre Model Analysis of GFRP I-beams and GFRP-UFC Beams with a Small Temperature Gradient

Fibre model analysis was carried out for the GFRP I-beams (G-60 and G-90) and for the GFRP-UFC composite beams (GC-20, GC-60, and GC-90) with a small temperature gradient across the beam cross-section. The reason for considering a small temperature gradient across beam cross-section is to simulate the beam experiment and thereby compare the experiment and analysis results. The relationships between load and midspan deflection of the GFRP I-beams, obtained from experiment and analysis are shown in Fig. 5.5. According to the analysis results, the fibre model can well predict the flexural behaviour of the GFRP I-beams where there is a small temperature gradient across the beam cross-section. The load and deflection relationship in the GFRP I-beams at elevated temperature is linear up to beam failure because there are no UFC segments. The difference in the failure load of the experiment and analysis was 1% in G-60 beam and 8% in G-90 beam. However, the flexural capacity of the G-90 beam was overestimated by fibre model and this may be due to the occurrence of web kink failure in the experiment whereas in the analysis, that effect was not taken into consideration.

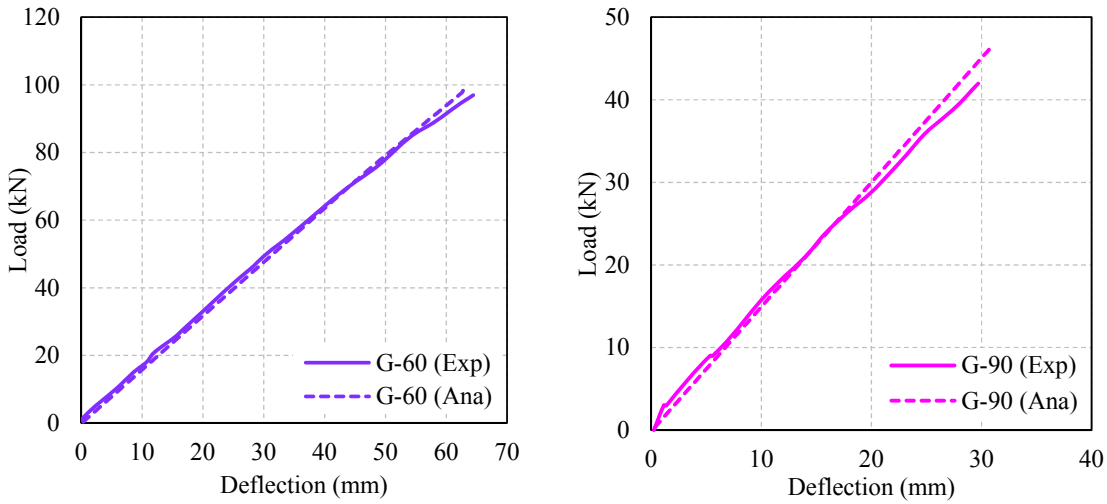

(a) G-60 beam (b) G-90 beam

Fig. 5.5 Analytical and experimental load-deflection relationships of GFRP I-beams

Fig. 5.6 shows the relationships between load and midspan deflection of the GFRP and UFC composite beams, obtained from the experiment and analysis. Fig. 5.6a shows a relatively good agreement between the experiment and the FMA results in beam GC-20. In beams GC-60 and GC-90, the load-deflection relationships were agreed up to the occurrence of slipping of the UFC segments (Fig. 5.6b and c). This is because, in the FMA, full interaction between the UFC segments and the GFRP flange was assumed. The vertical load corresponding to the ultimate shear capacity of the epoxy adhesive in beams GC-60 and GC-90 was obtained by the FMA (see lines ② and ④ in Fig. 5.6b and c, respectively). Similarly, the vertical load corresponding to the ultimate shear capacity of the FRP bolts in GC-60 and GC-90 beams was determined by the fibre model (see lines ① and ③ in Fig. 5.6b and c, respectively). According to the FMA results it was confirmed that the slipping of the UFC segments occurred in both GC-60 and GC-90 beams when the vertical load is approximately equal to the load corresponding to the shear capacity of the epoxy adhesive. The difference in the vertical load corresponding to the slipping of the UFC segments between the experiment and the FMA was about 5.5% and 7.5% in beam GC-60 and in beam GC-90, respectively.

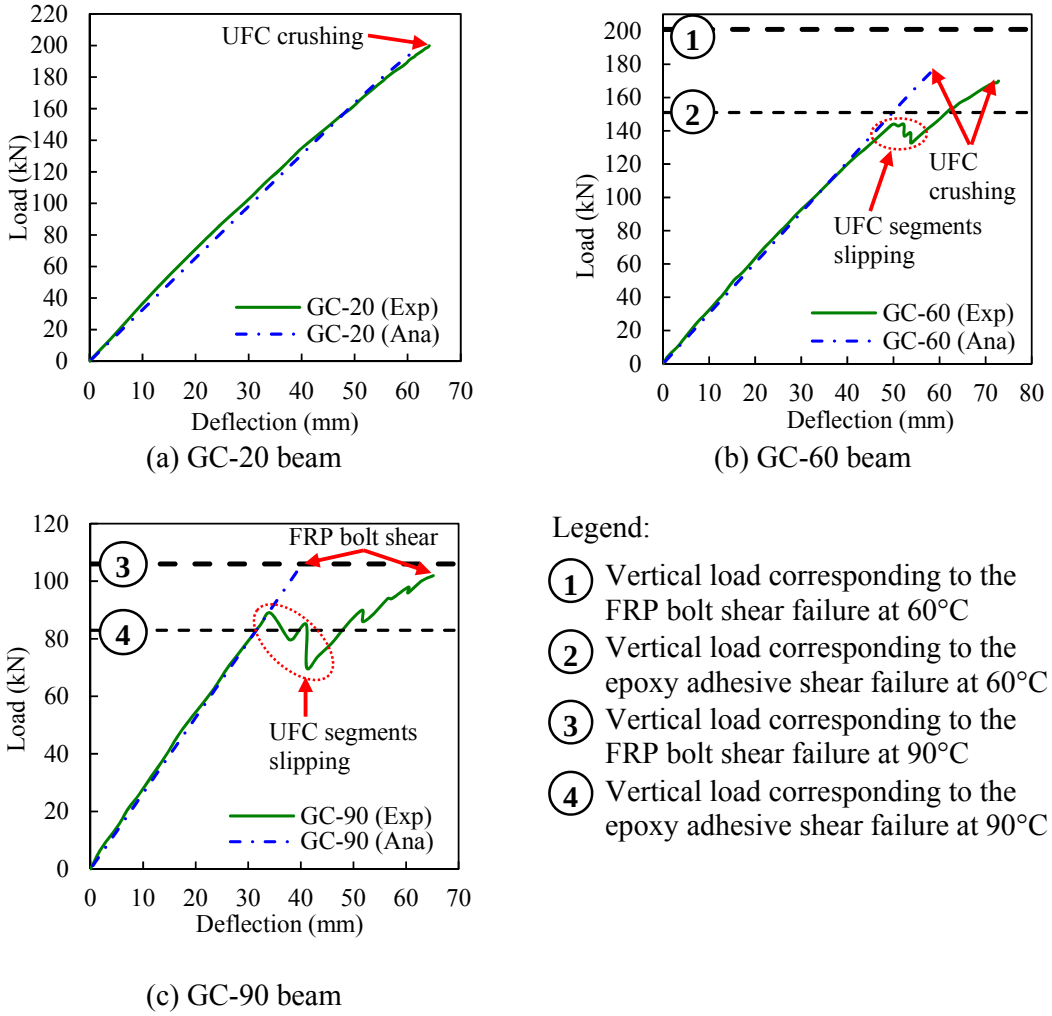

Fig. 5.6 Analytical and experimental load-deflection relationships of GFRP and UFC beams

In both GC-20 and GC-60 beams, the ultimate compressive strain (ε_{cu}) of the UFC slab was reached at midspan before the FRP bolt shear capacity was attained. Therefore, those beams failed by crushing of the UFC slab at the midspan. The FMA results of beam GC-90 showed that the total FRP bolt shear capacity at the UFC-GFRP interface was exceeded at the beam failure and that was confirmed by the experiment results (Fig. 5.6c). The reason for the different failure mode observed in beam GC-90 was the significant degradation of the shear capacity of the FRP bolts between 60°C and 90°C temperatures.

5.3 Fibre Model Analysis of GFRP and UFC Beams with a Large Temperature Gradient

These GFRP and UFC composite beams were developed for outdoor constructions, where the main source of heat is solar radiation. In contrast to the experiment described in Chapter 4, in actual circumstances, the GFRP and UFC composite beams may experience a large temperature gradient across the beam cross-section. Therefore, as shown in Fig. 5.7, the beam top temperature will be the highest and the beam bottom temperature will be almost the same as the ambient temperature. The flexural performance of the GFRP and UFC composite beams under this condition was analysed by the FMA. Three temperature cases were analysed and Table 5.1 shows the temperatures of different parts of the GFRP and UFC composite beams for each case. Temperatures for CASE 1 were determined based on the field investigation conducted by Sirimanna, et al. [37] and those for CASE 2 and CASE 3 were assumed by the authors. The fibre model analysis was processed until the shear failure of epoxy adhesive occurs.

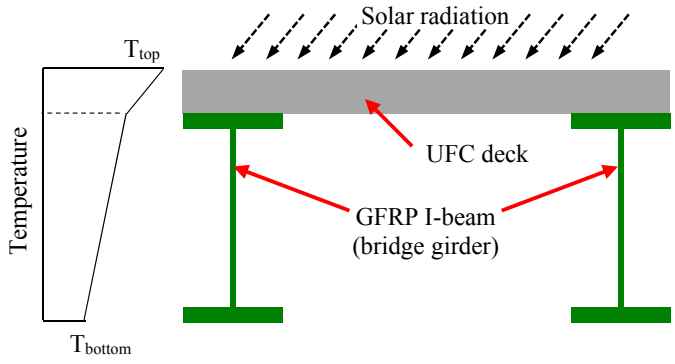

Fig. 5.7 Typical temperature distribution across GFRP and UFC bridge cross-section

The FMA results of the GFRP and UFC composite beams with a large temperature gradient are shown in Fig. 5.8a. For comparison purpose, the FMA results of beam GC-60 (small temperature gradient) also included in Fig. 5.8a. CASE 1 beam failed by crushing of the UFC segments and there was no slip of the UFC segments up to beam failure (Fig. 5.8b). On the other hand, there was a slipping of the UFC segments in the GC-60 beam even though the maximum temperature at the GC-60 beam top was identical to CASE 1 beam. As a result of the shear failure of the epoxy adhesive, CASE 2 and CASE 3 beams exhibited slipping of the UFC segments at the load of 151 kN and 127 kN, respectively (Fig. 5.8b). This result confirms that

the full composite behaviour of the GFRP and UFC beam is lost at relatively low vertical loads when the UFC slab of the composite beam is subjected to elevated temperature.

As shown in Fig. 5.8a, the stiffness of CASE 1, CASE 2, and CASE 3 beams was not significantly affected by the temperature gradient. On the other hand, the stiffness of beams GC-60 and GC-90 which had a small temperature gradient across beam cross-section degraded significantly (Fig. 4.12). Therefore, the GFRP and UFC composite beam's stiffness may not be significantly affected by the actual warm temperature conditions, where there is a large temperature gradient across the beam cross-section. This is attributed to the fact that the temperature increment in the GFRP bottom flange and the GFRP web is comparatively lower than that of the top parts of the composite beam in the actual warm temperature environments.

Table 5.1 Temperatures of the parts of the GFRP and UFC beams in FMA

	Temperature (°C)				
Case	UFC slab	Epoxy adhesive	Top flange	Web	Bottom flange
CASE 1	60	50	40	30	30
CASE 2	70	60	50	40	30
CASE 3	80	70	60	40	40

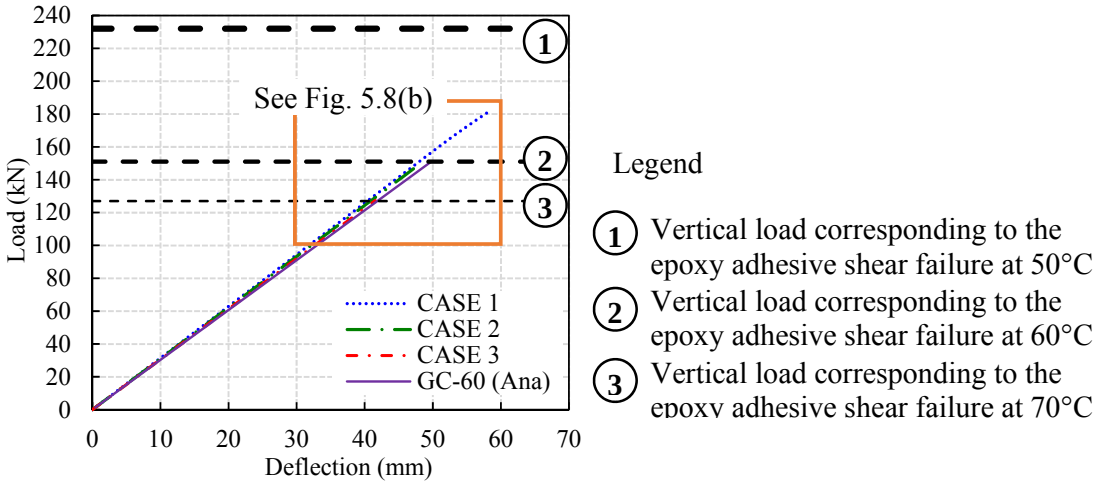

(a)

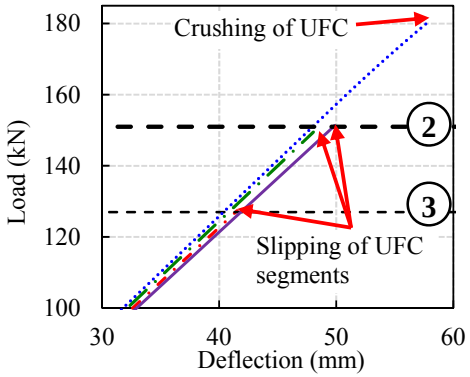

(b)

Fig. 5.8 (a) Analysis results of GFRP and UFC beams with a large temperature gradient; (b) Enlarged view

5.4 Concluding remarks

Fibre model analysis of the GFRP I-beams and the GFRP-UFC composite beams under room and elevated temperatures is demonstrated in this chapter. The analysis results were verified by the experiment results and the FMA was used to predict the flexural behaviour of the GFRP and UFC composite beams where there is a large temperature gradient across the beam cross-section. The main conclusions of the study are as follows.

- The fibre model analysis can be used to analyse the flexural behaviour of the GFRP I-beams at temperatures between 20°C and 90°C.

- The proposed fibre model analysis method can be used to predict the flexural behaviour of the GFRP and UFC composite beams until the slip of the UFC segments occurs.
- The difference between the beam failure loads in the analysis and the experiment is less than 8% in the GFRP I-beams and that is less than 1% in the GFRP and UFC composite beams with full interaction.
- Under the actual circumstances, the GFRP and UFC composite beams may experience a large temperature gradient across beam top to bottom. According to the analysis, it was found that the stiffness of the GFRP and UFC composite beams, which is related to the main design criterion of the FRP bridges, is not significantly affected by the temperature gradient in the real situations. However, the flexural capacity of the GFRP and UFC composite beams at the slipping of the UFC segments is greatly influenced by the temperature of the beam top.

Chapter 6

Flexural Performance of Short span Pedestrian Bridge Consisting of GFRP and UFC Composite Beams

6.1 Introduction

The GFRP and UFC composite beams described in this document are used for construction of short span pedestrian bridges. These beams can be used as the bridge girders in such bridges. As demonstrated in Chapter 2, the GFRP and UFC composite beams consisting of FRP bolts showed flexural performance similar to the GFRP-UFC beams having steel bolts. In Chapter 4, the temperature dependence of the GFRP-UFC composite beams (having FRP bolts) subjected to temperatures between 20°C and 90°C is described. Even though an actual pedestrian bridge would never reach 90°C, the bridge deck temperature can reach up to 50°C to 60°C [36, 37]. Warm temperatures in the bridges will exist when they are located in very hot climates and in the industrial environments. In general, the structural design of the FRP bridges depends mostly on the deflection limitation due to the low stiffness of the FRP [31]. Therefore, the FRP composite beams are suitable for constructions of short span bridges. The American Association of State Highway and Transportation Officials (AASHTO) and the Japan Society of Civil Engineers (JSCE) suggest that the deflection limit for pedestrian bridges should be less than $L/500$, where L corresponds to the bridge span [32, 33]. According to that limitation, the overall flexural capacity of the GFRP-UFC composite beams cannot be utilized. In this chapter, the details of a short span bridge constructed using the GFRP and UFC composite beams and the details of the static loading tests conducted on that bridge are described.

The short span pedestrian bridge was constructed at a fishery harbour in Onagawa city, Miyagi prefecture, Japan. It was constructed in 2012 by a group of universities, local governments, and companies. As shown in Fig. 6.1, it is located in a harbour, where corrosion severely affects the durability of the structures. This pedestrian bridge is used to access a pontoon from the pier (Fig. 6.1).

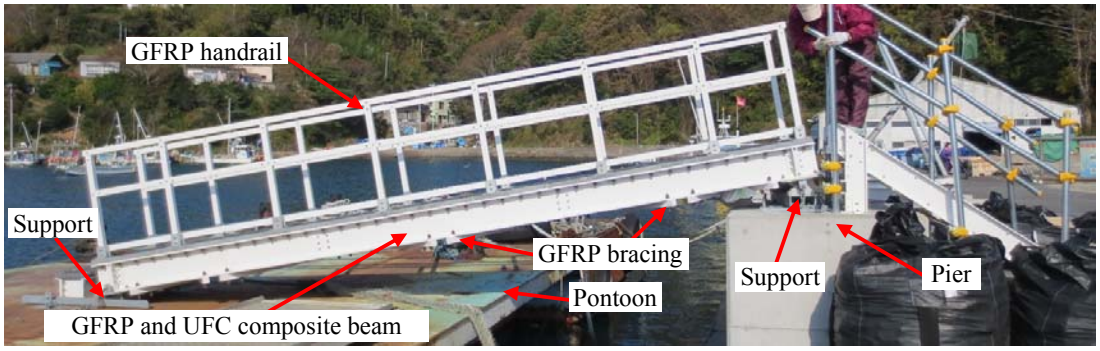

Fig. 6.1 GFRP and UFC pedestrian bridge in Miyagi prefecture, Japan

In order to improve corrosion resistance, non-corroding materials were used for the other main parts of the bridge such as handrails and bracings. Two GFRP and UFC composite beams were used in the pedestrian bridge and the overall length and width of the bridge are 6,000 mm and 960 mm, respectively. The GFRP I-beams, UFC slab segments and all the other members (handrails and bracings, etc.) can be pre-fabricated in a factory and can be easily transported to the construction site. The UFC segments avoid unwarranted cracks during transportation and during installation compared to a full length monolithic UFC slab. Thus, the GFRP and UFC composite beams are attractive in accelerated short span bridge construction. The Precast UFC segments were used as the decking of the bridge and they were connected to the GFRP I-beam top flange by 16 mm diameter FRP bolts and epoxy adhesive. Technical details of this high corrosion resistant short span bridge are given in Fig. 6.2a, b, and c. The bridge was designed according to the guidelines for short span bridges by the Japan Highway Association [51]. As suggested in the guidelines, a 3.5 kN/m^2 design live load on each GFRP and UFC composite beam and a 5.0 kN/m^2 design live load on the floor area of the short span bridge were taken into account. The total design load on the bridge is 25.86 kN and the allowable deflection limit for this bridge is 12 mm (L/500) [33].

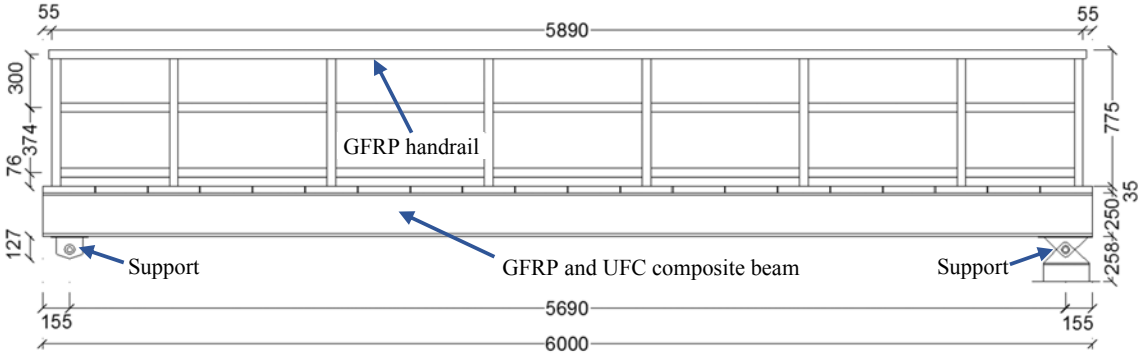

(a) Elevation

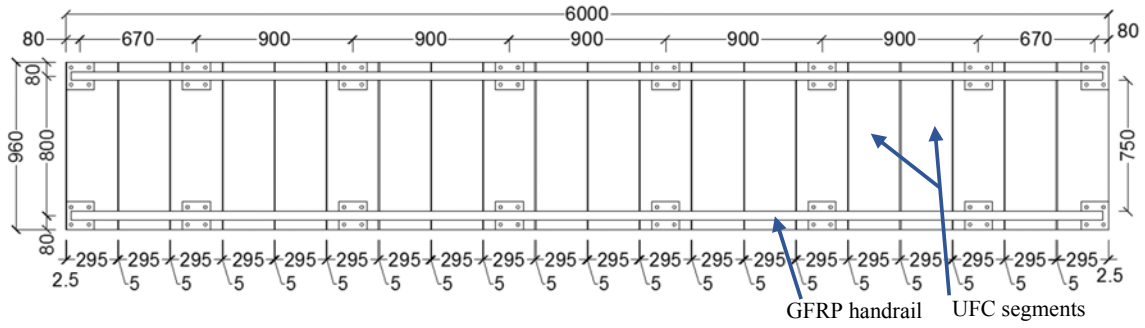

(b) Plan view

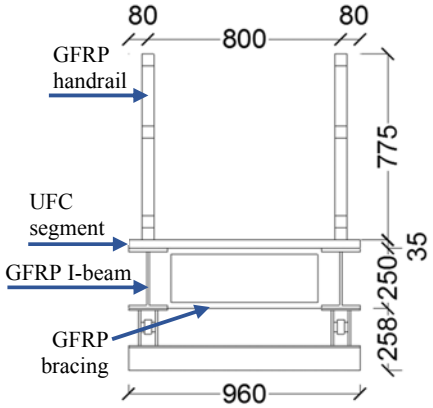

(c) Cross-section

Fig. 6.2 Details of the GFRP and UFC short span pedestrian bridge in Miyagi, Japan (Units: mm)

6.2 Experiment details of the static loading tests on the short span bridge

The flexural performance of the GFRP and UFC bridge was investigated through static loading tests. A maximum load of 8.02 kN was applied by 12 people standing on the bridge in three different loading patterns. The applied loading patterns are 1) concentrated load, 2) distributed load along the centreline, and 3) eccentric distributed load. The details of the applied load and the details of the loading patterns are given in Table 6.1 and Table 6.2, respectively. At each loading pattern, load was increased as steps. At each loading step, two people get on to the bridge. The loading pattern 3 was applied on each GFRP and UFC beams, separately. To check the strain distribution at the midspan, four strain gauges were attached at the midspan cross-section of each GFRP and UFC composite beam. Strain gauge locations were top of the UFC slab, bottom of the UFC slab, middle of the GFRP web, and GFRP bottom flange. There were two deflection gauges connected to the bottom flange of each beam at the midspan and the deflection of the beams were recorded at each loading step.

Table 6.1 Details of the applied load on the bridge

Number of people	1	2	3	4	5	6	7	8	9	10	11	12
Load (kg)	71	66	60	87	70	61	50	54	63	79	64	93
Cumulative applied load (kN)	0.70	1.34	1.93	2.79	3.47	4.07	4.56	5.09	5.71	6.48	7.11	8.02

Table 6.2 Details of loading patterns

Name	Loading pattern	Method of loading
Pattern 1	Concentrated load	People are standing in two rows at the centre of the bridge (Fig. 6.3a).
Pattern 2	Distributed load (along centreline)	People are standing in a row, along the centreline of the bridge (Fig. 6.3b).
Pattern 3	Distributed load (eccentric)	People are standing in a row, towards one of the GFRP and UFC composite beam (Fig. 6.3b).

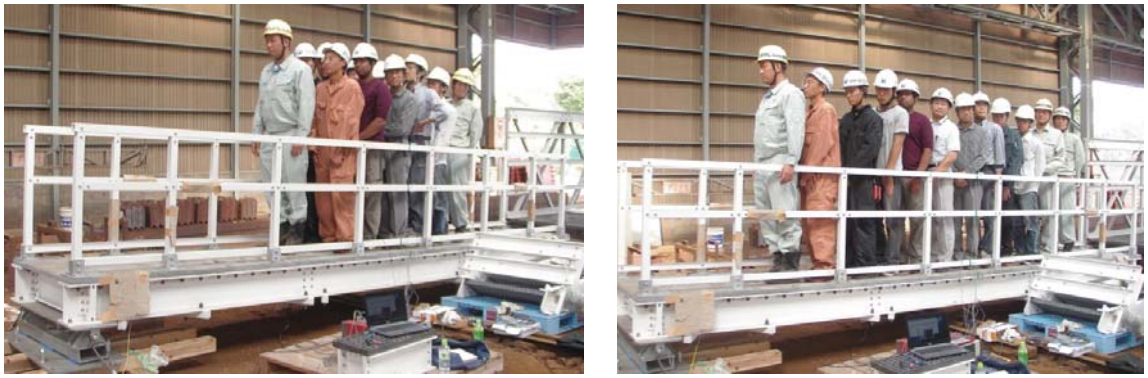

(a) Concentrated load (b) Distributed load

Fig. 6.3 Loading patterns

6.3 Results and discussion

At the deflection limit suggested by the design guidelines (L/500), the effective flexural capacity of the GFRP and UFC composite beams (beam length 6,000 mm) which can be utilized under different temperatures is shown in Fig. 6.4. According to the experiment results demonstrated in Chapter 4, at the deflection limit of the GFRP and UFC composite beams, only 11.5%, 13%, and 17.6% of the ultimate flexural capacity can be utilized at 20°C, 60°C, and 90°C, respectively. Therefore, further developments are required to improve the stiffness of these composite beams.

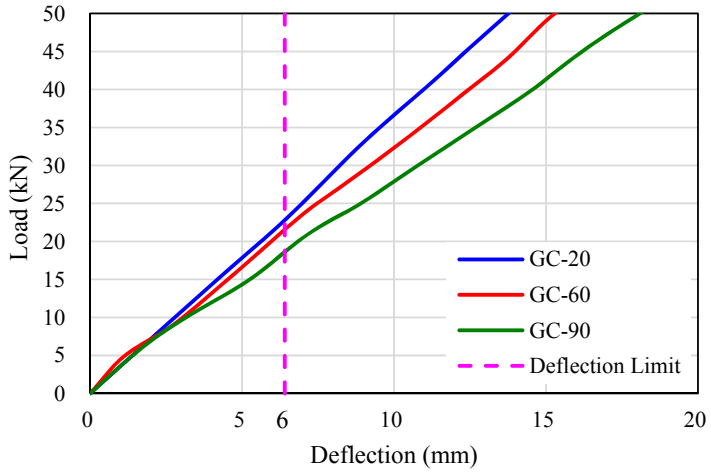

Fig. 6.4 Flexural capacity utilized in GFRP and UFC composite beams at different temperatures

The load and deflection relationship of the GFRP and UFC composite beams under different loading patterns are given in Fig. 6.5. The maximum deflection of beam 1 and beam 2 was less

than 4 mm in all loading patterns, which is less than the deflection limit (12 mm) of the bridge. When the distributed load was applied on the bridge, the increment of the deflection was reduced as the load increases (Fig. 6.5b, c, and d). This is due to non-uniformly distribution of the load because of the different weights of the humans (Table 6.1). The eccentric distributed load showed the maximum deformation at midspan compared to the other loading patterns. The maximum deflection of the pedestrian bridge, subjected to eccentric distributed load, at the design load (25.86 kN) was predicted and shown in Fig. 6.6. According to Fig. 6.6, the deflection of the pedestrian bridge at the design load is less than 12 mm (the deflection limit of the bridge). Therefore, performance of the GFRP and UFC composite beams in the Miyagi pedestrian bridge is satisfactory.

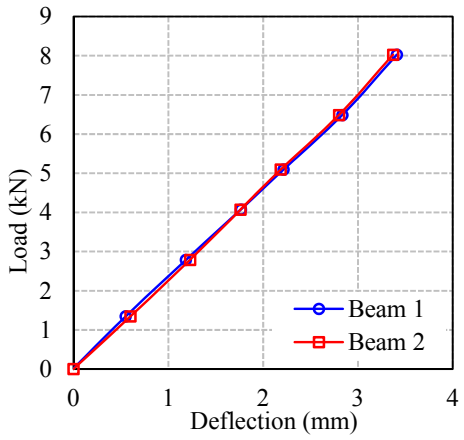

(a) Pattern 1 – Concentrated load

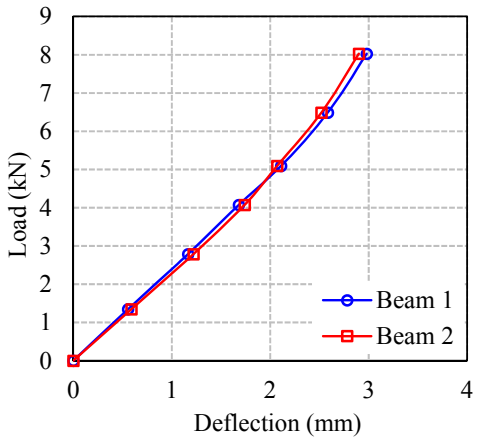

(b) Pattern 2 – Distributed load (along centreline)

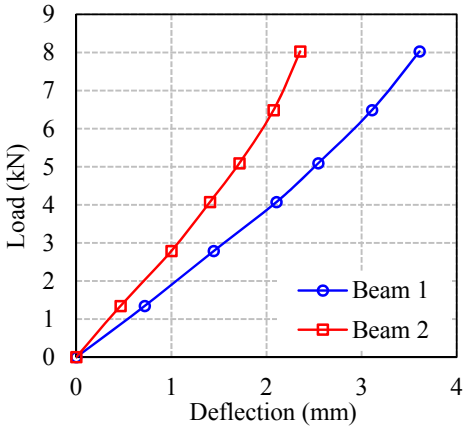

(c) Pattern 3 – Eccentric distributed load on beam 1

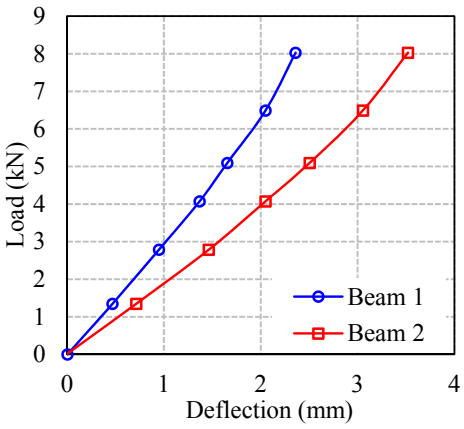

(d) Pattern 3 – Eccentric distributed load on beam 2

Fig. 6.5 Load and deflection relationships of the bridge under different loading patterns

As shown in Fig. 6.5, the maximum deflection of the beam was obtained from the concentrated load (Pattern 1) and eccentric distributed load (Pattern 3). The maximum deflection of the composite beam subjected to eccentric distributed load was nearly 21% higher than that of the beam subjected to distributed load along the centreline of the bridge. Because of that, loading pattern 1 and pattern 3 need to be considered when checking the deflection limitation of the bridges consisting of the GFRP-UFC composite beams. The midspan strain distribution of each GFRP and UFC composite beam under loading pattern 1 is shown in Fig. 6.7. The section depth was measured from the bottom flange of the GFRP I-beam. There is a linear strain distribution along the midspan cross-section throughout the loading test and that implies the full composite behaviour of the GFRP and UFP composite beams. This strain distribution is similar to the strain distribution observed in the GFRP and UFC composite beam test at 20°C (Fig. 4.14).

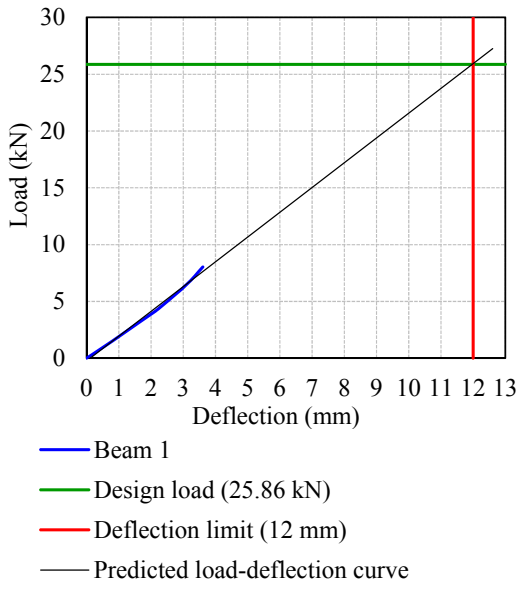

Fig. 6.6 Deflection of the pedestrian bridge at the design load

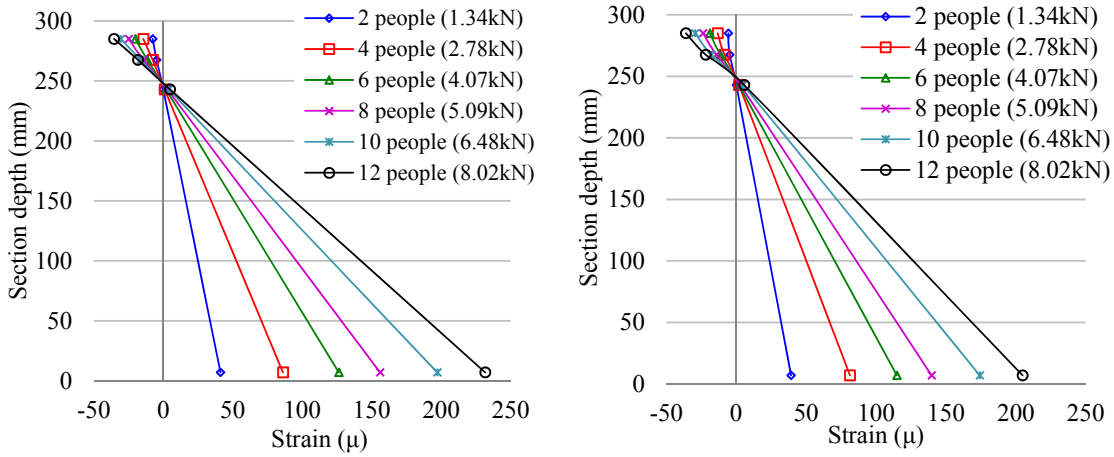

(a) Beam 1 (b) Beam 2

Fig. 6.7 Strain distribution at midspan cross-section of GFRP and UFC composite beams – Loading pattern 1

6.4 Concluding remarks

Application of the GFRP and UFC composite beams for construction of short span pedestrian bridges is described in this chapter. The GFRP and UFC composite beams are used for the girders of the bridges. The static loading tests were conducted under actual working loads on the bridge and its flexural performance was checked. The conclusions of the study are as follows.

- High corrosion resistant composite beams consisting of the GFRP I-beam and UFC segments can be used for accelerated construction of short span pedestrian bridges in severe corrosive environments.
- The short span pedestrian bridge satisfied the deflection limitation suggested in the Japan Society of Civil Engineers (JSCE) guidelines and the American Association of State Highway and Transportation Officials (AASHTO) guidelines under the design loads and working loads.
- Because of the low stiffness of the GFRP and UFC composite beams, they exceed the design deflection limit at low loads. Therefore, the ultimate flexural capacity of the composite beams cannot be utilized. To overcome this, the stiffness of the GFRP and UFC composite beams need to be further improved.

Chapter 7

Conclusions and recommendations for future studies

7.1 Flexural Behaviour of GFRP and UFC Composite Beams Having FRP Bolts as Shear Connectors

Large-scale beam flexural tests were carried out to check the performance of the FRP bolts in the GFRP and UFC composite beams. The FRP bolts were used instead of the steel bolts to improve the corrosion resistance of the composite beams so that they can be used in severe corrosive environments. The experiment results were used for construction of a short span pedestrian bridge in a fishery harbour in Japan (Chapter 6). The following conclusions were drawn from the study.

- The FRP bolts can be used instead of steel bolts in the GFRP and UFC composite beams and can have flexural capacity and stiffness similar to the GFRP and UFC composite beams with steel bolts. Because of the FRP bolts, the corrosion resistance of these composite beams will be increased and hence, they can be used for construction of short span pedestrian bridges in severe corrosive environments.
- The influence of the gap between the UFC segments on the flexural behaviour of the GFRP and UFC composite beams is very small where the gap is less than 10 mm. Provision of gaps between the UFC segments allows ease of fixing the UFC segments to the GFRP I-beams.
- The volume of the FRP material inside the UFC segment affects the stiffness of the composite beams. Therefore, the FRP bolts without bolt-heads are recommended to use as the shear connectors.

7.2 Influence of Elevated Temperature on the Mechanical Properties of Materials Used in FRP and UFC Composite Beams

The temperature dependence of the mechanical properties of the materials used in the GFRP/HFRP and UFC composite beams were investigated through laboratory tests. The main conclusions of the study are given below.

- The glass transition temperatures of the materials used in the GFRP/HFRP and UFC composite beams are in between 50°C and 60°C. Therefore, the flexural capacity and the

stiffness of the GFRP/HFRP and UFC composite beams can be significantly reduced at temperatures beyond 60°C.

- The coefficients of thermal expansion (in the longitudinal direction of the composite beam) of GFRP flange, HFRP flange, GFRP web, and UFC are constant at all temperatures between 20°C and 85°C. There is no significant influence on the longitudinal thermal expansion rates of these materials by their glass transition temperatures.
- Tensile strength of the GFRP flange and GFRP web is greatly affected by the glass transition of the vinylester resin whereas in the HFRP flange and in the FRP bolts, the tensile strength is not significantly affected by glass transition of polymer resin matrix.
- In contrast to the tensile strength, the compressive strength of the GFRP flange, GFRP web, HFRP flange, and the FRP bolts is significantly affected by the glass transition of their polymer resin matrices. The UFC doesn't contain temperature dependent materials and hence, its compressive strength remained almost constant with the temperature.
- Shear strength of the FRP bolts is rapidly reduced at the temperatures beyond 60°C, caused by the glass transition of the resin inside the FRP bolts. On the other hand, the shear capacity of the epoxy adhesive significantly reduced with temperature regardless its glass transition temperature.

7.3 Flexural Behaviour of FRP I-beams and FRP-UFC Composite Beams Subjected to Elevated Temperature

Large-scale beam flexural tests were conducted at room and elevated temperatures to study the influence of elevated temperature on the flexural behaviour of the GFRP I-beams, GFRP-UFC composite beams, and HFRP-UFC composite beams. The following conclusions can be drawn.

- The flexural capacity and the stiffness of the GFRP I-beams, GFRP-UFC composite beams, and HFRP-UFC composite beams are degraded by elevated temperature due to glass transition of the vinylester resin. However, more than 85% of the flexural capacity (compared to the flexural capacity at 20°C) of three beam types can be retained when the beam temperature is below 60°C. As the beam temperature increases beyond 60°C, the flexural capacity of these beams was severely degraded.
- The use of the UFC segments significantly improves the ultimate flexural capacity and the stiffness of the GFRP I-beams at temperatures in between 20°C to 90°C. This is because the UFC segments can prevent the premature delamination and kink failure of the GFRP I-beam

compression flange. As a result, the tensile strength of the GFRP I-beam can be effectively utilized. Similarly, the UFC segments will improve the flexural capacity and the stiffness of the HFRP I-beams.

- The bi-material bending effect in the GFRP/HFRP and UFC composite beams is negligible due to approximately close thermal expansion rates of the GFRP, HFRP, and UFC materials.
- The slippage of the UFC segments observed in the GFRP/HFRP and UFC composite beams above 60°C was due to the failure of the epoxy adhesive caused by elevated temperature. It was found that the full composite behaviour of the GFRP/HFRP and UFC beams lose after the slippage of the UFC segments and there will be partial interaction between the UFC segments and the GFRP/HFRP I-beams.
- Both the GFRP-UFC composite beams and the HFRP-UFC composite beams are affected by elevated temperature and their flexural capacities are reduced when the beam temperature increases. The failure mechanism (flexural failure or shear failure) of these composite beams was governed by the shear capacity of the FRP bolts at the beam temperature.

7.4 Fibre Model Analysis

Fibre model analysis was carried out for the GFRP I-beams and the GFRP-UFC composite beams under room and elevated temperatures. A small temperature gradient across the GFRP-UFC beam cross-section was assumed to simulate the bending test conditions described in Chapter 4. The analysis results were compared with the experiment results. In actual circumstances, when the GFRP-UFC composite beams are exposed to direct solar radiation, there will be a large temperature gradient across the beam cross-section. The flexural behaviour of the GFRP-UFC composite beams under this criterion was studied using the fibre model analysis. The main conclusions of the study are as follows.

- The fibre model analysis can be used to analyse the flexural behaviour of the GFRP I-beams at temperatures between 20°C and 90°C.
- The proposed fibre model analysis method can be used to predict the flexural behaviour of the GFRP and UFC composite beams until the slip of the UFC segments occurs.
- The difference between the beam failure loads in the analysis and the experiment is less than 8% in the GFRP I-beams and that is less than 1% in the GFRP and UFC composite beams with full interaction.

- Under the actual circumstances, the GFRP and UFC composite beams may experience a large temperature gradient across beam top to bottom. According to the analysis, it was found that the stiffness of the GFRP and UFC composite beams, which is related to the main design criterion of the FRP bridges, is not significantly affected by the temperature gradient in the real situations. However, the flexural capacity of the GFRP and UFC composite beams at the slipping of the UFC segments is greatly influenced by the temperature of the beam top.

7.5 Flexural Performance of Short span Pedestrian Bridge Consisting of GFRP and UFC Composite Beams

The GFRP and UFC composite beams describe in this study are developed to use as bridge girders in short span pedestrian bridges. Because of the high corrosion resistance, they can be used in severe corrosive environments. Static loading tests were conducted under actual working loads and the performance of the bridge was checked with the design guidelines. The conclusions of the study are as follows.

- High corrosion resistant composite beams consisting of the GFRP I-beam and UFC segments can be used for accelerated construction of short span pedestrian bridges in severe corrosive environments.
- The short span pedestrian bridge satisfied the deflection limitation suggested in the Japan Society of Civil Engineers (JSCE) guidelines and the American Association of State Highway and Transportation Officials (AASHTO) guidelines under the design loads and working loads.
- Because of the low stiffness of the GFRP and UFC composite beams, they exceed the design deflection limit at low loads. Therefore, the ultimate flexural capacity of the composite beams cannot be utilized. To overcome this, the stiffness of the GFRP and UFC composite beams need to be further improved.

7.6 Recommendations for future studies

- Because of the low stiffness of the FRP materials, the design criterion of the short span pedestrian bridges is governed by the deflection limit. Therefore, the ultimate flexural capacity of the GFRP/HFRP and UFC composite beams cannot be utilized. Therefore, it is

recommended to carry out further researche to improve the stiffness of the GFRP-UFC composite beams and the HFRP-UFC composite beams.

- The glass transition temperature of the materials used in the GFRP/HFRP and UFC composite beams is generally in between 50°C and 60°C. Therefore, it is recommended to carry out further material tests and composite beam flexural tests at temperatures between 50°C and 80°C for better understanding of the influence of T_g on the flexural behaviour of the composite beams.
- In order to predict the flexural behaviour of the GFRP and UFC composite beams after slipping the UFC segments, partial interaction at the UFC-GFRP interface need to be considered in the future analysis.

PUBLICATIONS

Journal article

Wijayawardane, I.S.K., Mutsuyoshi, H., Nguyen, H., and Manalo A., "Flexural Behaviour of GFRP and Ultra-High Strength Fibre-Reinforced Concrete Composite Beams Subjected to Elevated Temperature", *Advances in Structural Engineering*, 2016. (Accepted for publishing)

Peer reviewed conference proceedings

Wijayawardane, I.S.K., Mutsuyoshi, H., and Perera, S.V.T. J., "Innovative composite girders using FRP I-beams and precast UFC slab segments", *The 7th International Conference on FRP Composites in Civil Engineering (CICE-2014)*, Vancouver, Canada, 2014.

Wijayawardane, I.S.K., Mutsuyoshi, H., Perera, S.V.T. J., and Hai, N.D., "FRP and ultra high-strength concrete slab composite girders for accelerated bridge construction", *9th International Conference on Short and Medium Span Bridges (SMSB-2014)*, Alberta, Canada, 2014.

Wijayawardane, I.S.K., Mutsuyoshi, H., Endo, T., and Moriya, K., "Flexural behavior of GFRP and ultra-high strength concrete composite girders subjected to elevated temperature", *JCI Annual Convection*, Chiba, Japan, 2015.

Wijayawardane, I. S.K., and Mutsuyoshi, H., "Development of GFRP and ultra-high strength concrete composite beams for short span bridges", *5th International Conference on Construction Materials: Performance, Innovations and Structural Implications (CONMAT-15)*, Whistler, Canada, 2015.

Wijayawardane I., and Mutsuyoshi H., "Influence of elevated temperature on the flexural behavior of GFRP and UFC composite beams", *7th International Conference on Advanced Composite Materials in Bridges and Structures, (ACMBS-VII)*, Vancouver, Canada, 2016. (will be published in 2016)

Wijayawardane, I.S.K., and Mutsuyoshi, H., "High corrosion resistant GFRP-UFC composite beams for short span pedestrian bridges", *The 8th International Conference on Concrete Under Severe Conditions - Environment & Loading (CONSEC-2016)*, Lecco, Italy, 2016. (will be published in 2016)

Wijayawardane, I.S.K., and Mutsuyoshi, H., "Effect of glass transition temperature on the flexural behavior of the GFRP and UFC composite beams", *The 7th International Conference on FRP Composites in Civil Engineering (CICE-2016)*, Hong Kong, China, 2016. (will be published in 2016)

Other conference proceedings

Wijayawardane, I.S.K., Mutsuyoshi, H., Perera, S.V.T. J., and Kanaya, Y., "Behavior of GFRP and UHF composite girders with FRP bolts", *Japan Society of Civil Engineers (JSCE) 15th International Summer Symposium*, Tokyo, Japan, 2013.

Wijayawardane, I.S.K., Mutsuyoshi, H., Perera, S.V.T. J., and Kanaya, Y., "Development of GFRP and UHF composite girders", *13th East Asia-Pacific Conference on Structural Engineering and Construction (EASEC-13)*, Sapporo, Japan, 2013.

Wijayawardane, I.S.K., Mutsuyoshi, H., and Perera, S.V.T. J., "Flexural behavior of composite girders consisting of HFRP and UHSFRC slabs", *4th International Symposium on Life-Cycle Civil Engineering (IALCCE-2014)*, Tokyo, Japan, 2014.

Publications as a co-author

Endo T., Mutsuyoshi H., and Wijayawardane I.S.K., "FRP 桁と超高強度繊維補強プレキャストコンクリート床版から成る合成桁の曲げ性状", *JCI Annual Convection*, Chiba, Japan, 2015 (in Japanese). (Peer reviewed conference paper)

Mutsuyoshi, H., and Wijayawardane, I.S.K., "Development of composite short span bridge consisting of FRP and ultra-high strength concrete", *2nd Second International Conference on Sustainable Urbanization (ICSU 2015)*, Hong Kong, China, 2015. (International conference abstract)

Mutsuyoshi, H., Wijayawardane, I.S.K., and Phuong, N.D., "Application of FRP to Pedestrian Bridges in Japan", *14th East Asia-Pacific Conference on Structural Engineering and Construction (EASEC-14)*, Ho Chi Minh, Vietnam, 2016. (Conference paper)

Mutsuyoshi, H., and Wijayawardane, I.S.K., "Design and construction of a short span pedestrian bridge using high corrosion resistant hybrid FRP composite beams", *The 7th International Conference on FRP Composites in Civil Engineering (CICE-2016)*, Hong Kong, China, 2016. (will be published in 2016) (Peer reviewed conference paper)

REFERENCES

[1] USDOT, *2006 status of the nation's highways, bridges, and transit: conditions and performance*: U.S. Department of Transportation (USDOT), 2007.

[2] I. Nishizaki, N. Takeda, Y. Ishizuka, and T. Shimomura, "A case study of life cycle cost based on a real FRP bridge," in *Proceedings of Third International Conference on FRP Composites in Civil Engineering (CICE)*, Florida, USA, 2006, pp. 99-102.

[3] H. Tanaka, H. Tazawa, M. Kurita, and T. Shimomura, "A case study on life-cycle assessment of environmental aspect of FRP structures," in *Proceedings of Third International Conference on FRP Composites in Civil Engineering (CICE)*, Florida, USA, 2006, pp. 175-178.

[4] R. Shenoi, S. Moy, and L. Hollaway, *Advanced polymer composites for structural applications in construction*, 2000.

[5] C. B. Lawrance, *Composites for constuction - Structural design with FRP materials*: John Wiley & Sons, Inc., 2006.

[6] L. C. Bank, T. R. Gentry, and A. Barkatt, "Accelerated test methods to determine the long-term behavior of FRP composite structures: environmental effects," *Journal of Reinforced Plastics and Composites,* vol. 14, pp. 559-587, 1995.

[7] J. Summerscales and D. Short, "Carbon fibre and glass fibre hybrid reinforced plastics," *Composites,* vol. 9, pp. 157-166, 1978.

[8] P. J. D. Mendes, J. A. O. Barros, J. M. Sena-Cruz, and M. Taheri, "Development of a pedestrian bridge with GFRP profiles and fiber reinforced self-compacting concrete deck," *Composite Structures,* vol. 93, pp. 2969-2982, 2011.

[9] I. Kalnin, "Evaluation of unidirectional glass-graphite fiber/epoxy resin composites," presented at the Composite Materials: Testing and Design (second conference), ASTM STP 497, 1972.

[10] R. Dukes and D. L. Griffiths, "Marine aspects of carbon fibers and glass fiber/carbon fiber composites," in *First International Conference on Carbon Fibers*, 1971, pp. 226-231.

[11] H. Wells and N. L. Hancox, "Stiffening and strengthening GFP beams with CFRP Composites," 1971, pp. 147-151.

[12] N. Uno and N. Kitayama, "Design, fabrication and erection of the pedestrian bridge in the road-park of Ikei-Tairagawa in Okinawa," *IHI Engineering Review,* vol. 36, pp. 35-39, 2003.

[13] P. J. Szak, B. N. Robson, I. E. Harik, and B. Brailsford, "The clear creek hybrid composite I-girder pedestrian bridge," *Journal of Composites for Construction,* vol. 3, pp. 101-104, 1999.

[14] H. Nguyen, H. Mutsuyoshi, and W. Zatar, "Push-out tests for shear connections between UHPFRC slabs and FRP girder," *Composite Structures,* vol. 118, pp. 528-547, 2014.

[15] C. Bakis, L. C. Bank, V. Brown, E. Cosenza, J. Davalos, J. Lesko*, et al.*, "Fiber-reinforced polymer composites for construction-state-of-the-art review," *Journal of Composites for Construction,* vol. 6, pp. 73-87, 2002.

[16] M. W. Braestrup, "Footbridge constructed from glass-fibre-reinforced profiles, Denmark," *Structural engineering international,* vol. 9, pp. 256-258, 1999.

[17] N. D. Hai, H. Mutsuyoshi, S. Asamoto, and T. Matsui, "Structural behavior of hybrid FRP composite I-beam," *Construction and Building Materials,* vol. 24, pp. 956-969, 2010.

[18] I. S. K. Wijayawardane, H. Mutsuyoshi, and S. V. T. J. Perera, "Innovative composite girders using FRP I-beams and precast UFC slab segments," in *Proceedings of 7th International Conference on FRP Composites in Civil Engineering (CICE)*, Vancouver, Canada, 2014.

[19] A. Manalo, T. Aravinthan, H. Mutsuyoshi, and T. Matsui, "Composite behaviour of a hybrid FRP bridge girder and concrete deck," *Advances in Structural Engineering,* vol. 15, pp. 589-600, 2012.

[20] H. Nordin and B. Täljsten, "Testing of hybrid FRP composite beams in bending," *Composites Part B: Engineering,* vol. 35, pp. 27-33, 2004.

[21] J. A. Gonilha, J. R. Correia, and F. A. Branco, "Structural behaviour of a GFRP-concrete hybrid footbridge prototype: Experimental tests and numerical and analytical simulations," *Engineering Structures,* vol. 60, pp. 11-22, 2014.

[22] M. M. Schwartz, *Composite materials. Vol.2, Processing, fabrication, and applications*. Upper Saddle River, NJ: Prentice Hall, 1997.

[23] S. K. Foster and L. A. Bisby, "Fire survivability of externally bonded FRP strengthening systems," *Journal of Composites for Construction,* vol. 12, pp. 553-561, 2008.

[24] L. A. Bisby, M. F. Green, and V. K. R. Kodur, "Response to fire of concrete structures that incorporate FRP," *Progress in Structural Engineering and Materials,* vol. 7, pp. 136-149, 2005.

[25] S. Cao and Z. Wu, "Tensile properties of FRP composites at elevated and high temperatures," *Journal of Applied Mechanics,* vol. 11, pp. 963-970, 2008.

[26] V. M. Karbhari and Q. Wang, "Multi-frequency dynamic mechanical thermal analysis of moisture uptake in E-glass/vinylester composites," *Composites Part B: Engineering,* vol. 35, pp. 299-304, 2004.

[27] ACI, *Guide for the design and construction of externally bonded FRP systems for strengthening concrete structures (ACI 440.2R-08)*. Farmington Hills, Michigan, USA: American Concrete Institute, 2008.

[28] Strongwell, *Strongwell Design Manual*. Virginia, USA, (CD ROM): Strongwell Inc. (http://www.strongwell.com/), 2002.

[29] D. N. Farhey, "Long-term performance monitoring of the Tech 21 all-composite bridge," *Journal of Composites for Construction,* vol. 9, pp. 255-262, 2005.

[30] T. Keller, Y. Bai, and T. Vallée, "Long-term performance of a glass fiber-reinforced polymer truss bridge," *Journal of Composites for Construction,* vol. 11, pp. 99-108, 2007.

[31] E. J. Barbero, S. H. Fu, and I. Raftoyiannis, "Ultimate bending strength of composite beams," *Journal of Materials in Civil Engineering,* vol. 3, pp. 292-306, 1991.

[32] AASHTO, *Guide specifications for design of FRP pedestrian bridges (1st edition)*. Washington, USA: American Association of State Highway and Transportation Officials (AASHTO), 2008.

[33] JSCE, *Guidelines for Design and Construction of FRP Footbridges*: Japan Society of Civil Engineers (in Japanese), 2011.

[34] B. M. Shahrooz, A. R. Neumann, and R. M. Reising, "Durability of FRP composite bridge decks–construction and temperature effects," *International Journal of Materials and Product Technology,* vol. 28, pp. 66-88, 2007.

[35] D. Ho and C. Liu, "Temperature distribution in concrete bridge decks," *INSTITUTION OF CIVIL ENGINEERS (GREAT BRITAIN),* vol. 91, 1991.

[36] J. Dai, W. Y. Gao, and J. G. Teng, "Bond-slip model for FRP laminates externally bonded to concrete at elevated temperature," *Journal of Composites for Construction,* vol. 17, pp. 217-228, 2012.

[37] C. Sirimanna, M. Islam, and T. Aravinthan, "Temperature effects on full scale FRP bridge using innovative composite components," in *Advances in FRP Composites in Civil Engineering*, ed: Springer, 2011, pp. 376-380.

[38] S. C. Kwon, P. K. Dutta, Y. H. Kim, S. H. Eum, D. H. Shin, and R. Lopez-Anido, "Fatigue studies of FRP composite decks at extreme environmental conditions," *Key Engineering Materials,* vol. 261, pp. 1301-1306, 2004.

[39] N. Watanabe, H. Musha, and K. Yoshinaga, "Design and performance tests for bridge using ultra high strength fiber reinforced concrete," in *23th US–Japan Bridge Engineering Workshop*, 2007.

[40] P. Mehta, "Durability of High-Strength Concrete," *ACI Special Publication,* vol. 122, 1990.

[41] S. J. Perera, H. Mutsuyoshi, and N. D. Hai, "Flexural Behaviour of Composite Girders Using FRP and Precast Ultra-High-Strength Fiber-Reinforced Concrete Slabs," in *Third International Conference on Sustainable Construction Materials and Technologies*, Kyoto, Japan, 2013.

[42] JIS, *Testing Methods for Transition Temperatures of Plastics (K7121)*. Tokyo, Japan: Japanese Industrial Standard, Japanese Standards Association, 1987.

[43] J. G. T. L. Hollaway, "Strengthening and rehabilitation of civil infrastructures using fibre-reinforced polymer (FRP) composites," ed: CRC Press, 2008, pp. 67-71.

[44] H. H. S.V. Hoa, J. Lo, A. Yokoyama, "Design manufacturing composites - Proceedings of the Third International Canada-Japan Workshop," ed: Technomic, 2000, pp. 113-120.

[45] R. Park and T. Paulay, *Reinforced Concrete Structures*. New York: John Wiley and Sons, Inc., 1975.

[46] A. Manalo and T. Aravinthan, "Behaviour of glued fibre composite sandwich structure in flexure: Experiment and Fibre Model Analysis," *Materials & Design,* vol. 39, pp. 458-468, 2012.

[47] H. Nguyen, H. Mutsuyoshi, and W. Zatar, "Flexural behavior of hybrid composite beams," *Transportation Research Record: Journal of the Transportation Research Board,* vol. 2332, pp. 53-63, 2013.

[48] S. V. T. J. Perera and H. Mutsuyoshi, "Flexural Behavior of Composite Girders Consisting of Hybrid FRP and Precast Ultra High-strength fiber-reinforced Concrete Slabs," in *The Seventh International Structural Engineering and Construction Conference (ISEC-7)*, Honolulu, Hawai, 2013.

[49] H. Mutsuyoshi, N. D. Hai, K. Shiroki, T. Aravinthan, and A. Manalo, "Experimental investigation of HFRP composite beams," *ACI Special Publication,* vol. 275, 2011.

[50] JSCE, *Recommendations for Design and Construction of Ultra High Strength Fiber Reinforced Concrete Structures (Vol. 9)*. Tokyo, Japan: JSCE Guidelines for Concrete, Japan Society of Civil Engineers 2004.

[51] J. H. Association, "Technical Standard for Solid Crossing Facilities (in Japanese)," 1979.

Annexure: A

Failure patterns of the test specimens

GFRP or HFRP coupon tensile test

GFRP flange 30°C

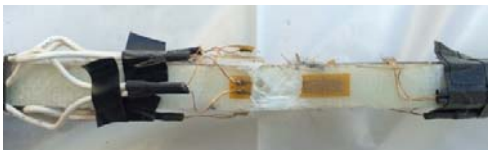

GFRP web 30°C

GFRP flange 50°C

GFRP web 50°C

GFRP flange 70°C

GFRP web 70°C

GFRP flange 90°C

GFRP web 90°C

Fig. A1 Tensile failure patterns of GFRP flange and GFRP web coupons

HFRP flange 30°C

HFRP flange 50°C

HFRP flange 70°C

HFRP flange 90°C

Fig. A2 Tensile failure patterns of HFRP flange coupons

GFRP and HFRP coupon compression test

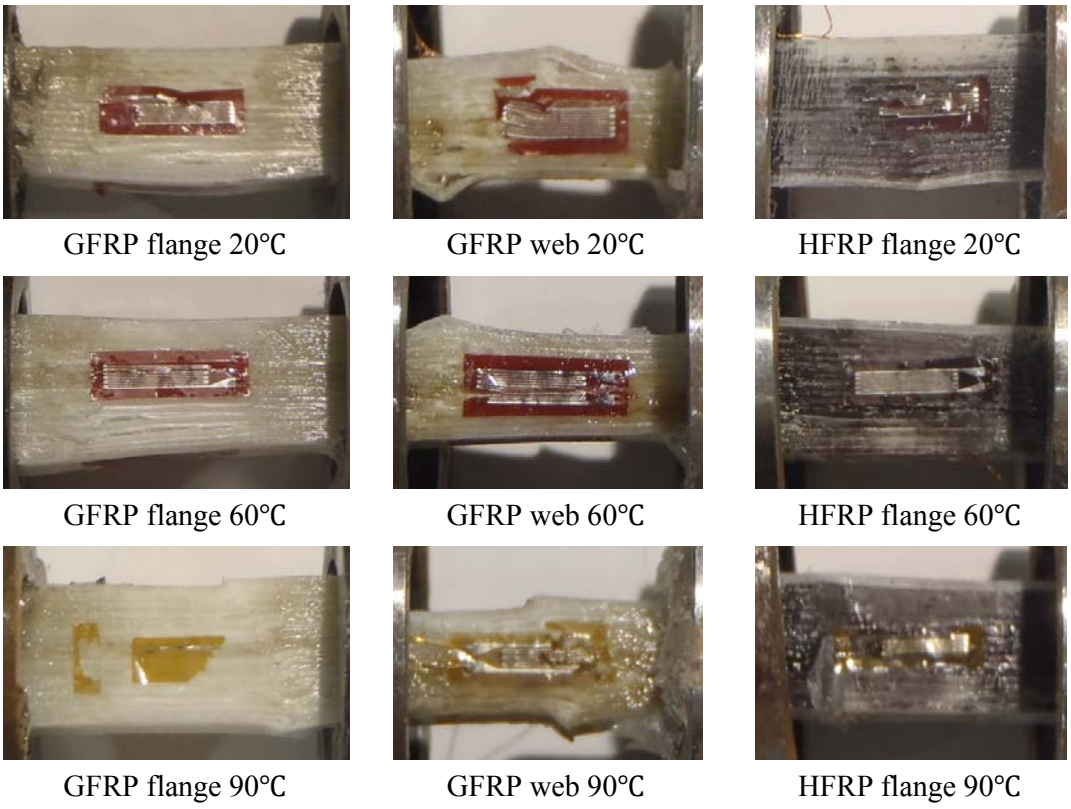

GFRP flange 20℃ GFRP web 20℃ HFRP flange 20℃

GFRP flange 60℃ GFRP web 60℃ HFRP flange 60℃

GFRP flange 90℃ GFRP web 90℃ HFRP flange 90℃

Fig. A3 Compression failure patterns of GFRP/HFRP flange and GFRP web coupons

UFC compression test

Fig. A4 Typical compression failure pattern of UFC cylinders (at all temperatures)

FRP bolt tensile test

20°C 50°C

70°C 90°C

Fig. A5 Failure patterns of FRP bolt tensile test specimens

FRP bolt compression test

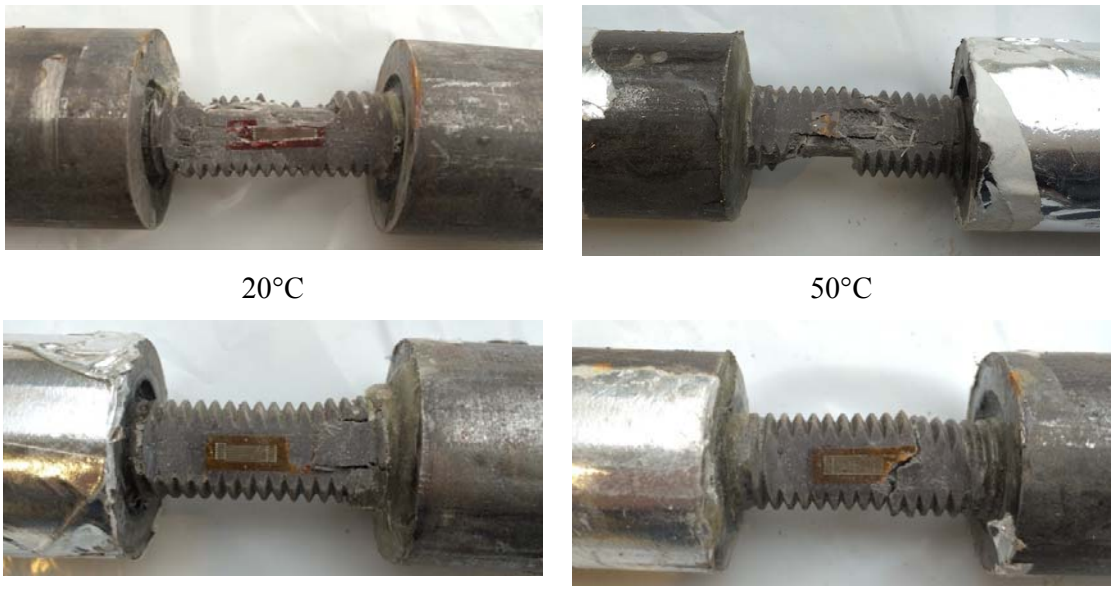

20°C 50°C

70°C 90°C

Fig. A6 Failure patterns of FRP bolt compression test specimens

FRP bolt lap-shear test

Fig. A7 Typical failure pattern of FRP bolt lap-shear test specimens (at 20°C, 60°C, and 90°C)

Epoxy adhesive lap-shear test

30°C 60°C 90°C

Fig. A8 Failure patterns of epoxy adhesive lap-shear test specimens